Compound Flood Hazards in Chinese Coastal Cities

Xu, H.

DOI
10.4233/uuid:63ebc028-a791-4efe-a32d-2def2ba248d3

Publication date
2024

Document Version
Final published version

Citation (APA)
Xu, H. (2024). *Compound Flood Hazards in Chinese Coastal Cities*. [Dissertation (TU Delft), Delft University of Technology]. https://doi.org/10.4233/uuid:63ebc028-a791-4efe-a32d-2def2ba248d3

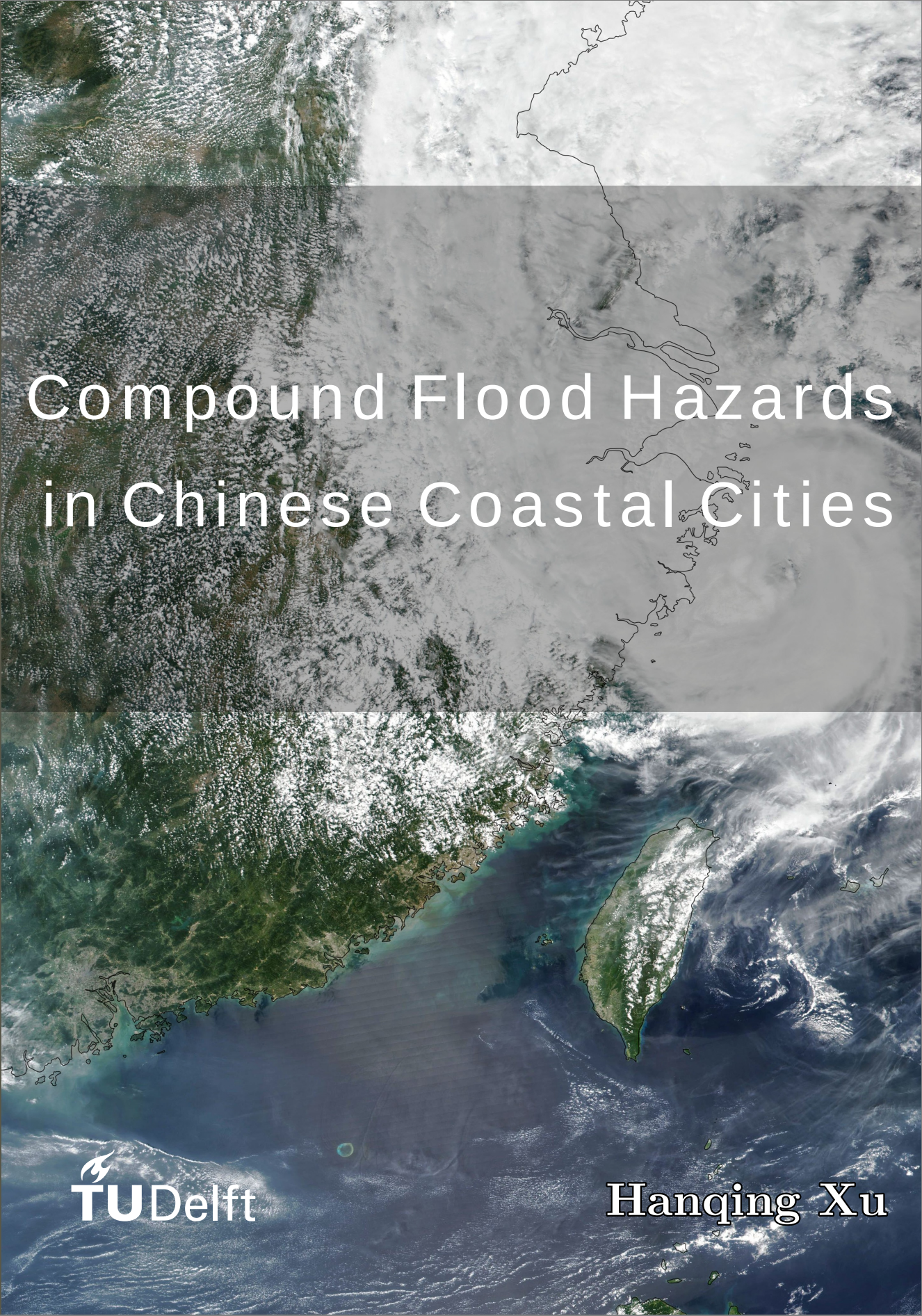

Compound Flood Hazards in Chinese Coastal Cities

TU Delft

Hanqing Xu

COMPOUND FLOOD HAZARDS IN CHINESE COASTAL CITIES

中国沿海城市复合洪涝灾害

COMPOUND FLOOD HAZARDS IN CHINESE COASTAL CITIES

Dissertation

for the purpose of obtaining the degree of doctor
at Delft University of Technology
by the authority of the Rector Magnificus Prof.dr.ir. T.H.J.J. van der Hagen,
chair of the Board for Doctorates
to be defended publicly on
Tuesday 3 September 2024 at 10:00 o'clock

by

Hanqing XU

Master of Science in Applied Chemistry, Shanghai Institute of Technology, China
born in Lianyungang, China.

This dissertation has been approved by the promotors.

Composition of the doctoral committee:

Rector Magnificus,	chairperson
Prof. dr. ir. S.N. Jonkman,	Delft University of Technology, promotor
Prof. dr. J. Wang,	East China Normal University, promotor
Dr. E. Ragno,	Delft University of Technology, co-promotor

Independent members:

Prof. dr. ir. M. Kok,	Delft University of Technology
Prof. dr. J. Yin,	East China Normal University
Dr. ir. O.M. Napoles,	Delft University of Technology
Dr. D. Pasquali,	University of L'Aquila
Prof. dr. ir. Z.B. Wang,	Delft University of Technology, reservelid

The doctoral research has been carried out in the context of an agreement on joint doctoral supervision between East China Normal University, China and Delft University of Technology, the Netherlands.

This study is a product of the projects the National Natural Science Foundation of China (42371088, 51761135024), the Netherlands Organization for Scientific Research (NWO) (ALWSD.2016.007), the Engineering and Physical Sciences Research Council of the UK (R034214/1). The author is partially supported by the China Scholarship Council.

Keywords: Climate change; Compound flood; Coastal city; Copula function; Numerical modelling

Front & Back: Hanqing Xu

ISBN 978-94-6384-620-2

An electronic version of this dissertation is available at http://repository.tudelft.nl/.

CONTENTS

SUMMARY

Coastal regions are at risk of flooding because of their natural layout. Evidence of a changing climate, like sea levels rise and more extreme weather events, along with growing populations and cities, can make the impact of floods on society even greater. Additionally, estuary regions are threatened by compound floods, i.e., flood events generated when multiple physical drivers, e.g., the water level and river discharge, interact, even if each driver on its own might not seem threatening.

Along the Chinese coastline, particularly in the south, cities like Shanghai and Haikou are prone to flood, especially during the typhoon season. When typhoons hit the coast, high storm surges and heavy rainfall can interact leading to severe impacts. Characterizing compound flooding in coastal regions poses different challenges, including identifying the physical drivers that potentially generate a flood event, selecting an appropriate numerical model to describe the interaction between these drivers in terms of frequency and magnitude, and ensuring the quality and representativity of the available observations.

This thesis aims to tackle these challenges using cities along the Chinese coast as case studies. It seeks to (i) provide a probabilistic characterization of the physical drivers of compound floods, considering the effect of sea level rise, and (ii) integrate this quantification with a hydrodynamic model to assess the extent and depth of compound flood impacts in inundated areas. This approach can lay a solid foundation for developing flood-resilient strategies and mitigating potential impacts.

Chapter 2 introduces a design approach via conditional probability for quantifying compound flood hazards in coastal regions and its implication for infrastructure design considering the seasonal variation in surge peak occurrence. We found that along the southern coast of China, the severity of the expected rainfall events in case of a storm surge peak is larger compared to the expected severity inferred from the probability distribution of annual maxima of precipitation. Consequently, from a design perspective, implementing rainwater storage systems and facilities to mitigate hydrograph peaks is crucial for these regions.

Chapter 3 focuses on Shanghai and investigates how relative sea level rise (RSLR) affects design values for flood protection systems. We employed the D-Flow FM ocean storm surge model to reconstruct 210 historical typhoon storm surge events in Shanghai to overcome the constraint of unavailable water level records. We then applied a copula-based approach to calculate the joint probability and design value of peak water level and accumulated rainfall with the impact of RSLR. This research improves our understanding of how storm surges, rainfall, and RSLR interact, revealing how they collectively contribute to the risk of flood in coastal areas. Thus, it is crucial to monitor and predict the interplay of these factors for developing future design standards for better flood preparedness.

Chapter 4 reveals distinct patterns in the relationship between flooded areas and volume for both single-driven and multi-driven flood scenarios at the coastal city of Haikou by implementing an ocean storm surge generator and urban overland hydrodynamic model. The results highlighted storm tide (a combination of surge and astronomical tide) as the predominant factor contributing to compound flooding in Haikou. Only examining single-driven factors would underestimate flood hazard.

Chapter 5 investigates the sensitivity of inundated areas to the relative timing between the occurrence of the rainfall peak and the storm surge peak in Shanghai and provides a characterization of the consequent inundated areas based on the main flood driver(s). This is achieved by inferring from the probabilistic model the severity of the expected pairs of storm surges and rainfall events. They are then used as forcing of a hydrodynamic model to generate flood extent. We showed that the relative time between the peak of flood drivers affects the extent and depth of the flood and the flood zone classification. This can better suggest potential strategies for dealing with different types of compound flooding for coastal cities.

摘要

气候变化影响极端天气事件的发生频率和变率增加，台风风暴潮、极端降水、相对海平面上升等多致灾因子在时空维度遭遇、耦合或并发，导致复合洪涝已成为沿海地区影响最严重的自然灾害，给沿海人居环境和可持续发展造成严峻挑战。在气候变化背景下，准确理解多源复合洪涝灾害对沿海城市的影响，进而揭示多致灾因子之间的复杂作用机制和复合洪灾的形成机制，从而有效应对复合洪涝灾害，提高防灾减灾能力，已当前国际社会和学术界普遍关注的热点和前沿科学问题。

本研究立足于沿海超大城市上海和海口，基于Copula统计模型和D-Flow FM水动力模型耦合方法，探讨了沿海城市复合洪涝灾害的作用机理，构建了复合洪涝情景和复合洪涝数值模型，系统模拟了不同重现期的复合洪涝灾害，深刻揭示了多源复合洪涝灾害的形成机理与致灾机制。本研究的主要创新性认识如下：

（1）得益于河口海岸学和统计学理论交叉，基于超阈值模型和Copula联合概率统计模型，在沿海流域尺度开展复合洪涝多致灾因子的识别和评估，对我国沿海流域的极端风暴潮与降水事件的特征和依赖结构进行了有效评估，并将给定潮位的降雨与年极值降雨进行频率分析，认为在我国东南沿海地区，以年极值降雨频率分析的设防标准设计难以满足复合洪涝多致灾因子的设计需要。

（2）为了评估台风风暴潮和极端降雨对沿海城市的复合影响，通过耦合Holland台风模和D-Flow FM水动力模型，构建台风风暴潮模型和城市洪涝模型，开展典型复合洪涝灾害事件（1997年台风“温妮”、2013年台风“菲特”和2019年台风“利奇马”）的模拟和验证。结果表明Holland台风模型、台风风暴潮模型和城市洪涝模型均能较为准确地模拟历史复合洪涝事件下风速、风向、天文潮、风暴潮、淹没范围和积水深度的变化特征，可用于不同重现期复合洪涝的淹没模拟和定量分析。

（3）为了定量表征极值水位和累积降雨的依赖结构和相互关系，通过使用Copula函数构造210场台风事件极值水位和累积降雨的联合分布函数。结果表明Gaussian Copula函数能够较好地描述上海市台风期间典型雨潮遭遇事件的联合分布及相关性。利用极大似然方法估计Copula联合分布函数在不同重现期的概率设计值。结果表明，Copula函数方法能够更加准确地表达极值水位和累积降雨之间的相互作用和依赖结构，揭示台风期间雨潮复合洪涝情景的变化规律，优化台风风暴潮—暴雨内涝共同作用下的复合洪涝典型情景，为雨潮复合洪涝的模拟和适应提供更为科学合理的情景方案。

（4）利用台风风暴潮模型和城市洪涝模型，对不同重现期单灾种洪涝情景（台风风暴潮和暴雨内涝）和多灾种复合洪涝情景进行模拟。结果表明，台风风暴潮的淹没范围主要集中在三角洲沿海与沿江区域，由于降雨导致的淹没范围主要位于城市地势低洼的区域。台风风暴潮决定了淹没范围内的积水深度，而暴雨内涝则主要表现为淹没范围的空间变化。在雨潮复合洪涝研究中，通过对比单灾种洪涝和复合洪涝的淹没面积和淹没体积，表明单灾种洪涝与复合洪涝的淹没面积之间存在“1+1>2”的关系，而单灾种洪涝与复合洪涝的淹没体积之间是“1+1<2”的关系。

（5）该研究耦合Copula统计模型和DFlow FM水文水动力模型，定量评估了上海地区由台风风暴潮与台风降雨遭遇引发的复合洪涝事件。研究首先使用基于Copula统计模型定义复合事件，之后利用DFlow FM水文水动力模型模拟复合洪涝积水淹没情况。研究发现流域极端降雨发生在河口潮位峰值之前会引发复合洪涝淹没的“最坏情景”，洪涝最为严重，合理利用防潮除涝设施规避复合洪涝多致灾因子之间的“时滞效应”是关键。与此同时，研究开展了复合洪涝不同致灾因子的影响区域的区划研究，识别关键基础设施洪涝影响的关键驱动因素，认为空间合理布局防洪设施，能够更有效的开展复合洪涝风险应对。

关键词：复合洪涝；沿海城市；水文水动力模型；台风风暴潮；暴雨内涝

1

INTRODUCTION

1

1.1. MOTIVATION

The United Nations Intergovernmental Panel on Climate Change (IPCC) Sixth Assessment Report (AR6) highlights the acceleration of climate change, driven by the convergence of natural variability and human activities. Coastal urban areas in regions where land and sea interact are highly susceptible to frequent extreme weather events, making them hotspots for climate hazards. These events include typhoon-driven storm surges, heavy rainfall, and rising sea levels (Adler et al., 2022). The increased tropical cyclone activity, which altered rainfall patterns and raised storm surge intensity, combined with sea-level rise collectively poses a growing risk to coastal communities, challenging their safety and sustainable development (Dutton et al., 2015; Kossin et al., 2020). Chinese cities are an example. Over 70% of Chinese cities are situated in the southeast coastal regions which are exposed to seasonal typhoons (Figure 1.1)(Yi et al., 2021). In 2019 only, storm surges and high waves caused direct economic losses of 1.826 billion USD leading to 22 deaths and disappearances, surpassing historical averages (State Oceanic Administration, 2019). Furthermore, rapid urbanization and human-induced land subsidence exacerbate relative sea-level rise, resulting in an "amplification effect" for flood events on the Chinese coast (Wang et al., 2018). The interplay between climatic and environmental factors calls for developing sustainable solutions for compound flooding risk reduction. This will advance climate-resilient urban planning and management in coastal regions and contribute to sustainable development and social stability.

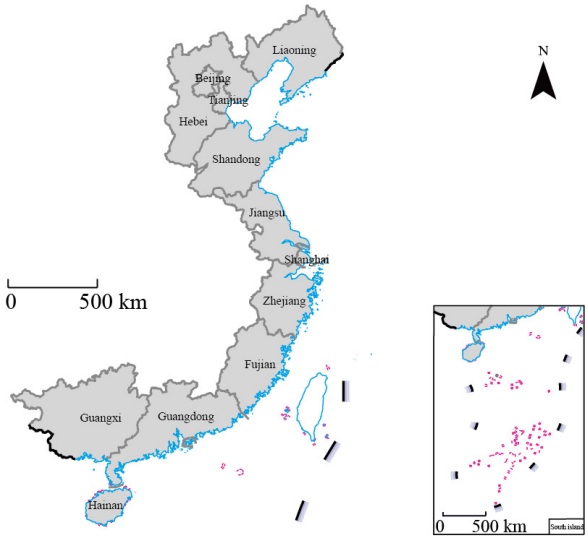

Figure 1.1: Map of Chinese coastal cities.

The global scientific community has recently launched several research projects focused on climate-related impacts on societies, infrastructures, and ecosystems to develop adaptation strategies. One of these projects, the "Integrated Research on Disaster Risk Program (IRDR)," operating under the International Union of Sciences (ICSU), has gained significant momentum (Handmer et al., 2021). Other important research projects

in this domain include, for example, the United States Global Change Research Program (USGCRP), the Sendai Framework for Risk Reduction Strategies, and the European Climate Adaptation Platform (Climate-ADAPT).

1.2. COMPOUND FLOODING

1.2.1. DEFINITION OF COMPOUND FLOODING

The IPCC Special Report on extreme events defines compound events in climate science as (i) two or more extreme events occurring simultaneously or successively, (ii) combinations of extreme events with underlying conditions that amplify the impact of the events, or (iii) combinations of events that are not themselves extremes but lead to an extreme event or impact when combined (Seneviratne et al., 2012). Types of compound events could be, for example, hot-and-dry events (e.g., AghaKouchak et al., 2014; Bevacqua et al., 2022), wildfires (e.g., Richardson et al., 2022), and floods (e.g., Bevacqua et al., 2017).

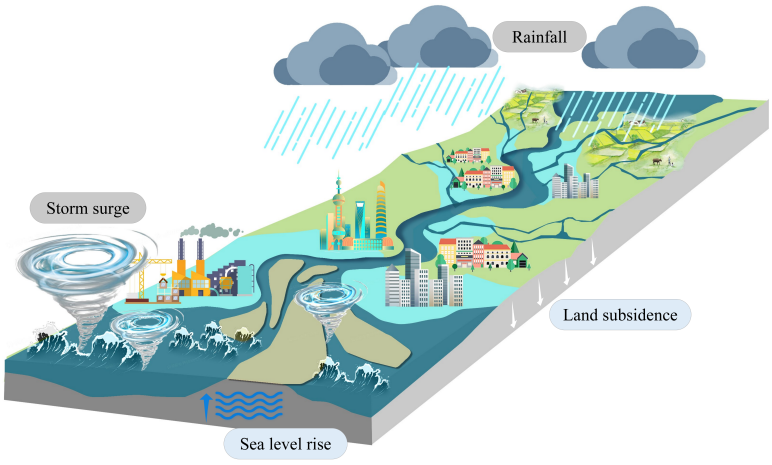

Figure 1.2: Conceptual model of compound flooding event in coastal cities.

In coastal regions, three main flood drivers can be identified: sea levels which comprised of storm surge, high astronomical tides, and/or waves (coastal flood); river discharge (fluvial flood); and direct surface run-off from rainfall events (pluvial flood) (Figure 1.2) (Fang et al., 2021). The interaction between such drivers can lead to compound floods. In the current literature, compound floods have been widely investigated as the interaction between river discharge and storm surge (e.g., Bevacqua et al., 2017; Couasnon et al., 2020; Ganguli and Merz, 2019; Ganguli et al., 2020; Moftakhari et al., 2017; Paprotny et al., 2020; Wu et al., 2021) and heavy precipitation and storm surge (e.g., Bevacqua, Vousdoukas, Zappa, et al., 2020; Feng et al., 2023; Lai et al., 2021; Paprotny et al., 2020; Santos et al., 2021; Wahl et al., 2015), when precipitation is used as a proxy for river discharge. Other studies investigated compound floods as a combination of river discharge, surge, and wave height (Eilander et al., 2023); heavy rainfall on saturated soil or coinciding with snowmelt (Poschlod et al., 2020); ENSO states, precipitation, surface runoff, and the global averaged temperature (Liu et al., 2018).

In recent years, Hurricane Isaac in 2012 over southern Mississippi and southeastern Louisiana, Typhoon Haiyan in 2013 struck the Philippines, Hurricane Irma (U.S. mainland) and Hurricane Florence (North Carolina) in 2018, and Typhoon Lekima (China) in 2019 led to severe damages due to the combined effect of heavy rainfall, strong winds, and high storm surges (Fang et al., 2021). Understanding the driving processes of compound floods and their frequency of occurrence is important for flood mitigation and reduction strategies, especially in a changing climate (Fang et al., 2021; Wahl et al., 2015).

1.2.2. METHODS FOR MODELLING AND ANALYZING COMPOUND FLOODING

Two main approaches have been employed to model and analyze compound flooding: data-driven and physical-based models. Each method offers unique advantages and challenges, depending on the specific research objectives, data availability, and computational resources. Data-driven models, e.g., dependence models, often rely on multivariate distribution, e.g., copula families, to describe the dependence structure between the event's physical drivers. From these models, it is possible to generate synthetic event sets and infer low-probability events in a way that the drivers maintain the observed dependence structure. Examples are the studies by Bevacqua et al., 2017; Couasnon et al., 2018; Moftakhari et al., 2017; Wahl et al., 2015. Both observed (e.g., Ward et al., 2018) and hindcasts (e.g., Bevacqua, Vousdoukas, Shepherd, et al., 2020; Couasnon et al., 2020) data have been implemented in such methods.

On the other hand, physical-based models explicitly resolve the interaction between flood drivers over time and space providing information on the extent and depth of the flood. Hydrodynamic model simulations have been used to understand the complex physical interactions between drivers and their relative importance for the total flood hazard (Couasnon et al., 2020; Shi et al., 2020; Yin et al., 2016) also during tropical cyclones (Kumbier et al., 2018; Zellou and Rahali, 2019), enhancing our comprehension of region-specific compound flooding generating mechanisms.

Recent research has integrated dependence models for the probabilistic characterization of compound events with hydrodynamic models, to enhance the quantification of compound flooding hazards. For example, Bevacqua et al. (2019) modelled the sea level via the hydrodynamic method and evaluated the potential probability of compound flooding hazards arising from heavy rainfall with high tidal levels via copula functions across Europe. Moftakhari et al. (2019) proposed a method linking bivariate statistical models and hydrodynamic models to estimate compound flooding resulting from upstream discharge and downstream water levels in tidal estuaries. Gori et al. (2020) investigated compound flooding hazards under climate change by integrating physical models and joint probability analysis, demonstrating its effectiveness in reducing computational time for simulating compound flooding events.

1.2.3. COMPOUND FLOODING AROUND THE WORLD

Studies investigating compound flooding generally require long observation records. Hence, most of the studies are located in the US (e.g., Bates et al., 2021; Ghanbari et al., 2021) and in Europe (e.g., Svensson and Jones, 2002, 2004; van den Hurk et al., 2015). Other studies, for example, Zheng et al. (2014), Zheng et al. (2013) and Wu et al. (2018) have investigated compound floods in Australia. Fang et al. (2021) investigated the com-

pound along the Chinese coast during typhoon season. At the same time, few studies, e.g., Couasnon et al., 2020; Ward et al., 2018, investigated the potential of compound floods at the global scale by assessing the dependence between flood drivers via measures of correlation.

1.3. KNOWLEDGE GAPS

Due to their unique geographical location and complex ecological environment, Chinese southeastern coastal cities are highly susceptible to flood hazards induced by typhoons (Shi et al., 2015). Extreme rainfall and high storm surges during the typhoon season serve as primary flood drivers contributing to the frequent occurrence of compound floods (Wu et al., 2021). Even though compound flooding has been extensively studied globally, the limited availability of water level records during typhoon events and the small sample sizes of precipitation and storm surge observations limited compound flooding studies along the Chinese coast (Fang et al., 2021). Moreover, the presence of multiple drivers generating floods can challenge current engineering practices when determining design values for infrastructures (Tian et al., 2023).

1.4. OBJECTIVES AND RESEARCH QUESTIONS

Following from section 1.1, section 1.2 and section 1.3, the most important challenge is the limited insight into the quantification of compound flooding hazards generated by storm surge and rainfall in Chinese coastal cities, especially during typhoon season.

This challenge is addressed in this thesis through two main objectives:

1. *Probabilistic characterization of compound floods' physical drivers, i.e., rainfall and storm surge, along the Chinese coast, also under relative sea level rise.*

2. *Integrating statistical and physical-based models to assess compound flooding hazards in Shanghai.*

To achieve these two objectives, four associated research questions are formulated:

I. *What are the geographical and physical factors determining the relationship between peak surge and rainfall along the Chinese coastline?*

Despite compound flooding receiving significant attention globally, research on this phenomenon in Chinese coastal regions remains scarce due to the complexity of typhoon events, limited availability of data, and rapid urbanization. Here, we investigated the relationship between surge and rainfall along the Chinese coast to assess hotspots for potential compound floods, especially in relation to the occurrences of typhoons.

II. *What is the added value of explicitly modelling the dependence between peak surge and rainfall when inferring design values for compound flooding in coastal regions?*

Traditional approaches for infrastructure design rely on methods investigating one single flood driver. Floods generated by multiple drivers however require differ-

ent approaches. For example, modelling the dependence between multiple flood drivers can provide new information for design purposes.

III. *Why do synthetic generated data provide valuable options for compound flooding hazards assessment when available observations are limited?*

The limited availability of historical data poses challenges for comprehensive hazard assessment. In such a case, synthetic data can offer a valuable option to enlarge historical records.

IV. *What are the potential benefits of combining probabilistic modelling and hydrodynamic modelling for flood hazard quantification in urban environments?*

The relative occurrence of the peak of rainfall and surge can alter the characteristics (extent and depth) of the inundated land. Hence, the advantages and disadvantages of combining statistical models providing event magnitudes and frequencies with a physical-based model explicitly calculating the interaction between the drivers are explored for the city of Shanghai.

1.5. OUTLINE OF THIS THESIS

This thesis has six chapters (Figure 1.3). Chapter 1 and Chapter 6 are introduction and conclusions, respectively. In Chapter 1, an exhaustive exploration of compound flooding is presented, including an overview of the phenomenon, challenges associated with comprehending the interplay of contributing factors, particularly human-induced influences, and the formulation of key research questions. Chapter 6 provides conclusive findings and insightful suggestions for future research directions. The main body of the thesis is the collection of previous publications and is organized into two parts:

1. Probability quantification of storm surge and rainfall alone Chinese coast under relative sea level rise (Chapter 2 and 3)

2. Compound flooding hazards quantification via hydrodynamic model in Chinese coastal megacity. (Chapter 4 and 5)

Chapter 2 presents a copula-based framework for modelling the interdependence between surge and rainfall along the Chinese coast. This framework is applied to estimate the expected conditional probability of rainfall levels for different surge event magnitudes, which is useful for mitigating urban pluvial flooding hazards and enhancing urban flood resilience during the season when surge peaks are predominant in specific estuarine regions.

Chapter 3 extends the analysis of Chapter 2 to Shanghai, employs the D-Flow Flexible Mesh model to reconstruct the historical peak water level, which includes storm surge, astronomical tide, and relative sea level rise (RSLR). Then, we applied a copula-based method to compute the joint probability between peak water levels and rainfall during the typhoon period.

Chapter 4 introduces a method for developing a 'Typhoon Storm Surge - Heavy Rainfall' compound flooding hydrodynamic model. This chapter focuses on the examination of compound flooding through the construction of a storm surge model and an overland

flooding model using D-Flow FM. Based on these models, we quantify the implications of compound flooding when compared to individual single-hazard flooding (storm tide flooding and rainstorm inundation).

Chapter 5 employs the same frequency amplification method and copula function to develop a library of compound flooding hazard scenarios. Then, we investigate the sensitivity of inundated areas to the timing of peak occurrences of rainfall and storm surges in Shanghai. By analysis of compound flooding inundation maps, we identify primary flood drivers and delineate flood zones in Shanghai.

Chapter 6 summarizes the main findings and contributions of the thesis, discusses the limitations and uncertainties, and provides recommendations for future research and practice.

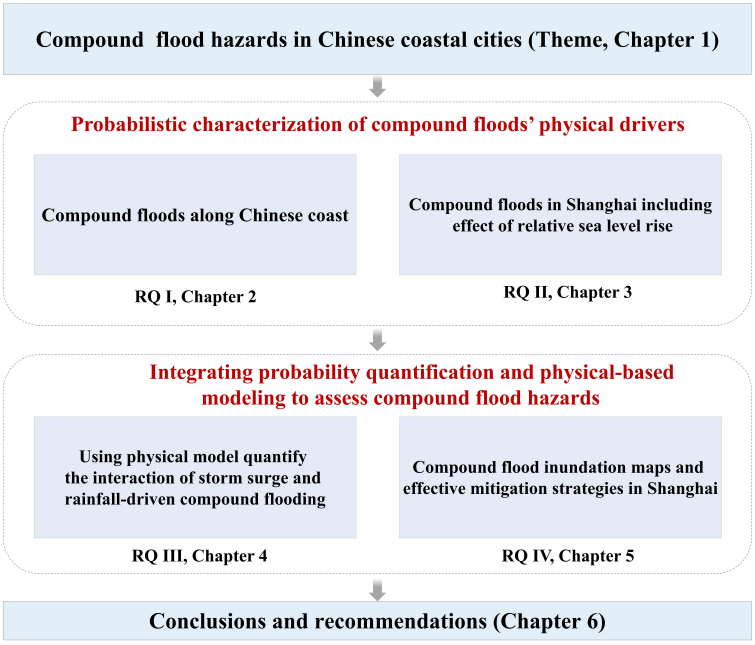

Figure 1.3: An overview of the content and structure of this thesis.

BIBLIOGRAPHY

Adler, C., Wester, P., Bhatt, I., Huggel, C., Insarov, G., Morecroft, M., Muccione, V., & Prakash, A. (2022). Cross-chapter paper 5: Mountains. In H. O. Pörtner, D. C. Roberts, M. Tignor, E. S. Poloczanska, K. Mintenbeck, A. Alegría, M. Craig, S. Langsdorf, S. Löschke, V. Möller, A. Okem, & B. Rama (Eds.), *Climate change 2022: Impacts, adaptation and vulnerability. contribution of working group ii to the sixth assessment report of the intergovernmental panel on climate change* (pp. 2273–2318). Cambridge University Press. https://doi.org/10.1017/9781009325844.022.2273

AghaKouchak, A., Cheng, L., Mazdiyasni, O., & Farahmand, A. (2014). Global warming and changes in risk of concurrent climate extremes: Insights from the 2014 california drought. *Geophysical Research Letters*, *41*(24), 8847–8852.

Bates, P. D., Quinn, N., Sampson, C., Smith, A., Wing, O., Sosa, J., Savage, J., Olcese, G., Neal, J., Schumann, G., et al. (2021). Combined modeling of us fluvial, pluvial, and coastal flood hazard under current and future climates. *Water Resources Research*, *57*(2), e2020WR028673.

Bevacqua, E., Maraun, D., Hobæk Haff, I., Widmann, M., & Vrac, M. (2017). Multivariate statistical modelling of compound events via pair-copula constructions: Analysis of floods in ravenna (italy). *Hydrology and Earth System Sciences*, *21*(6), 2701–2723.

Bevacqua, E., Maraun, D., Vousdoukas, M., Voukouvalas, E., Vrac, M., Mentaschi, L., & Widmann, M. (2019). Higher probability of compound flooding from precipitation and storm surge in europe under anthropogenic climate change. *Science advances*, *5*(9), eaaw5531.

Bevacqua, E., Vousdoukas, M. I., Shepherd, T. G., & Vrac, M. (2020). Brief communication: The role of using precipitation or river discharge data when assessing global coastal compound flooding. *Natural Hazards and Earth System Sciences*, *20*(6), 1765–1782.

Bevacqua, E., Vousdoukas, M. I., Zappa, G., Hodges, K., Shepherd, T. G., Maraun, D., Mentaschi, L., & Feyen, L. (2020). More meteorological events that drive compound coastal flooding are projected under climate change. *Communications earth & environment*, *1*(1), 47.

Bevacqua, E., Zappa, G., Lehner, F., & Zscheischler, J. (2022). Precipitation trends determine future occurrences of compound hot–dry events. *Nature Climate Change*, *12*(4), 350–355.

Couasnon, A., Eilander, D., Muis, S., Veldkamp, T. I., Haigh, I. D., Wahl, T., Winsemius, H. C., & Ward, P. J. (2020). Measuring compound flood potential from river discharge and storm surge extremes at the global scale. *Natural Hazards and Earth System Sciences*, *20*(2), 489–504.

Couasnon, A., Sebastian, A., & Morales-Nápoles, O. (2018). A copula-based bayesian network for modeling compound flood hazard from riverine and coastal interac-

tions at the catchment scale: An application to the houston ship channel, texas. *Water*, *10*(9), 1190.

Dutton, A., Carlson, A. E., Long, A. J., Milne, G. A., Clark, P. U., DeConto, R., Horton, B. P., Rahmstorf, S., & Raymo, M. E. (2015). Sea-level rise due to polar ice-sheet mass loss during past warm periods. *science*, *349*(6244), aaa4019.

Eilander, D., Couasnon, A., Sperna Weiland, F. C., Ligtvoet, W., Bouwman, A., Winsemius, H. C., & Ward, P. J. (2023). Modeling compound flood risk and risk reduction using a globally applicable framework: A pilot in the sofala province of mozambique. *Natural Hazards and Earth System Sciences*, *23*(6), 2251–2272.

Fang, J., Wahl, T., Fang, J., Sun, X., Kong, F., & Liu, M. (2021). Compound flood potential from storm surge and heavy precipitation in coastal china: Dependence, drivers, and impacts. *Hydrology and Earth System Sciences*, *25*(8), 4403–4416.

Feng, J., Li, D., Li, Y., & Zhao, L. (2023). Analysis of compound floods from storm surge and extreme precipitation in china. *Journal of Hydrology*, *627*, 130402.

Ganguli, P., & Merz, B. (2019). Trends in compound flooding in northwestern europe during 1901–2014. *Geophysical Research Letters*, *46*(19), 10810–10820.

Ganguli, P., Paprotny, D., Hasan, M., Güntner, A., & Merz, B. (2020). Projected changes in compound flood hazard from riverine and coastal floods in northwestern europe. *Earth's Future*, *8*(11), e2020EF001752.

Ghanbari, M., Arabi, M., Kao, S.-C., Obeysekera, J., & Sweet, W. (2021). Climate change and changes in compound coastal-riverine flooding hazard along the us coasts. *Earth's Future*, *9*(5), e2021EF002055.

Gori, A., Lin, N., & Xi, D. (2020). Tropical cyclone compound flood hazard assessment: From investigating drivers to quantifying extreme water levels. *Earth's Future*, *8*(12), e2020EF001660.

Handmer, J., Vogel, C., Payne, B., Stevance, A.-S., Kirsch-Wood, J., Boyland, M., Han, Q., & Lian, F. (Eds.). (2021). A framework for global science in support of risk informed sustainable development and planetary health. https://doi.org/10.24948/2021.07

Kossin, J. P., Knapp, K. R., Olander, T. L., & Velden, C. S. (2020). Global increase in major tropical cyclone exceedance probability over the past four decades. *Proceedings of the National Academy of Sciences*, *117*(22), 11975–11980.

Kumbier, K., Carvalho, R. C., Vafeidis, A. T., & Woodroffe, C. D. (2018). Investigating compound flooding in an estuary using hydrodynamic modelling: A case study from the shoalhaven river, australia. *Natural Hazards and Earth System Sciences*, *18*(2), 463–477.

Lai, Y., Li, J., Gu, X., Liu, C., & Chen, Y. D. (2021). Global compound floods from precipitation and storm surge: Hazards and the roles of cyclones. *Journal of Climate*, *34*(20), 8319–8339.

Liu, Z., Cheng, L., Hao, Z., Li, J., Thorstensen, A., & Gao, H. (2018). A framework for exploring joint effects of conditional factors on compound floods. *Water Resources Research*, *54*(4), 2681–2696.

Moftakhari, H., Salvadori, G., AghaKouchak, A., Sanders, B. F., & Matthew, R. A. (2017). Compounding effects of sea level rise and fluvial flooding. *Proceedings of the National Academy of Sciences*, *114*(37), 9785–9790.

Moftakhari, H., Schubert, J. E., AghaKouchak, A., Matthew, R. A., & Sanders, B. F. (2019). Linking statistical and hydrodynamic modeling for compound flood hazard assessment in tidal channels and estuaries. *Advances in Water Resources*, *128*, 28–38.

Paprotny, D., Vousdoukas, M. I., Morales-Nápoles, O., Jonkman, S. N., & Feyen, L. (2020). Pan-european hydrodynamic models and their ability to identify compound floods. *Natural Hazards*, *101*, 933–957.

Poschlod, B., Zscheischler, J., Sillmann, J., Wood, R. R., & Ludwig, R. (2020). Climate change effects on hydrometeorological compound events over southern norway. *Weather and climate extremes*, *28*, 100253.

Richardson, D., Black, A. S., Irving, D., Matear, R. J., Monselesan, D. P., Risbey, J. S., Squire, D. T., & Tozer, C. R. (2022). Global increase in wildfire potential from compound fire weather and drought. *NPJ climate and atmospheric science*, *5*(1), 23.

Santos, V. M., Casas-Prat, M., Poschlod, B., Ragno, E., Van Den Hurk, B., Hao, Z., Kalmár, T., Zhu, L., & Najafi, H. (2021). Statistical modelling and climate variability of compound surge and precipitation events in a managed water system: A case study in the netherlands. *Hydrology and Earth System Sciences*, *25*(6), 3595–3615.

Seneviratne, S., Nicholls, N., Easterling, D., Goodess, C., Kanae, S., Kossin, J., Luo, Y., Marengo, J., McInnes, K., Rahimi, M., et al. (2012). Changes in climate extremes and their impacts on the natural physical environment.

Shi, X., Han, Z., Fang, J., Tan, J., Guo, Z., & Sun, Z. (2020). Assessment and zonation of storm surge hazards in the coastal areas of china. *Natural Hazards*, *100*, 39–48.

Shi, X., Liu, S., Yang, S., Liu, Q., Tan, J., & Guo, Z. (2015). Spatial–temporal distribution of storm surge damage in the coastal areas of china. *Natural Hazards*, *79*(1), 237–247.

Svensson, C., & Jones, D. A. (2002). Dependence between extreme sea surge, river flow and precipitation in eastern britain. *International Journal of Climatology: A Journal of the Royal Meteorological Society*, *22*(10), 1149–1168.

Svensson, C., & Jones, D. A. (2004). Dependence between sea surge, river flow and precipitation in south and west britain. *Hydrology and Earth System Sciences*, *8*(5), 973–992.

Tian, Z., Ramsbottom, D., Sun, L., Huang, Y., Zou, H., & Liu, J. (2023). Dynamic adaptive engineering pathways for mitigating flood risks in shanghai with regret theory. *Nature Water*, *1*(2), 198–208.

van den Hurk, B., van Meijgaard, E., de Valk, P., van Heeringen, K.-J., & Gooijer, J. (2015). Analysis of a compounding surge and precipitation event in the netherlands. *Environmental Research Letters*, *10*(3), 035001.

Wahl, T., Jain, S., Bender, J., Meyers, S. D., & Luther, M. E. (2015). Increasing risk of compound flooding from storm surge and rainfall for major us cities. *Nature Climate Change*, *5*(12), 1093–1097.

Wang, J., Yi, S., Li, M., Wang, L., & Song, C. (2018). Effects of sea level rise, land subsidence, bathymetric change and typhoon tracks on storm flooding in the coastal areas of shanghai. *Science of the total environment*, *621*, 228–234.

Ward, P. J., Couasnon, A., Eilander, D., Haigh, I. D., Hendry, A., Muis, S., Veldkamp, T. I., Winsemius, H. C., & Wahl, T. (2018). Dependence between high sea-level and high river discharge increases flood hazard in global deltas and estuaries. *Environmental Research Letters*, *13*(8), 084012.

Wu, W., McInnes, K., O'grady, J., Hoeke, R., Leonard, M., & Westra, S. (2018). Mapping dependence between extreme rainfall and storm surge. *Journal of Geophysical Research: Oceans*, *123*(4), 2461–2474.

Wu, W., Westra, S., & Leonard, M. (2021). Estimating the probability of compound floods in estuarine regions. *Hydrology and Earth System Sciences*, *25*(5), 2821–2841.

Yi, X., Sheng, K., Wang, Y., & Wang, S. (2021). Can economic development alleviate storm surge disaster losses in coastal areas of china? *Marine Policy*, *129*, 104531.

Yin, J., Yu, D., Yin, Z., Liu, M., & He, Q. (2016). Evaluating the impact and risk of pluvial flash flood on intra-urban road network: A case study in the city center of shanghai, china. *Journal of hydrology*, *537*, 138–145.

Zellou, B., & Rahali, H. (2019). Assessment of the joint impact of extreme rainfall and storm surge on the risk of flooding in a coastal area. *Journal of Hydrology*, *569*, 647–665.

Zheng, F., Westra, S., Leonard, M., & Sisson, S. A. (2014). Modeling dependence between extreme rainfall and storm surge to estimate coastal flooding risk. *Water Resources Research*, *50*(3), 2050–2071.

Zheng, F., Westra, S., & Sisson, S. A. (2013). Quantifying the dependence between extreme rainfall and storm surge in the coastal zone. *Journal of Hydrology*, *505*(21), 172–187.

2

PERSPECTIVES ON COMPOUND FLOODING IN CHINESE ESTUARY REGIONS

This chapter explores how compound flooding affects the Chinese coastline. A comprehensive regional assessment of the compound flooding potential is currently missing due to the unavailability of water level records during typhoon events, small sample sizes of observations, and potential biases in the selection of rainfall gauges along the Chinese coast. Here, we analyzed 26 catchments along the Chinese coastline to identify areas at risk of compound flooding. Catchments with a significant statistical dependence between storm surge and rainfall are considered vulnerable. We propose a method using bivariate copulas to derive design values for flood protection systems that explicitly consider the dependence between flood drivers.

The results show that less than 40 % of the catchments (10 out of 26) are at risk of compound flooding, needing special attention when designing flood protection. Interestingly, some at-risk catchments are in northern China, not typically prone to typhoons. The findings have design implications. When explicitly considering the dependence between storm surge and rainfall, catchments in the south, exposed to typhoons, expect more severe rainfall than predicted based on annual maxima. In contrast, catchments in the north expect less severe rainfall. The actual impact of compound flooding depends on the geographical location and associated climate.

This chapter has been published as: Hanqing Xu, Elisa Ragno, Jinkai Tan, Alessandro Antonini, Jeremy D. Bricker, Sebastiaan N. Jonkman, Jun Wang. Perspectives on Compound Flooding in Chinese Estuary Regions. ***International Journal of Disaster Risk Science***, 2023: 14, 269-279.

2.1. INTRODUCTION

Around 70 % of the Chinese coastline is lower than 3 m above sea level (a.s.l.), making it extremely sensitive to coastal flooding (Shi et al., 2020). In estuary regions, the interactions of multiple flood drivers, such as local rainfall, wave effects, tidal amplitude, and surge-tide interactions can exacerbate the probability of flooding, causing great economic losses and casualties (Saleh et al., 2017; Vousdoukas et al., 2018). In the literature, flood events generated by the interaction between multiple physical drivers, which might not be extremes if considered in isolation, are referred to as compound flood events (Couasnon et al., 2020).

In China, high storm surges and extreme rainfall during the typhoon season are the major driving factors of flooding along the coast (Liu et al., 2022; Wu et al., 2021). Typhoons may produce strong onshore winds and an inverse barometric effect, which result in extreme surges, while simultaneously producing large quantities of rainfall over land, generating surface runoff. Moreover, high sea levels can prevent the normal discharge of surface runoff due to rainfall excesses, potentially leading to backwater effects along rivers and increasing the probability of compound flooding (Kossin, 2018; Ward et al., 2018).

China is one of the few countries in the world that are affected not only by tropical but also extra-tropical surges (Shi et al., 2015). Typhoon surges usually hit the South China Sea and the East China Sea coast with the characteristics of strong wind speeds, low atmospheric pressure, intense rainfall, large waves and storm surges, and thus strong destructive power (Day et al., 2018; Xiang et al., 2022). Many storms in the Yellow Sea and the Bohai Sea coast usually occur in the spring and autumn (W. Fang et al., 2016). For example, the combined effect of rainfall and storm tides during Typhoon Winnie (TC9711) in southeastern China killed 342 people and caused a direct economic loss of USD 4.3 billion (State Oceanic Administration, 1998). Also, severe flooding due to the combination of surge and rainfall during super typhoon Hato killed at least 12 people in Macau in 2017 (Wang et al., 2019). These examples emphasize the importance of studying the combination of surge and rainfall in estuaries and coastal regions (Wahl et al., 2015; Zheng et al., 2013) to avoid misrepresentations of the flood hazard and improve the resilience of coastal systems (Ghanbari et al., 2021; Wahl et al., 2015).

The relationship between rainfall and surge in estuary regions can have a substantial impact on coastal flood management, despite being challenging to detect from observations as the correlation between observed variables may not be significant (Bevacqua et al., 2020; Sadegh et al., 2018). Most of the available studies on compound flooding investigate locations in the United States and Europe, where tide gauges are densely distributed and provide more than 50 years of observed data (Bevacqua et al., 2017; Bevacqua et al., 2019). For example, Wahl et al. (2015) examined the dependence between precipitation and storm surge and reported an increase in compound flood risk during the past decades along the east coast of the United States. According to Zheng et al. (2013), precipitation and storm surge are significantly correlated in the coastal regions of Australia.

Although studies on compound coastal flooding in estuary locations across China are still scarce, recent work by J. Fang et al. (2021) showed that there is a positive dependence between rainfall and storm surge, especially during the typhoon season, calling

for a more in-depth investigation of compound flooding. The current studies have limitations, such as small sample sizes of observations, for example, the 23-year sample in J. Fang et al. (2021), and potential biases in the selection of rainfall gauges. The rainfall gauges selected are the ones closest to the tidal gauge without a check on whether the rainfall gauge falls within the drainage basin discharging into the sea and interacting with the tidal gauge (Zheng et al., 2013).

Hence, this study aimed to improve the current modelling of compound flooding in estuary regions along the Chinese coastline. This is done by analyzing longer records of rainfall (around 36 years) and carefully selecting the rainfall gauges to be representative of the inland water received by drainage basins discharging directly into the sea. Moreover, this study aimed to propose guidelines to derive design values for coastal infrastructure in relation to the season in which most of the pairs of surges and corresponding rainfall occur.

Specifically, we first developed a copula-based framework to model the dependence between surge and rainfall in this study, in which rainfall was used as a proxy of the amount of inland water discharged into the sea. Then, we implemented such a framework to derive information on expected rainfall as a function of the magnitude of the surge event in cases where the interaction between surge and rainfall cannot be neglected, that is, where a statistically significant correlation exists. Finally, we discuss the implication of this approach for reducing the risk of urban pluvial flooding and increasing urban flood resilience in the season in which most of the surge peaks in a specific estuary region occur. The structure of this chapter is structured as follows. Section 2.2 provides details of the dataset and study region. Section 2.3 presents the copula-based framework. Section 2.4 contains the results of the analysis. Section 2.5 discusses the advantages and limitations of this work. Finally, Section 2.6 provides a summary of the study.

2.2. DATA AND STUDY AREA

In this study, we are interested in estuary regions along the Chinese coast and prone to compound flooding generated by the interaction between rainfall and storm surge. For this reason, the following datasets are selected:

1) Catchment Shapefiles. HydroSHEDS database developed by the WWF-US (Figure 2.1) (Lehner et al., 2006) to retrieve catchment boundaries.

2) Rainfall. Daily rainfall (24h cumulative rainfall) time series gauges managed by the China Meteorological Administration (CMA) and covering the period between 1979 and 2014.

3) Storm surge. Surge reanalysis data from the Global Tide and Surge Reanalysis (GTSR, https://data.4tu.nl/) dataset. The GTSR dataset is the first global reanalysis dataset of surges and extreme sea levels, and it is based on hydrodynamic modelling (Muis et al., 2016). The GTSR covers the entire world's coastline and provides a near-coast time series of surges and tides from the Dynamic Interactive Vulnerability Assessment model from 1979 to 2014. The surge is simulated by forcing the global tide and surge model with wind and pressure fields from ERA-Interim. Numerical simulations were carried out at a 10-minute temporal resolution. Regarding the application of GTSR/Era-Interim for surge during typhoon season, the GTSR produced sufficient surge results and is widely used in

the East Asian region (Mori et al., 2019)

2.2.1. CATCHMENT SELECTION AND DESCRIPTION

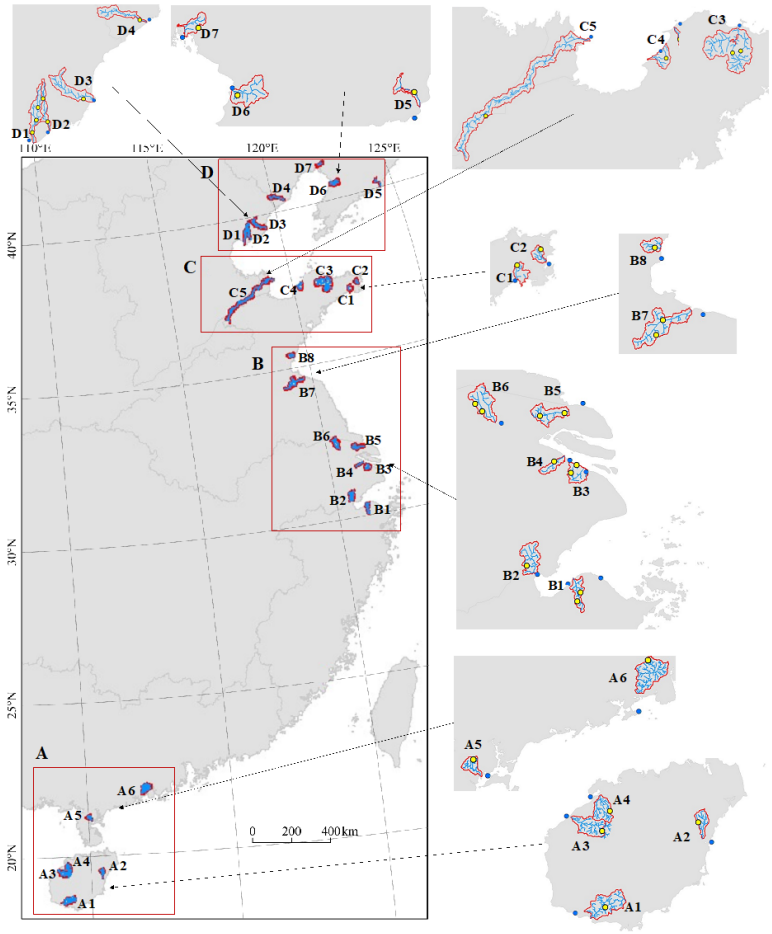

Figure 2.1: Location and area of 26 catchments along the Chinese coastline (blue dots represent tide gauges and yellow dots represent rainfall gauges). Label A refers to the region in southern China with a latitude of lower than 21.5 °*C*. Catchments labelled as B are located on the eastern coast of China, with latitudes ranging from 30 to 37 °*C*. Catchments labelled as C are located to the south of the Bohai Sea, with latitudes ranging from 37 to 38 °*C*. Finally, catchments labelled as D are located in northern China, with latitudes higher than 38 °*C*.

Since we are interested in estuary regions along the Chinese coast prone to coastal flooding, we need to select estuary locations for which catchment information, surge, and rainfall data are available. Hence, we simultaneously looked at the relative locations of catchment boundaries, rainfall gauges, and surge data. Then, we selected catchments discharging directly into the sea for which at least one rain gauge within the catchment

boundary and one surge station in the vicinity of the catchment outlet could be found. Following this approach, we identified 26 hydrological catchments across the entire Chinese coastline (Figure 2.1).

The selected catchments across the coastline have lengths up to 100 km and areas of up to 1000 km^2, except catchment C5 which has a length of 224 km and an area of 2876 km^2 (Figure 2.2(a) and Figure 2.2(b)). China's coastline covers approximately 14,500 km and a range of climates. The average annual temperature in the catchments ranges from 10.3 °C (north) up to 24.8 °C (south), Figure 2.2(c). Figure 2.2(d) shows that annual rainfall across the 26 catchments ranges from 575.6 mm (north) up to 2183.5 mm (south). For those catchments containing more than one rainfall gauge (8 among the 26 selected), the weighted average of the station rainfall was considered. The weight was estimated based on the distance to the catchment outlet. More specifically, the closest gauge has the highest weight. A small variability between rainfall peaks of stations in the same catchments is observed.

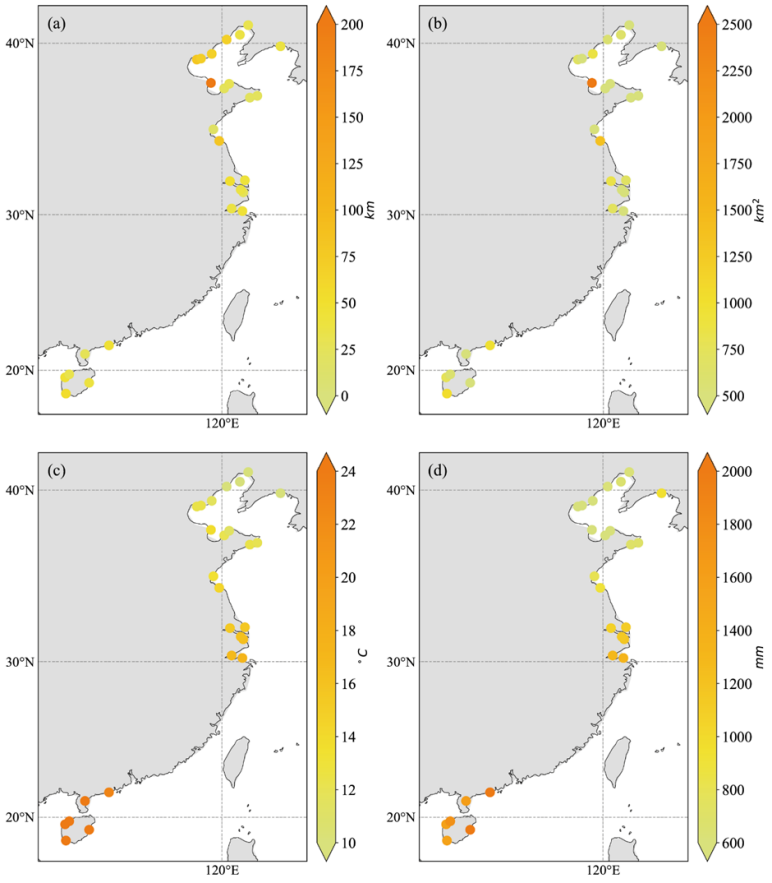

Figure 2.2: Catchments investigated in this study. (a) Catchment length; (b) Catchment area; (c) Annual mean temperature; (d) Annual mean rainfall.

2.2.2. PAIRS OF SURGES AND RAINFALL

To develop the copula-based framework, we constructed a dataset of pairs of surge peaks and corresponding rainfall potentially leading to compound flooding. First, we sampled surge peaks from the daily surge reanalysis data following the peak-over-threshold approach. To ensure independence between peaks, only peaks spaced at least three days apart were considered (Feng et al., 2018). Then, we ran a preliminary analysis on the correlation between surge peaks and accumulated rainfall over a window of time ranging from the day of the occurrence of the peak to seven days before it to investigate the lead time in the response of the catchments to a rainfall event. Based on this analysis, we selected the daily rainfall recorded on the day of the occurrence of the surge peak as the rainfall event, since this combination of surge peak and corresponding rainfall gives the highest correlation for most of the catchments. These pairs of surge and corresponding rainfall were then used to determine a copula-based framework for compound flooding.

2.3. METHODS

A copula-based framework was used to model the dependence between flood drivers. To quantify the probability of the compound hazard generated by the interaction between surge and rainfall, we first evaluated the marginal distributions of surge peaks and corresponding rainfall. Then, we selected a copula function to evaluate the probability of compound flooding. Finally, we estimated design values of surge and rainfall via conditional probability.

2.3.1. PEAKS OVER A HIGH THRESHOLD

We select surge peaks following the Peak Over Threshold (POT) approach. According to Coles et al. (2001) and Pickands III (1975), given a random variable X, the excess is $X_e x = x - u$, defined above a large enough threshold u. To ensure the independence of the excesses, a declustering technique was also implemented to ensure the independence of excesses (Antonini et al., 2018). The threshold u was selected based on the empirical mean residual life (MRL) and dispersion index (DI). The MRL provides a visual diagnostic tool to select the threshold u in which the average mean of $X_e x$ is plotted as a function of u. A suitable u was selected where the plot is approximately linear. On the other hand, the DI, being the ratio between the variance and the mean of the yearly occurrence of the peaks, was used to check whether the peaks above a given threshold u are independent and follow a Poisson distribution. The combination of MRL and DI can indicate a suitable u.

2.3.2. COPULA MODEL

Copula functions have gained popularity in hydrological studies following the work of De Michele and Salvadori (2003). The advantage of copula functions is their ability to model the dependence between two (or more) random variables independently of their marginal distributions (Sklar, 1973). Specifically, given two random variables X and Y with continuous marginal distributions $F(x)$ and $G(y)$, the joint distribution of X and Y is given by

$$F(x,y) = C[F(x), G(y)] = \mathrm{C}(u,v) \tag{2.1}$$

where C is the copula function and $u = F(x)$ and $v = G(y)$ are uniform margins.

In this study, we restricted our analysis to the most used copulas, namely Gaussian, Clayton, Frank, and Gumbel, as the candidate functions for modelling the joint probability distributions of compound events. This is because they are all one-parameter copulas that can cover different types of dependence behaviour, that is, symmetry in the data (Gaussian and Frank copulas) or greater association between variables at the tails, that is, Clayton can capture lower tail dependence and Gumbel upper tail dependence. Moreover, when the sample size of investigated pairs is small, more complex copulas might not provide any advantage. The parameters of each copula function were estimated based on the maximum likelihood estimation (MLE) method (Haseeb and Haqqi, 2013). To select the copula that best fits the data, the following metrics were considered: the Akaike information criterion (AIC), Bayesian information criterion (BIC), and root mean square error (RMSE).

The AIC and BIC are defined as follows:

$$AIC = -2L(\bar{\vartheta}|\ y) + 2K \tag{2.2}$$

$$BIC = -2L(\bar{\vartheta}|\ y)\ +\ Kln(n) \tag{2.3}$$

where K is the number of estimated parameters in the model including the intercept and $L(\theta|y)$ is the log-likelihood at its maximum point of the estimated model; n is the sample size. The smaller the AIC and BIC are, the better the fit (Burnham and Anderson, 2004).

The RMSE is defined as:

$$RMSE = \sqrt{\frac{1}{n}\sum_{i=1}^{n}\left(C_C\left(u_i,\ v_i\right) - C_n\left(u_i,\ v_i\right)\right)^2} \tag{2.4}$$

where n is the number of pairs (u,v); C_C is the theoretical copula, and C_n is the empirical copula. A low RMSE value indicates that the simulated and observed data are close to each other, showing better accuracy.

2.3.3. INFERRING DESIGN VALUES VIA CONDITIONAL PROBABILITY

A probabilistic dependence model, like the copula function, can be used to infer a design value based on the probability of occurrence of the event of interest. When dealing with dependent variables, the (statistical) occurrence of an event, for example, a flood event is defined as the occurrence of its physical drivers, that is, X and Y (or U and V in the copula domain).

In the bivariate case, the probability of occurrence of the flood event of interest depends on whether both the physical drivers exceed their respective thresholds u_d and v_d (AND scenario, Eq. (2.5)) or whether either one or both physical drivers exceed their respective thresholds (OR scenario, Eq. (2.6)) (Salvadori and De Michele, 2004). The "AND"

scenario is frequently employed in the studies of compound flooding, as flooding is often caused by a combination of excessive runoff and high sea levels, rather than by either factor alone.

$$P((U > u_d) \cap (V > v_d)) = 1 - u_d - v_d + C(u_d, v_d) \tag{2.5}$$

$$P((U > u_d) \cup (V > v_d)) = 1 + C(u_d, v_d) \tag{2.6}$$

For a fixed probability of exceedance, or return period, the pair of variables (u_d, v_d) can be inferred following the "most-likely" method, which selects the pair with the highest density, hence the method's name.

However, in some cases, one of the two physical drivers is the most important from a design perspective. For example, higher storm surges, which determine hydraulic loads on coastal and offshore structures, often result from intense typhoons in southeastern China. Higher sea water level reduces the discharge capabilities of inland drainage systems, potentially causing pluvial flooding. In such a case, a dependent model can be used to infer the design value of one physical driver, for example, rainfall, when the other one, for example, storm surge, is fixed via conditional probability.

$$P(V > v \mid U = u_d) = 1 - \frac{\partial C(u, v)}{\partial u} \tag{2.7}$$

2.4. RESULTS

In this section, we examine the dependence between extreme surges and corresponding rainfall events in 26 catchments along the Chinese coastline to identify where the two drivers more often occur together. Our analysis revealed a significant correlation between surge and rainfall in 10 catchments, primarily located in southern and northern China. Then, we implement a copula framework to model the observed dependence and examine changes in the probability of rainfall when conditioned on the specific value of storm surge.

2.4.1. PEAKS SELECTION AND DEPENDENCE QUANTIFICATION

We selected surge peaks greater than the thresholds u based on the MRL and DI plots. The thresholds (0.33-1.39 m) in all the catchments range between the $99_t h$ and $99.4_t h$ percentile of observed surges. The threshold u around Hainan Island is generally lower than other stations because the western side of Hainan Island (South China), and the mainland across the strait, are sheltered by Hainan Island itself, reducing the surge (Zhang et al., 2017). In addition, the eastern side of Hainan Island has a narrower continental shelf than the rest of the Chinese coast. Surge is proportional to the width of the continental shelf over which the wind blows. In general, a narrow continental shelf results in a smaller surge than a wider shelf. The highest threshold obtained is around Shanghai, at 1.3 m. A declustering time of three days is considered by Feng et al. (2018) to ensure independence between events selected. In the end, we obtained an average of 53 excesses in the 26 catchments over 36 years. The average amount of peaks/pairs is 1.5 per year for all catchments. The maximum number of peaks/pairs is located in Catchment

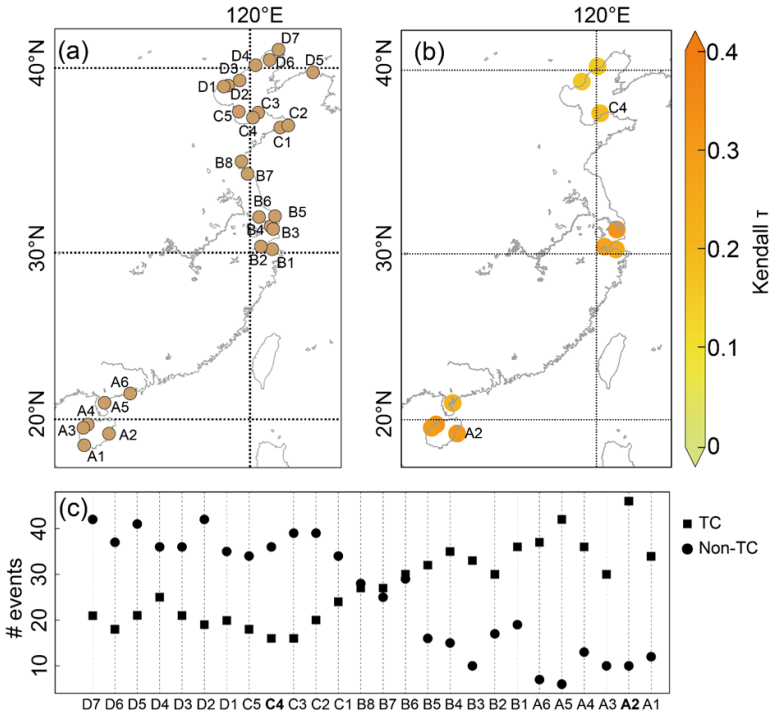

Figure 2.3: (a) Catchments investigated; (b) Catchments in which a significant dependence between extreme surge and rainfall was detected; (c) The occurrence of compound events in the typhoon season and the non-typhoon season. The catchments A2, A3, A4, A5, B1, B2, B3, C4, D3, and D4 exhibit significant correlations between extreme surge and rainfall. The levels of significance of both models emphasize the importance of events during the typhoon season (TC, black square) and the non-typhoon season (Non-TC, black circle). Among these catchments, the bold labels (A2 and C4) indicate those selected for further analysis. Catchment A2 was selected due to the highest occurrence of compound events and significant dependency during the typhoon season. Conversely, catchment C4 exhibits the strongest correlation during non-typhoon season although the number of compound events is not the largest.

D7 and the minimum number of peaks/pairs is in Catchment A3. For each excess, we selected the total daily rainfall recorded on the same day to form pairs of surges and rainfall. We quantified the dependence between entire excess pairs of surge peak and rainfall via Kendall's rank correlation coefficient τ significance test (Hauke and Kossowski, 2011) (Figure 2.3(a)). We detected a significant correlation (with a level of significance $\alpha = 0.05$) in 10 of the 26 catchments analyzed, especially in southern China (Figure 2.3(b)). Catchments A2, A3, A4, A5 (south), B1, B2, B3 (center), C4, D3 and D4 (north) show a significant correlation between surge and rainfall (with a level of significance $\alpha = 0.05$). Eastern Hainan Island (catchment A2) shows the highest correlation ($\tau = 0.35$). This is reasonable since Hainan Island is highly affected by typhoons and this implies that extreme surge conditions are often accompanied by high rainfall during typhoon events. We also find statistical dependence between rainfall and surge in three catchments around the Bohai Sea (C4, D3, and D4 gauges, Figure 2.3(b)). Northern China is affected by extra-tropical

Table 2.1: Performance measures of the estimated Copula functions.

Catchments	Copula type	Max-likelihood	AIC	BIC	RMSE
A2	Gaussian	214.8	427.6	425.6	0.1615
	Clayton	192.7	383.4	381.4	0.2395
	Frank	223.5	445.1	443.1	0.1381
	Gumbel	217.5	433.1	431.1	0.1537
C4	Gaussian	202.5	403.1	401.1	0.1468
	Clayton	196.3	390.6	388.6	0.1654
	Frank	206.3	410.6	408.6	0.1365
	Gumbel	210.5	419.1	417.1	0.1258

storms outside the typhoon season (mainly in the late winter and early spring), which can often cause flooding and damage.

To better understand the influence of seasonality, we count the number of events in the typhoon season (July to October) and the non-typhoon season (November to June of the following year) separately. Figure 2.3(c) shows the number of compound events in the typhoon season and the non-typhoon season. After an analysis of the surge peak events, we found that in the south, most of the compound events occur in the typhoon season while in the north, most of the compound events occur during the non-typhoon season.

2.4.2. SELECTING THE COPULA MODEL

To further analyze the dependence between surge and rainfall and the implication of such dependence on infrastructure design, we focus the following analysis on two locations: Hainan Island (catchment A2) and the Bohai Sea (catchment C4). These locations show positive and significant correlations between storm surge and rainfall. However, in catchment A2 (τ =0.35) the highest number of surge peaks (46) are observed during typhoon season, while in catchment C4 (τ = 0.24) the highest number of surge peaks are observed during the non-typhoon season (36). Based on the results in terms of AIC, BIC, and RMSE (Table 2.1), the copulas that best fit the observations are Frank for catchment A2 and Gumbel for catchment C4. Here, empirical margins are assumed.

Following the most-likely approach and based on the "AND" hazard scenario, that is, both rainfall and surge should be above their respective thresholds, Figure 2.4 shows the pairs of surge and rainfall corresponding to return periods of 50, 100 and 200-yr. The design events (yellow squares in Figure 2.4) are given by the point of maximum relative probability density (most likely method) on the isoline associated with a fixed return period. The processes of simulating samples from the fitted copulas, estimating the relative likelihood along the isolines, and extracting the most likely event, were then repeated to determine the three design events associated with the 50, 100 and 200-yr return periods. The most extreme observed compound event with rainfall of 123.8 mm and a surge peak of 1.4 m (close to 200-yr return period) in Figure 2.4(b) was during typhoon Meari (June 2011). This typhoon caused floods in 17 counties of three provinces on the east coast of China.

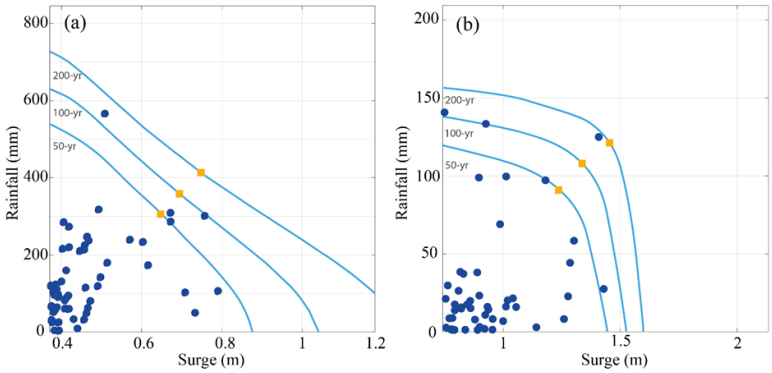

Figure 2.4: Isolines of extreme paired data based on the Frank and Gumbel copulas. (a) Catchment A2; (b) Catchment C4. The yellow squares show the design values under different joint return periods between the extreme surge and rainfall using the most-likely method.

2.4.3. CONDITIONAL DESIGN VALUE OF RAINFALL

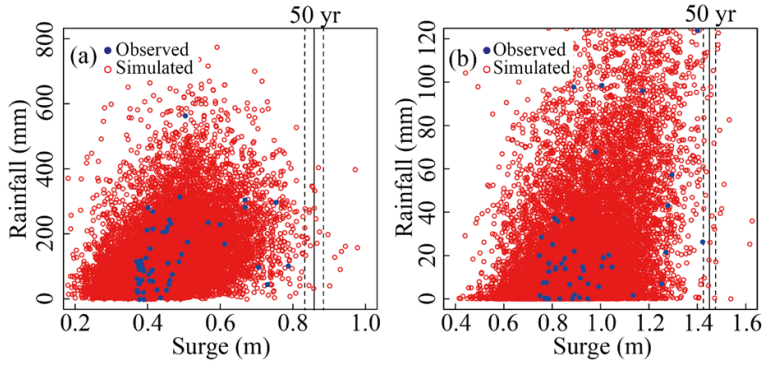

Figure 2.5: Simulated surges and rainfall under the joint copula model. (a) Catchment A2; (b) Catchment C4. The vertical solid line represents the value of the surge at 50 year return period, while the dashed lines represent the range percentiles beside the solid line.

In coastal areas, coastal flooding is driven by sea water level, which depends on both storm surge and astronomical tide. However, sea level might also affect pluvial flooding, since high sea level might prevent inland water discharge by gravity. Hence, we used the dependence model obtained above to assess changes in rainfall probability distribution when information about storm surge is known in relation to the probability distribution of annual maximum rainfall.

From the dependence model (Frank copula for catchment A2 and Gumbel copula for catchment C4) we randomly sampled 10,000 dependent surge and rainfall pairs (red dots in Figure 2.5). Then, we selected pairs for which the surge level is close to the 50 year return period event in the univariate case, that is, 0.86 m (0.835-0.885 m) for catchment A2 and 1.45 m (1.425-1.475 m) for catchment C4 (Figure 2.5), to obtain the distribution

of rainfall conditioned on the 50 year return period surge event.

Figure 2.6(a) shows that for catchment A2 (eastern Hainan Island, South China), where the majority of surge peaks occurred during typhoon season, we observe a shift in the rainfall median when rainfall is conditioned on storm surge. Specifically, the median of the rainfall condition on the 50-yr return period storm event (258.76 mm/day) is about 40.8% higher than the median of annual maxima rainfall (183.69 mm/day). This result implies that extreme rainfall events during typhoon season are generally more intense compared to most annual maxima events, requiring extra attention when developing a flood protection intervention. For catchment C4 (the Bohai Sea, North China), where the majority of surge peaks occurred outside the typhoon season, we observe the opposite behavior: the median rainfall event conditioned on the 50-yr return period surge event (49.43 mm/day) is smaller than the median of the annual maxima rainfall event (88.15 mm/day).

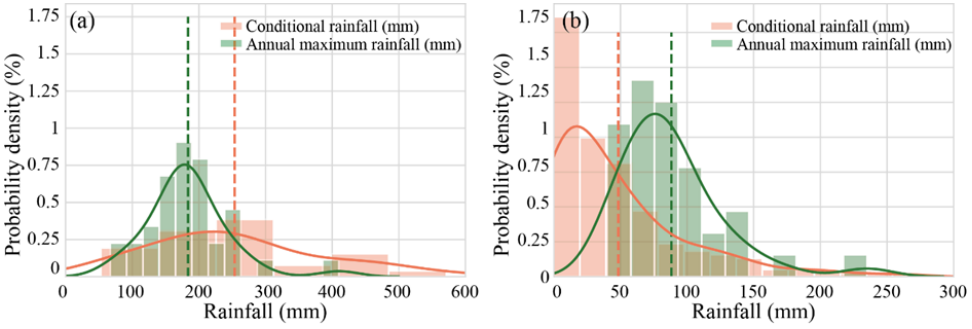

Figure 2.6: Comparison of annual maximum rainfall and conditional rainfall at A2 (a) and C4 (b) locations with all the pairs; dashed vertical lines are the median value of rainfall.

2.5. DISCUSSION

Highly urbanized centers such as Chinese coastal cities are prone to flooding from the combined occurrence of surge peaks and high rainfall events. Hence, we investigated the degree of dependence between surge peaks and corresponding rainfall events and its implication in terms of infrastructure design accounting for the seasonality of the surge peak occurrence.

Even though the GTSR dataset used in this study might underestimate surges during typhoon events (Muis et al., 2017; Muis et al., 2016), other studies proved that the use of the GTSR dataset in East Asia is possible and the results are plausible (Mori et al., 2019). Moreover, we showed that a probabilistic framework for modelling the dependence between environmental variables, such as the copula-based framework proposed here, can provide valuable inputs to propose risk reduction strategies against floods. Specifically, we found that around eastern Hainan Island, where the potential for compound flooding is the highest during typhoon season, surge events are associated with more severe rainfall events. For example, the intensity of rainfall events is about 40.8% higher than the median of annual maxima rainfall (Sun et al., 2021). We also found that in the Bo-

hai Sea area where the majority of extreme events occur during the extra-tropical storm season, the intensity of rainfall events associated with extreme surge conditions has a median value smaller than the median of annual maxima events (88 mm/day). This implies that the severity of the expected rainfall event in case of a storm surge peak is smaller compared to the expected severity inferred from the probability distribution of annual maxima precipitation.

From a design perspective, such a result calls for a more in-depth and case-specific understanding of the interaction between surge and rainfall and an evaluation of which strategy (dependent model versus independent model) for assessing design values is the most appropriate to avoid under-preparedness. For example, the sensitivity of the river to backwater effects can lead to pluvial flooding even for moderate rainfall events hence additional flood protection measures along riverbanks or within the city should be considered. Moreover, the implementation of rainwater storage and hydrograph peak reduction facilities (that is, detention basins) can strengthen the coastal flood protection system's capabilities and enhance the safety of the city (Ke et al., 2018; Najafi et al., 2021), especially when it is expected that surges are associated with higher than expected rainfall, such as along the southern coast of China. It is important, however, to consider that effective water discharges are influenced by several hydrological factors, including topography, land use, soil type, and vegetation cover and neglecting such factors might lead to a misrepresentation of flood risk. More in-depth and case-specific investigations can, for example, be performed via hydrodynamic models that explicitly simulate the interaction between rainfall events and surge conditions.

2.6. CONCLUSIONS

In this study, we proposed a copula-based framework to quantify flood hazards in coastal regions that are exposed to the combination of storm surge and pluvial flooding. This can provide insights into adaptation strategies that account for coastal and pluvial flooding protection infrastructure. We observed that in southern China the highest number of extreme surge events occur during typhoon seasons, while in the northern part of the country, the majority of the surge peaks occur during the non-typhoon season. This is expected because typhoons largely affect the southern region.

Our main results are that: (1) There is a positive and significant correlation between surge peaks and rainfall in 10 of the 26 catchments investigated; (2) The probability of rainfall conditional on a specific surge event can provide valuable information for the design of flood protection systems in estuary regions; (3) In southern China (Hainan Island), extreme rainfall events during the typhoon season are generally more intense compared to most annual maxima events. The framework developed in this study can be applied to other coastal cities or regions in East and Southeast Asia and around the world.

One of the main limitations of this study is the relatively small number of tide gauge sites and the 36 years of data available, especially during typhoons. There is an urgent need for longer datasets to be used in order to better assess compound flood risk, especially for southeastern China coasts, which are prone to typhoons. Therefore, monitoring and prediction of rainfall, storm surge, and sea level rise should be an important component of the development of future adaptation and flood management.

BIBLIOGRAPHY

Antonini, A., Raby, A., Caputo, P., Brownjohn, J., Papas, A., & D'Ayala, D. (2018). Survivability assessment of fastnet lighthouse. *Coastal Engineering Proceedings*, (36), 46–46.

Bevacqua, E., Maraun, D., Hobæk Haff, I., Widmann, M., & Vrac, M. (2017). Multivariate statistical modelling of compound events via pair-copula constructions: Analysis of floods in ravenna (italy). *Hydrology and Earth System Sciences*, *21*(6), 2701–2723.

Bevacqua, E., Maraun, D., Vousdoukas, M., Voukouvalas, E., Vrac, M., Mentaschi, L., & Widmann, M. (2019). Higher probability of compound flooding from precipitation and storm surge in europe under anthropogenic climate change. *Science advances*, *5*(9), eaaw5531.

Bevacqua, E., Vousdoukas, M. I., Shepherd, T. G., & Vrac, M. (2020). Brief communication: The role of using precipitation or river discharge data when assessing global coastal compound flooding. *Natural Hazards and Earth System Sciences*, *20*(6), 1765–1782.

Burnham, K. P., & Anderson, D. R. (2004). Multimodel inference: Understanding aic and bic in model selection. *Sociological methods & research*, *33*(2), 261–304.

Coles, S., Bawa, J., Trenner, L., & Dorazio, P. (2001). *An introduction to statistical modeling of extreme values* (Vol. 208). Springer.

Couasnon, A., Eilander, D., Muis, S., Veldkamp, T. I., Haigh, I. D., Wahl, T., Winsemius, H. C., & Ward, P. J. (2020). Measuring compound flood potential from river discharge and storm surge extremes at the global scale. *Natural Hazards and Earth System Sciences*, *20*(2), 489–504.

Day, J. A., Fung, I., & Liu, W. (2018). Changing character of rainfall in eastern china, 1951–2007. *Proceedings of the National Academy of Sciences*, *115*(9), 2016–2021.

De Michele, C., & Salvadori, G. (2003). A generalized pareto intensity-duration model of storm rainfall exploiting 2-copulas. *Journal of Geophysical Research: Atmospheres*, *108*(D2).

Fang, J., Wahl, T., Fang, J., Sun, X., Kong, F., & Liu, M. (2021). Compound flood potential from storm surge and heavy precipitation in coastal china: Dependence, drivers, and impacts. *Hydrology and Earth System Sciences*, *25*(8), 4403–4416.

Fang, W., Zhong, X., & Shi, X. (2016). Typhoon disasters in china. *Natural disasters in China*, 103–131.

Feng, J., Li, D., Li, Y., Liu, Q., & Wang, A. (2018). Storm surge variation along the coast of the bohai sea. *Scientific reports*, *8*(1), 11309.

Ghanbari, M., Arabi, M., Kao, S.-C., Obeysekera, J., & Sweet, W. (2021). Climate change and changes in compound coastal-riverine flooding hazard along the us coasts. *Earth's Future*, *9*(5), e2021EF002055.

Haseeb, A., & Haqqi, T. M. (2013). Immunopathogenesis of osteoarthritis. *Clinical immunology*, *146*(3), 185–196.

Hauke, J., & Kossowski, T. (2011). Comparison of values of pearson's and spearman's correlation coefficients on the same sets of data. *Quaestiones geographicae*, *30*(2), 87–93.

Ke, Q., Jonkman, S. N., Van Gelder, P. H., & Bricker, J. D. (2018). Frequency analysis of storm-surge-induced flooding for the huangpu river in shanghai, china. *Journal of Marine Science and Engineering*, *6*(2), 70.

Kossin, J. P. (2018). A global slowdown of tropical-cyclone translation speed. *Nature*, *558*(7708), 104–107.

Lehner, B., Verdin, K., & Jarvis, A. (2006). Technical documentation version 1.0. *USGS Earth Resources Observation and Science: Sioux Falls, SD, USA*.

Liu, Q., Xu, H., & Wang, J. (2022). Assessing tropical cyclone compound flood risk using hydrodynamic modelling: A case study in haikou city, china. *Natural Hazards and Earth System Sciences*, *22*(2), 665–675.

Mori, N., Shimura, T., Yoshida, K., Mizuta, R., Okada, Y., Fujita, M., Khujanazarov, T., & Nakakita, E. (2019). Future changes in extreme storm surges based on mega-ensemble projection using 60-km resolution atmospheric global circulation model. *Coastal Engineering Journal*, *61*(3), 295–307.

Muis, S., Verlaan, M., Nicholls, R. J., Brown, S., Hinkel, J., Lincke, D., Vafeidis, A. T., Scussolini, P., Winsemius, H. C., & Ward, P. J. (2017). A comparison of two global datasets of extreme sea levels and resulting flood exposure. *Earth's Future*, *5*(4), 379–392.

Muis, S., Verlaan, M., Winsemius, H. C., Aerts, J. C., & Ward, P. J. (2016). A global reanalysis of storm surges and extreme sea levels. *Nature communications*, *7*(1), 11969.

Najafi, M. R., Zhang, Y., & Martyn, N. (2021). A flood risk assessment framework for interdependent infrastructure systems in coastal environments. *Sustainable Cities and Society*, *64*, 102516.

Pickands III, J. (1975). Statistical inference using extreme order statistics. *the Annals of Statistics*, 119–131.

Sadegh, M., Moftakhari, H., Gupta, H. V., Ragno, E., Mazdiyasni, O., Sanders, B., Matthew, R., & AghaKouchak, A. (2018). Multihazard scenarios for analysis of compound extreme events. *Geophysical Research Letters*, *45*(11), 5470–5480.

Saleh, F., Ramaswamy, V., Wang, Y., Georgas, N., Blumberg, A., & Pullen, J. (2017). A multi-scale ensemble-based framework for forecasting compound coastal-riverine flooding: The hackensack-passaic watershed and newark bay. *Advances in Water Resources*, *110*, 371–386.

Salvadori, G., & De Michele, C. (2004). Frequency analysis via copulas: Theoretical aspects and applications to hydrological events. *Water resources research*, *40*(12), W12511.

Shi, X., Han, Z., Fang, J., Tan, J., Guo, Z., & Sun, Z. (2020). Assessment and zonation of storm surge hazards in the coastal areas of china. *Natural Hazards*, *100*, 39–48.

Shi, X., Liu, S., Yang, S., Liu, Q., Tan, J., & Guo, Z. (2015). Spatial–temporal distribution of storm surge damage in the coastal areas of china. *Natural Hazards*, *79*(1), 237–247.

Sklar, A. (1973). Random variables, joint distribution functions, and copulas. *Kybernetika*, *9*(6), 449–460.

State Oceanic Administration. (1998). *State oceanic administration bulletin of oceanic disaster of china in 1997*. China Ocean Press.

Sun, X., Li, R., Shan, X., Xu, H., & Wang, J. (2021). Assessment of climate change impacts and urban flood management schemes in central shanghai. *International Journal of Disaster Risk Reduction*, *65*, 102563.

Vousdoukas, M. I., Mentaschi, L., Voukouvalas, E., Bianchi, A., Dottori, F., & Feyen, L. (2018). Climatic and socioeconomic controls of future coastal flood risk in europe. *Nature Climate Change*, *8*(9), 776–780.

Wahl, T., Jain, S., Bender, J., Meyers, S. D., & Luther, M. E. (2015). Increasing risk of compound flooding from storm surge and rainfall for major us cities. *Nature Climate Change*, *5*(12), 1093–1097.

Wang, Q., Xu, Y., Wei, N., Wang, S., & Hu, H. (2019). Forecast and service performance on rapidly intensification process of typhoons rammasun (2014) and hato (2017). *Tropical Cyclone Research and Review*, *8*(1), 18–26.

Ward, P. J., Couasnon, A., Eilander, D., Haigh, I. D., Hendry, A., Muis, S., Veldkamp, T. I., Winsemius, H. C., & Wahl, T. (2018). Dependence between high sea-level and high river discharge increases flood hazard in global deltas and estuaries. *Environmental Research Letters*, *13*(8), 084012.

Wu, W., Westra, S., & Leonard, M. (2021). Estimating the probability of compound floods in estuarine regions. *Hydrology and Earth System Sciences*, *25*(5), 2821–2841.

Xiang, C., Wu, L., & Qin, N. (2022). Characteristics of extreme rainfall and rainbands evolution of super typhoon lekima (2019) during its landfall. *Frontiers of Earth Science*, *16*, 64–74.

Zhang, H., Cheng, W., Qiu, X., Feng, X., & Gong, W. (2017). Tide-surge interaction along the east coast of the leizhou peninsula, south china sea. *Continental Shelf Research*, *142*, 32–49.

Zheng, F., Westra, S., & Sisson, S. A. (2013). Quantifying the dependence between extreme rainfall and storm surge in the coastal zone. *Journal of Hydrology*, *505*(21), 172–187.

3

COMPOUND FLOOD IMPACT OF WATER LEVEL AND RAINFALL DURING TYPHOON PERIOD IN COASTAL MEGACITY

This chapter explores the physical factors driving compound floods in Shanghai under a changing climate when data are limited. In this study, we utilized the D-Flow Flexible Mesh model to generate synthetic data on seawater levels in Shanghai from 1961 to 2018. The simulation incorporated storm surge, astronomical tide, and relative sea level rise (RSLR). Subsequently, a copula-based methodology was applied to quantify the joint probability between peak water level and rainfall during historical typhoons.

The results show that in Shanghai the probability of extreme flooding events increases due to a 0.55 m rise in Relative Sea Level Rise (RSLR) from 1961 to 2018. Analysis using copula functions reveals a notable shift in the joint distribution of peak water level and rainfall during Tropical Cyclones (TCs) due to RSLR. Seven potential compound flood events have been identified, wherein astronomic tide typically serves as the primary driver, with storm surge acting as a supplementary factor in one instance. The combined influences of astronomic tide, storm surge, and RSLR collectively contribute to peak water levels, underscoring the necessity of considering all these factors during the typhoon season.

This chapter has been published as: Hanqing Xu, Zhan Tian, Laixiang Sun, Elisa Ragno, Jeremy D. Bricker, Ganquan Mao, Qinghua Ye, Jinkai Tan, Jun Wang, Qian Ke, Shuai Wang, Ralf Toumi. Compound flood impact of water level and rainfall during tropical cyclone period in a coastal city: The case of Shanghai. ***Natural Hazards and Earth System Sciences***. 2022: 22 (7), 2347-2358.

3.1. INTRODUCTION

Compound flooding is generated when two or more flood drivers, e.g., water level, rainfall, and high river discharges, occur simultaneously or in close succession. Such flood drivers can amplify each other and lead to greater impacts than when they occur in isolation (Chao et al., 2021; Leonard et al., 2014; Visser-Quinn et al., 2019; Zscheischler et al., 2018). Coastal cities like Shanghai are particularly prone to compound flooding associated with tropical cyclones (TCs), which often bring heavy rainfall and storm surges. For a more accurate assessment of compound floods in the coastal regions, a thorough understanding of the interdependence between multiple flood drivers is necessary. In other words, an enriched knowledge about the dynamic interaction between flood drivers would significantly improve the quantification of compound flooding risks in estuarine environments (Feng and Beighley, 2020). As such, the joint probability theory has been incorporated into the analysis of compound flood risk to take advantage of Sklar's Theorem (M. Sklar, 1959). According to Sklar's Theorem, any multivariate joint cumulative distribution function can be expressed in terms of univariate marginal distribution functions and a copula that describes the structure of dependency between the variables (Bevacqua et al., 2019).

Coastal regions are usually the most densely populated and economically developed areas of a country, and they are also the most vulnerable regions to the risk of compound flooding from heavy rainfall and extreme storm surge due to this large population and property density (Neumann et al., 2015). Shanghai is the largest and most developed coastal megacity in China. Rainstorms and storm surges caused by typhoons from June to October often cause substantial losses (W. Li et al., 2018). For example, extreme storm flooding caused nearly 30 thousand casualties in 1905 (M. Li et al., 2018). In 1962, storm flooding inundated half of the downtown region for nearly 10 days due to 46 failures along the floodwalls of the Huangpu River and its branches and led to huge losses of 1/6 of the local Gross Domestic Product (GDP) in Shanghai (Ke, 2014). In 1997, Typhoon Winnie killed seven people and flooded more than 5,000 households due to the extreme storm surge and rainfall (Ke et al., 2021). Although the construction of flood control measures in the past 50 years (especially after typhoon Winnie in 1997) has effectively reduced the risk of storm surge and rainstorm floods, Typhoon Matsa in 2005 (US $2.23 billion damage), Typhoon Fitow in 2013 (US $10.4 billion damage), and Typhoon Lekima in 2019 (US $2.55 billion damage) also brought significant damage to Shanghai (Du et al., 2020). Given the substantial damage caused by compound flooding, comparing the encounters of rainfall and storm surges during typhoon season is urgent in order to understand the driving mechanisms and frequency of compound flooding in Shanghai. However, owing to the unavailability of water level records, there is little research that has been able to estimate the dependency between peak water level and accumulated rainfall during historical TCs.

The copula method is widely used in statistics to model the interdependence between two or more variables (Anandalekshmi et al., 2019; Balistrocchi et al., 2019). Recent research using the copula model emphasizes the importance of studying the combined effects of rainfall and water level processes in estuaries and coastal regions (Wahl et al., 2015; Zellou and Rahali, 2019). For example, Xu et al. (2018) showed the existence of some positive dependences between rainfall and water level in the coastal city

of Hainan Island, while the water level poses an additional risk of flooding. The study Xu et al. (2018) confirmed that the copula method is a promising tool for studying multivariate problems in hydrology and coastal engineering. However, when applying the copula-based methods to 3 dimensions, controversies arise and uncertainty can become explosive (Bevacqua et al., 2017; Santos et al., 2021). The univariate flood driver cannot provide an accurate evaluation if the underlying drivers are modelled as independent extreme events (Khanal et al., 2019).

Flood induced by TCs is the most frequent natural disaster in the eastern coastal region of China (Zhang et al., 2020). The East Asian typhoon season is characterized by heavy inland rainfall and high storm tides, which are the major driving factors of coastal flood hazards in China. The slowdown in forward speed of landfalling TCs in the Northwest Pacific over 1949-2015 had increased the risk of flooding from water level and rainfall even without considering the changes in storm strength (Kossin, 2018). The simultaneous and/or consecutive occurrence, both in time and space, of heavy rainfall and high tide can lead to compound flooding (Bilskie et al., 2021; Liu et al., 2022; Wahl et al., 2015). Furthermore, the risk posed by the interactions between hydro-meteorological events under the condition of sea level rise and changing tidal regimes is bound to increase in the future (Idier et al., 2020). Despite the increasing threat of compound flooding events along the Chinese coast, owing to the unavailability of water level records during typhoon events, the associated joint probabilities and driving mechanisms have not been explored (Fang et al., 2021). This research intends to fill this important niche.

The TCs often produce strong onshore winds and low barometric pressure, which would cause extreme storm surges at the same time, and generate heavy rainfall in the coastal region (Hoque et al., 2018; Sohn et al., 2021). The peak water level during TCs not only results from the combination of storm surge and astronomical tide. Additionally, the combination of absolute sea level rise (SLR) due to global warming and land subsidence due to urbanization has caused relative sea level rise (RSLR) (Jebbad et al., 2022). According to the Regulations of Shanghai Municipality on the Administration of Land Subsidence Prevention and Control, the land subsidence rate was 6.19 mm/yr from 1965 to 2001. Since 2001, the land subsidence rate has been controlled to varying degrees by adaptation measures such as recharging water to aquifers.

This study establishes the joint distribution of peak water level and rainfall during typhoon events in the Shanghai estuary region, with the aim of better understanding the risk of compound flooding and improving the assessment of flood-defence design standards for adaptation strategies. Our modelling framework couples a state-of-the-art hydrodynamic model and a statistic model. This model coupling enables us to quantify the joint distribution of rainfall and storm surge events during typhoon season and also to consider the comparative cases with and without RSLR for Shanghai. The procedure of the modelling framework is as follows. First, the peak water levels, consisting of astronomical tides, storm surges associated with TCs, and RSLR, in Shanghai over 1961-2018 are generated using the D-Flow Flexible Mesh (D-Flow FM) model, then a compound hazard scenario for deriving design values is chosen. Second, we compare and investigate the peak water level with and without RSLR, and select the extreme compound flood events according to the design standard of the joint hazard scenario. Finally, we analyze the contribution of storm surge, astronomical tide, and RSLR to peak water level based

on the top seven extreme compound flood events over the study period. We provide a framework that could be applied to other coastal cities that face the similar constraint of unavailable water level records. The findings from our research could be useful for decision-makers in developing coastal flood defence measures in Shanghai and other East Asian coastal cities. This is the major contribution of this research.

3.2. MATERIALS AND METHODS

3.2.1. STUDY AREA

Shanghai is surrounded by water on three sides, and the Huangpu River and Suzhou River pass through the city (Figure 3.1). The total area of Shanghai is 6,340.5 km^2 with a population of 24.87 million in 2020. The annual rainfall is around 1,200 mm. June to September are the rainy months. From late August to early September, Shanghai is frequently affected by typhoons and rainstorms (Yin et al., 2021). Storm flooding caused by typhoons is the main natural disaster in Shanghai. Shanghai's flood risk is about US $63 million/year under an optimistic scenario of a maximum protection level of 1/1000 per year (Hallegatte et al., 2013). Although the construction of flood control measures in the past 50 years has effectively reduced the risk of storm floods, TC Matsa in 2005, the 2013 TC Fitow, and the 2019 TC Lekima caused substantial losses in Shanghai. Particularly, typhoon Winnie in 1997 led to direct economic damage of over US $100 million. During the typhoon Winnie period, the peak water level at Huangpu Park (city center) rose to 5.72 m, equivalent to the water level with a 500-year return period. During typhoon Fitow in 2013, the water level at Mishidu in the inland area of the Huangpu River was recorded at WD (Wusong Datum is adopted as the reference) as 4.61 m, which broke the record (Ke et al., 2018). In the context of climate change, relative sea level rise, and urban expansion, Shanghai will face higher compound flood risks and challenges from TCs, storm surges, and extreme rainstorms in the future.

3.2.2. DATA

This study systematically collected the geographic and meteorological data of the study area, including TC tracks (1961-2018), and daily accumulated rainfall (1961-2018). Due to the unavailability of measured water level data from historical TCs, in this study, we evaluate the dependence coefficient (Spearman's ρ and Kendall τ) between rainfall and water level based on observed rainfall and simulated peak water level during TCs. Observations come from a set of rain gauge measurements. The International Best Track Archive for Climate Stewardship (IBTrACS) from NOAA's National Climatic Data Center contains the 6-hourly TC center's longitude and latitude, minimum central pressure (P_c), and sustained maximum surface wind velocity (V_max). Multiple agencies provide TC's best tracks in the West Pacific, and we opt to use the best track from Hong Kong Observatory (www.hko.gov.hk). This choice was made because it includes the most complete set of observations from TCs making landfall in China (Chen et al., 2011). Based on the modelled TC data, we use the D-Flow FM model (Knapp et al., 2010) to simulate water levels during TC periods.

We analyzed the historical TCs influencing Shanghai between 1961 and 2018. We first defined a 6-degree-latitude square box around Shanghai (Figure 3.2). The area covered

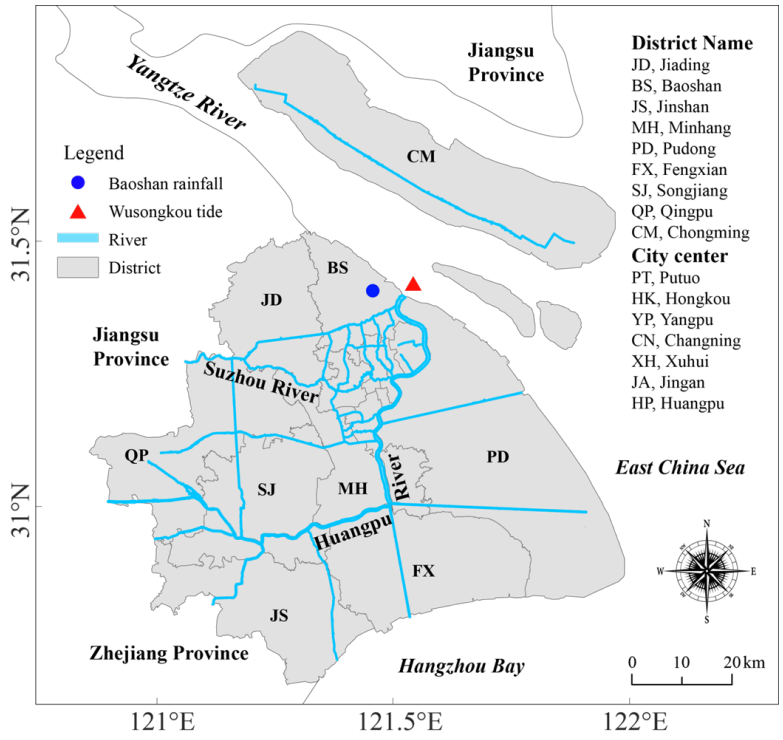

Figure 3.1: Location map of Shanghai.

by the blue box can be regarded as an alert area in terms of a TC causing potential damage in Shanghai. The size of the blue box was designed to be just large enough to include the partial tracks of the top 10 most severe TCs for Shanghai since 1949 (personal communication with Shanghai Climate Centre). We then selected historical TCs lasting for at least 24 hours in the blue box. After this best-track pre-processing, 210 TCs for the period of 1961-2018 are selected in this study (Figure 3.2). Additionally, we obtained tidal level data (1997) at the Wusongkou tide gauge from the Shanghai Municipal Water Authority, which is used for hydrodynamic model validation.

Daily rainfall records from 1961 to 2018 are collected from the China Meteorological Administration (CMA, http://data.cma.cn) for the Baoshan gauge station, being the closest to the Wusongkou surge station (Figure 3.1). The annual precipitation in Shanghai is 1,200 mm with the rainiest months being from June through September. Rainfall data are used in this study to approximate the TC-induced runoff. To implicitly account for the rainfall travel time to the catchment outlet, 1-, 2-, and 3-day accumulated rainfall was also estimated and the correlation between such accumulated rainfall and peak water level was then estimated.

According to the Chinese Sea Level Bulletin of 2020, which was compiled by the State Oceanic Administration of China, the absolute sea level rose at a rate of 3.4 mm/yr. According to the Regulations of Shanghai Municipality on the Administration of Land Sub-

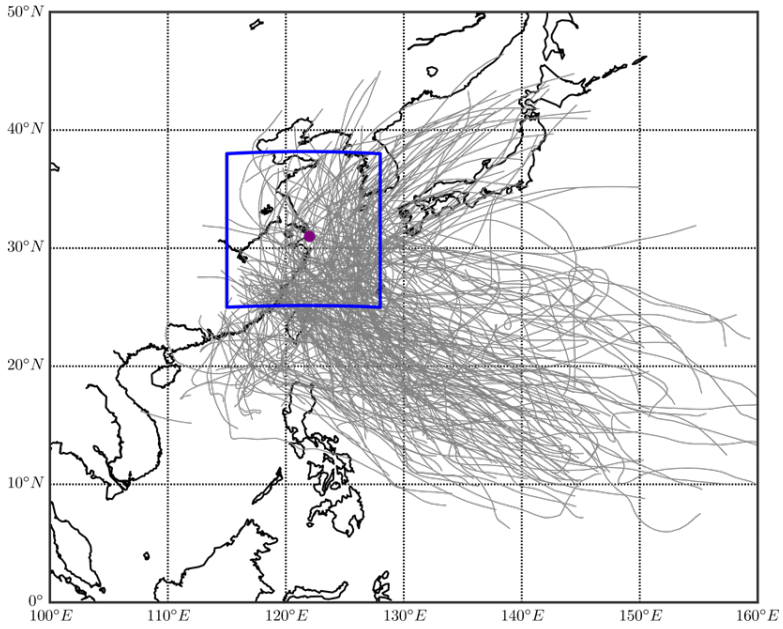

Figure 3.2: Location map for the area of interest. (Grey-coloured lines indicate major historical typhoon tracks within the region. The blue box indicates the selection criteria).

sidence Prevention and Control, the land subsidence rate was 27.93 mm/yr from 1921 to 1964. From 1965 to 2001, the land subsidence rate was 6.19 mm/yr. After 2001, the land subsidence rate has been under varying extents of control by adaptation measures such as recharging water to aquifers, and in most regions being 5-15 mm/yr. We use 10 mm/yr as the land subsidence rate from 2001 to 2018. The downside of such an assumption is that it fails to consider possible accelerating factors such as population growth, vertical and horizontal urban expansion, and deep strata motions, but these complex factors are beyond the scope of this research.

3.2.3. THE FRAMEWORK

The objectives of this study are to overcome the limitation of unavailable water level records during TCs and set up a framework to improve the methods for selecting the most suitable TCs for the research and for investigating TCs' influence on water levels. Due to the limited water level data availability, we employ an empirical track model for pressure and wind fields, followed by a physics-based ocean model to simulate storm tides and astronomical tides during TCs in Shanghai. A numerical simulation is carried out to better understand the distribution and timing of the peak water level and the areas of the country affected. The physics-based ocean model was calibrated using the recorded atmospheric pressure and focused on the ones with the most severe damages, comparing well with the results of the field survey data (Ke et al., 2021). Following this, the copula function was used to connect peak water level with accumulated rainfall and construct a joint distribution. After that, we compare and investigate the difference be-

tween peak water level and accumulated rainfall under the effect of RSLR, and select the extreme compound flood events according to the design value of the joint hazard scenario. Finally, we analyze the contribution of storm surge, astronomical tide, and RSLR to peak water level for the extreme compound flood events (Figure 3.3).

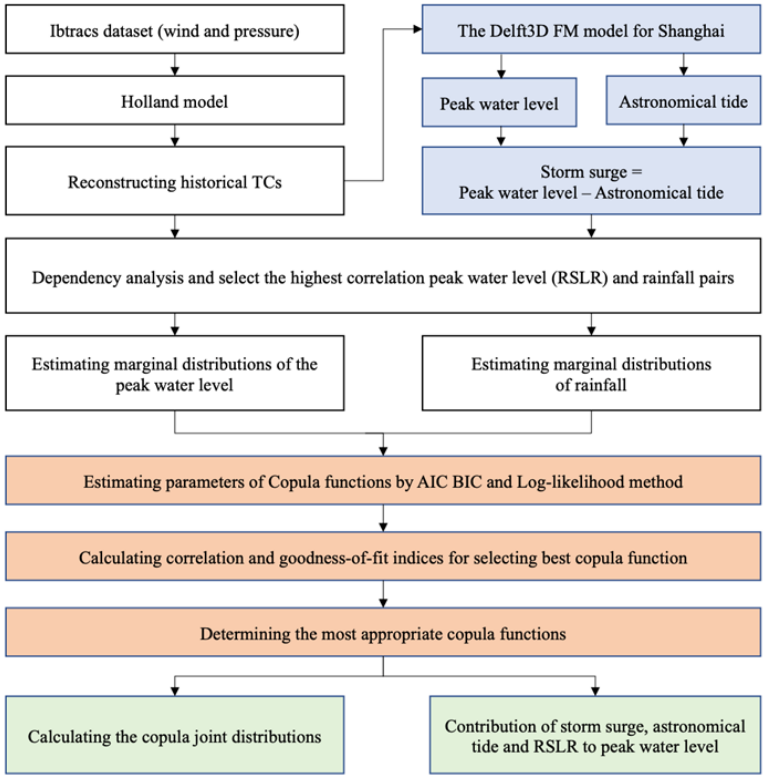

Figure 3.3: Flowchart of this study.

3.2.4. D-FLOW FM MODEL

Delft3D WES (Wind Enhance Scheme), a built-in module in Delft3D, is used to generate wind and air pressure fields of each TC according to the Holland formula (Holland et al., 2010). It can generate tropical cyclone wind and pressure fields around storm center positions on a high-resolution grid. Delft3D WES slightly improves on this by including asymmetry. This asymmetry is included by the use of the translational speed of the cyclone center's displacement by the steering flow, and the rotation of the wind velocity due to friction (Takagi and Wu, 2016). The output of Delft3D WES is suitable as input for the D-Flow FM model to simulate water level including the effect of storm surge.

The D-Flow FM module as part of the Delft3D Flexible Mesh suite solves the non-linear shallow water equations for unsteady flow and transport phenomena derived from the three-dimensional Navier Stokes equations for incompressible free surface flow. The

hydrodynamic model D-Flow FM is employed in this study to solve multi-disciplinary problems in coastal, river, and estuarine environments (Deltares, 2018). The domain of the model covers the East China Sea, Hangzhou Bay, the Yangtze Estuary, and the downstream reach of the Yangtze River, ranging from 24 to 34°N and 118 to 128°E, and consists of 69,000 mesh cells. The model has been validated with observed storm tide and astronomical tide at 10 stations around Shanghai during TC Winnie in 1997 (Ke et al., 2021). The storm tide and astronomical tide of 210 TCs are calculated in this D-Flow FM model. Then, the peak storm tide is selected from each TC. In addition, the storm surge is calculated by using storm tide minus astronomical tide at the same time as peak storm tide. In this study, we assume the Yangtze River discharge equals its annual mean at 31000 m^3/s.

3.2.5. DEPENDENCE MODELLING AND DESIGN VALUE VIA COPULAS

We define the joint distribution of accumulated rainfall and peak water level, $F(R, WL)$ as $F(R, WL) = C(F_R, F_W L)$ where F_R and $F_W L$ are marginal distributions of accumulated rainfall and peak water level, and C is the associated dependence function, i.e., copula, modelling the dependence between accumulated rainfall and peak water level independently from their marginal distributions (Salvadori and De Michele, 2004; A. Sklar, 1973). Hence, we select marginal distributions among the most commonly used distribution functions for extremes, namely: Generalized Extreme Value (GEV), Pearson type III (P-III), Gumbel, Exponential, and Weibull.

The copula function raised by A. Sklar (1973) can model the dependence structure and joint probability distributions. The Gaussian, Clayton, Frank and Gumbel copula functions are selected to establish joint distribution between peak water level and accumulated rainfall. To evaluate the fitting error and select the appropriate copula function by the non-parametric estimation method, the Akaike information criterion (AIC), Bayesian information criterion (BIC), and root mean square error (RMSE) are employed.

$$AIC = -2\iota(\theta\hat{}|y) + 2K \tag{3.1}$$

$$BIC = -2\iota(\theta\hat{}|y) + Kln(n) \tag{3.2}$$

K is the number of estimated parameters in the model including the intercept and $\iota(\theta\hat{}|y)$ is the log-likelihood at its maximum point of the estimated model; n is the sample size. The rule of selection was that the smaller the value of AIC was, the better the model was, and similarly with the BIC.

$$RMSE = \sqrt{\frac{1}{n}\sum_{i=1}^{n}(X_C(i) - X_O(I))^2} \tag{3.3}$$

where n is the number of observations; X_C is the theoretical probability from the copula and X_O is the empirical observed probability. It is also worth noting that the dependence between accumulated rainfall and the peak water level is given by their linear correlation, i.e., Spearman's ρ, or concordant/discordant pairs, i.e. Kendall τ.

Following Salvadori and De Michele (2004), copulas allow a straightforward definition of two hazard scenarios, i.e., pairs with an occurrence probability greater than a

safety threshold, namely "AND" and "OR" scenarios. The "AND" scenario assumes that a hazardous condition is realized when both the dependent variables, in this case, rainfall and water level, exceed their predefined thresholds, while the "OR" scenario assumes that a hazardous condition can occur when either one of the two dependent variables exceeds their predefined thresholds. The "AND" scenario is commonly used for compound flooding mostly because the flooding can be generated by excessive runoff, high sea level, or a combination of both (Moftakhari et al., 2017; Moftakhari et al., 2019; Zellou and Rahali, 2019). The joint exceedance probability based on the "AND" scenario is given by Eq. (3.4).

$$P((U > ud) \cap (V > vd)) = 1 + u_d + v_d - C(u_d, v_d) \tag{3.4}$$

where $U = F_R$ and $V = F_{WL}$ are the marginal distributions and u_d and v_d are the safety threshold of accumulated rainfall and peak water level, respectively. The dependent design values ($R_d = (F_r - 1)(u_d), WL_d = (F_{WL} - 1)(v_d)$) can be inferred from Eq. (3.4) based on the level of safety desired.

The joint probability cannot be directly used as the reference value of the actual engineering fortification standard. We calculate the joint design value combinations with the joint return period, which can serve as a reference for the engineering design. For given peak water level and accumulated rainfall events, under the conditions of a given joint return period, we design a series of (u_d, v_d) combinations to maximize $P((U > u_d) \cap (V > v_d))$, thereby obtaining the optimal combination design value. In the practical calculation, the intersection of the diagonal of critical probabilistic surface and probability isoline is regarded as the design values of (u_d, v_d).

3.3. RESULTS

3.3.1. EFFECT OF RELATIVE SEA LEVEL RISE TO PEAK WATER LEVEL

The correlation between peak water level and accumulated rainfall is positive. The peak water level and 2-day accumulated rainfall have the highest correlation compared with 1-day and 3-day accumulated rainfall. The correlation between peak water level and accumulated rainfall is significant ($P_{value} < 0.05$) in all cases. Consequently, the remaining analysis will be performed considering 2-days accumulated rainfall, hereafter R_{2d}.

A probability density function is a useful tool for comparing peak water levels between the cases with and without RSLR. Results in Figure 3.4 show a clear shift in the distribution of peak water level during the TC periods. It demonstrates that RSLR increases both the mean and variance of peak water levels, thus resulting in a higher risk of flooding in Shanghai.

Table 3.1: Performance measures of the estimated copula functions (data of functions selected for this study are indicated in bold).

Copula type	Max. likelihood	AIC	BIC	RMSE
Without RSLR				
Gaussian	1024.1	-2046.1	-2042.8	0.1105
Clayton	1034.7	-2067.5	-2064.1	0.1050
Frank	1009.4	-2016.8	-2013.4	0.1185
Gumbel	972.0	-1941.1	-1938.7	0.1415
Presence of RSLR				
Gaussian	1038.8	-2075.5	-2072.2	0.1030
Clayton	1029.4	-2056.7	-2053.4	0.1077
Frank	1016.4	-2030.9	-2027.5	0.1146
Gumbel	992.7	-1983.5	-1980.2	0.1282

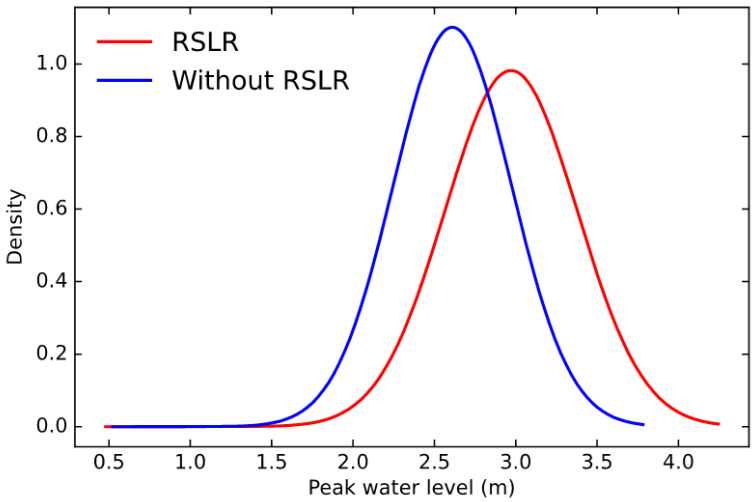

Figure 3.4: The shift of the probabilistic distribution of peak water level, "with RSLR" versus "without RSLR", in Shanghai during 1961-2018.

The marginal distributions are used to transform peak water level and R_{2d} into uniform marginals, u_{WL} and u_{R2d}, respectively. Then, the preferred copula is selected among the Clayton, Frank, Gumbel, and Gaussian copula. In the case without considering RSLR, the preferred copula is Clayton because it has the smallest AIC, BIC, and RMSE (the upper panel in Table 3.1). In the case with the presence of RSLR, the lower panel in Table 3.1 shows that the Gaussian copula has the smallest AIC, BIC, and RMSE. Therefore, the Gaussian copula is selected as the best fit for the peak water level and accumulated rainfall under the effect of RSLR.

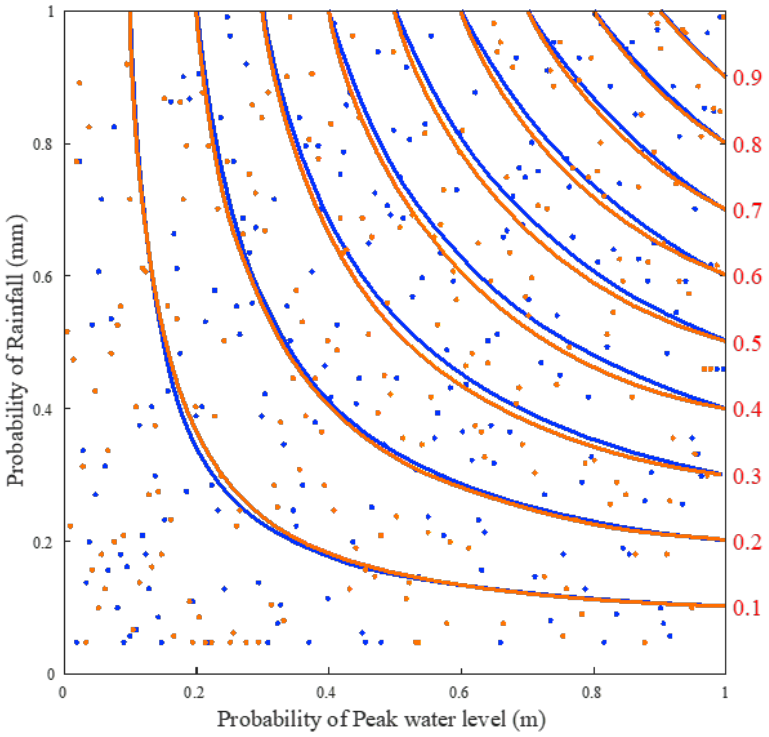

Figure 3.5: With RSLR (red) and without RSLR (blue) for 2 different copulas. Both peak water level (x-axis) and accumulated rainfall (y-axis) are presented in probability space. The red isolines are the fitted Gaussian copula, and the blue lines use a Clayton copula. Lines present the copula isolines and dots show observed data. The vertical axis on the right-hand side shows the joint probability value of isolines.

Figure 3.5 shows the difference between peak water level and accumulated rainfall with RSLR and without RSLR. This indicates that different copula families can return different dependence structures. In Figure 3.5, both peak water level and accumulated rainfall are presented in probability space. Gaussian and Clayton copula families are used to explain the bivariate dependence between peak water level and accumulated rainfall in this study. The red and blue isolines are fitted Gaussian copulas and Clayton copulas, respectively. Neither is among the commonly used copulas in the hydrological literature. This highlights the importance of the choice of the copula and quantifies the difference in results based on copula choice.

3.3.2. CONTRIBUTION OF STORM SURGE, ASTRONOMICAL TIDE AND RSLR TO PEAK WATER LEVEL

Figure 3.6 presents the scatter plot of peak water level and accumulated rainfall with and without RSLR. It shows that the influence of RSLR pushes up the design value of peak water level from 3.25 m to 3.36 m under the 10-yr joint return period, with the corresponding design value of rainfall at 90.39 mm. The univariate analysis approach

is to assume independence between rainfall and sea level, then the independence assumption would generally lead to lower design values compared to scenarios from the copula-based method. It usually depends on how one selects the pairs and the statistical model used (independent/dependent). This is a direct consequence of the difference in the sampling of extreme observations between both approaches.

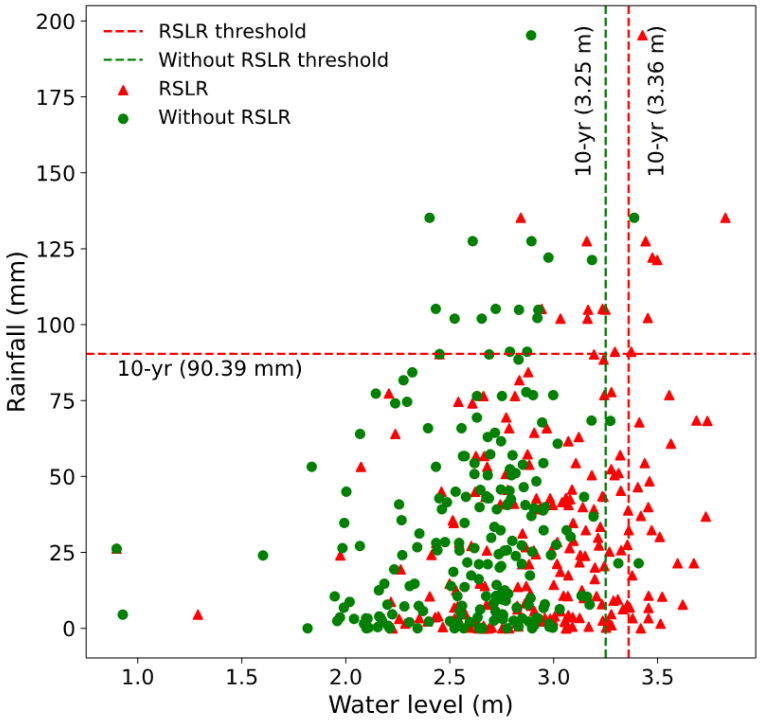

Figure 3.6: Scatter plot of water level and rainfall analyzed. Red lines show the design value of 10-yr joint return period with the effect of RSLR. Green lines show the design value of 10-yr joint return period without the effect of RSLR.

Based on the results in Figure 3.6, we defined the compound flood events as the peak water level and accumulated rainfall both being greater than their design values of 10-yr joint return period (i.e., peak water level > 3.36 m and accumulated rainfall > 90.39 mm). Based on this criterion, we identified seven compound flood events under the influence of RSLR (Figure 3.7).

Peak water level results from the combination of storm surge, astronomical tide, and RSLR. Figure 3.7 shows the contribution of storm surge, astronomical tide, and RSLR to peak water level from the seven extreme compound flood events in Shanghai. We consider the cases including the effect of RSLR and split the peak water level according to the contributions of its components, i.e., storm surge, astronomical tide, and RSLR, to investigate their shares of contribution.

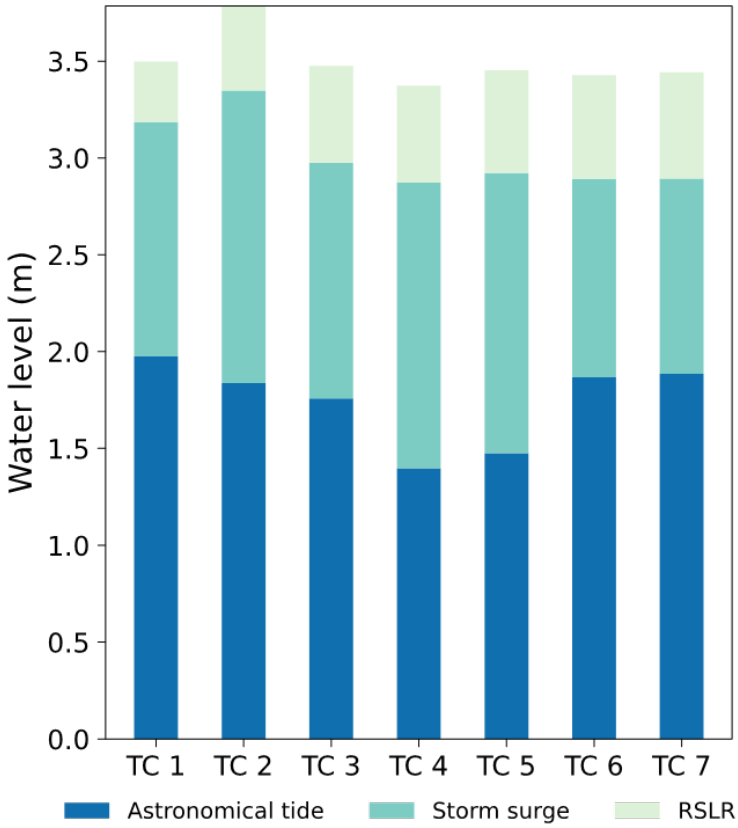

Figure 3.7: The contribution of storm surge, astronomical tide and RSLR to peak water level. (Cases are samples greater than the 10-yr joint return period.)

Overall, storm surge explains 32% of the peak water level, while astronomical tide accounts for 55% and RSLR accounts for 13% of the peak water level. The astronomical tide is in general the leading contributor to the peak water level, but storm surge can be the leading contributor in some cases, e.g., TC 4, in which the contribution of storm surge accounted for 45% of the peak water level. Under the scenario of future global warming and further urbanization, the impact of RSLR would increase and should not be treated as less important.

3.4. DISCUSSION

Coastal areas are the most densely populated and economically developed areas of many countries, and they are also the most vulnerable regions to the risk of compound floods from heavy precipitation and storm surges because of the high population and property density as well as storm surge risk (Shen et al., 2019). In this study, we provide a framework that could be applied in general to coastal cities that face the constraint of

unavailable water level records.

3.4.1. THE DEPENDENCY BETWEEN THE WATER LEVEL AND RAINFALL

The dependence among different drivers of compound floods has been widely studied. For example, Zheng et al. (2013) identified a significant dependence between precipitation and storm surge along the coastlines of Australia; Wahl et al. (2015) examined the enhanced dependence between precipitation and storm surge and reported an increasing trend in compound flood risk in the past decades along the coast of the US. These findings are critical to better understanding the changing compound flood risk and provide important references for the evaluation of simulation-based studies.

The correlations between rainfall and storm surge are determined by various factors such as meteorological conditions and regional topography. For example, compound floods from heavy precipitation and storm surges can occur during TCs (Bevacqua et al., 2019). TCs are one of the most important triggers of compound floods from heavy rainfall and storm surges in coastal regions. Even though compound floods are receiving attention, few studies have analyzed the dependency between water level and rainfall during historical TCs in China. This study enriches this stream of literature by quantifying the joint distribution of peak water level and rainfall during TCs in the Shanghai estuary region. On the other hand, it is worth noting that the record lengths of observational data in our study are relatively short and the uncertainties of simulation-based studies could be large. Therefore, further studies are needed once more observational data become available.

3.4.2. THE EFFECT OF RSLR ON PEAK WATER LEVEL

Deltas are especially vulnerable to RSLR because of their low elevation and commonly high rates of land subsidence (Higgins et al., 2014; Wang et al., 2012). Long-term tide gauge records show that global mean sea levels have risen by 1.7±0.3 mm/yr over the last century (Cipollini et al., 2017; Holgate, 2007). Nearly 90% of the world's river deltas suffer the impact of RSLR, including Shanghai and Manila (He and Silliman, 2019). The accelerated rise of global sea levels puts low-lying coastal regions at risk of increases in the frequency and magnitude of flooding (Cazenave and Le Cozannet, 2014). For example, the sea level rose on average by ~10 cm over the $20_t h$ century along the Italian coast, and flood frequency increased by more than seven times in the area (Kulp and Strauss, 2019). Increased flooding because of RSLR, in regions that experience storm surges from TCs, further increases the vulnerability of coastal regions to inundation (Edmonds et al., 2020).

Previous studies of Shanghai reported an increased risk of coastal floods due to global and local changes (Wang et al., 2012; Yan et al., 2016). Including the increased RSLR we estimated over the past 58 years (0.55 m), a 4.3 m projected RSLR due to additional land subsidence along the Yangtze River delta by 2100 would result in half of Shanghai being flooded by extreme storm-water levels (Wang et al., 2012). There are serval potential carbon emission scenarios used to project sea-level rise. Regardless of the methods and emission scenarios used to estimate future sea levels, the consensus is that sea levels are rising and its rate is expected to accelerate (Wahl et al., 2017). We investigated the effect of RSLR for a lower return period and under stationary climate conditions.

This approach needs adaptation if using climate projections for future climate change. By contrast, this thesis presents a probabilistic analysis of the impact of RSLR on peak water levels, accounting for the effects of sea level rise and land subsidence on coastal flooding, in Shanghai from 1961-2018. The findings from our research would provide a more solid foundation for scenario-based analysis in the future and be useful for the decision-making about the adaption via coastal flood defence measures for Shanghai.

3.4.3. MULTIPLE CONTRIBUTORS TO PEAK WATER LEVEL

Coastal flooding from peak water levels is one of the most devastating natural hazards to Shanghai. A storm with strong winds and low atmospheric pressure can produce a large storm surge and large waves. A storm surge is an increase in water level above normal sea level and is a function of storm intensity, duration, size, and location (Cooper et al., 2008). Tides are an astronomical phenomenon caused by the gravitational attraction of the moon and the sun on earth's oceans, while storm surge is a meteorological phenomenon (Karim and Mimura, 2008). If storm surge coincides with the astronomical high tide, these water levels superpose, and an extreme water level may be generated. Southeast Asia is highly vulnerable to, and frequently impacted by, extreme sea-level events of different origins: TCs cause severe storm surges and rainfall with potentially devastating impacts to the economy and environment and in many cases loss of human life.

Astronomical tides are deterministic and can be predicted far in advance, whereas storm surges can only be accurately hindcast from tide gauge records. Prediction of storm surge is possible days in advance of TC landfall, simulated by taking into account predicted forcing variables, such as wind stress and sea level pressure over the sea surface. Tide gauge records have been used to study sea level extremes. However, 90% of the tide gauges located in Southeast Asia have record lengths of less than 30 years. One way to overcome the absence of long tide gauge records is to employ numerical models to simulate the storm surge component using best-track TC data or meteorological reanalysis results, as we have done in this research (Park and Suh, 2012).

In this study, we demonstrate that the astronomical tide plays an important role in the total water level in Shanghai. Indeed, surges might occur at any tidal level and are especially strong in shallow estuaries. A high tide at Wusongkou gauge would extend to downtown Shanghai causing a fluvial flood. The flood extent, depth, and duration can be exacerbated by storm surge, and consequently, the disruptive impact increases strongly (Ke et al., 2018). Astronomical tides contribute to peak water levels during TCs (Sweet et al., 2009). Bacopoulos (2017) showed that in the St Johns River in Florida, the astronomical tide could contribute as much as 94% to the extreme water level. Our study highlights that the critical components to consider in the analysis of peak water levels during TCs are the astronomic tides, storm surge and RSLR. In future research, we will explore the applicability of the presented methodology to other regions where limited observational data availability has hampered a better understanding of peak water levels, storm surges and potential changes related to climate variability and change.

3.5. CONCLUSIONS

It is important to consider the compounding effects of multiple interdependent extremes or drivers to accurately characterize the underlying hazard. In this study, we focused on the joint impact of peak water level and accumulated rainfall in Shanghai, a coastal mega-city located in the Yangtze River Delta region. We showed that Shanghai is prone to compound flooding and this justifies the adoption of a probabilistic modelling framework to incorporate the interdependence of multiple flood drivers.

Between 1961 and 2018, the RSLR increased by 0.55 m in Shanghai. With the ongoing global warming and further urbanization vertically and horizontally in the city, the process of RSLR would continue and amplify the peak water levels in extreme flooding events. The sample data we consolidated show an increase in the probability of peak water level under the effect of RSLR. We also identify the extent of the shift in the joint distribution of peak water level and accumulated rainfall during TC periods between the theoretical setting without RSLR and the real setting with RSLR by employing the best-fitted copula functions. The shift indicates that the RSLR leads to an increase in both the mean and variance of peak water levels, thus a significantly higher level of flooding risk in Shanghai.

The design value of peak water level and accumulated rainfall are 3.36 m and 90.39 mm during TCs under the 10-yr joint return period and with the influence of RSLR. We selected the potential compound flood events according to this pair of design values and identified seven potential compound flood events. The analysis of these seven events shows that astronomic tide is in general the most important driver of the peak water level, however, there is one case in which storm surge is the leading driver of the peak water level. If the astronomic tide is relative to the mean high water instead of the mean sea level, the length of the tide part bars may be smaller. However, we argue that the peak water level is the most dangerous hazard to coastal cities. The combination of astronomical tide, storm surge and RSLR drives the peak water level. We cannot neglect the contribution of the tide during the typhoon season.

The framework developed in this study could be applied to other coastal cities or regions in East and Southeast Asia. The impact of the RSLR in amplifying the peak water level would significantly increase in the future. Therefore, the monitoring and prediction of the RSLR should be an important component in the development of future design standards for flood preparedness. Furthermore, RSLR caused by climate change and intensive use of urban land would also increase social vulnerability, which can be an interesting topic for future research.

BIBLIOGRAPHY

Anandalekshmi, A., Panicker, S. T., Adarsh, S., Muhammed Siddik, A., Aloysius, S., & Mehjabin, M. (2019). Modeling the concurrent impact of extreme rainfall and reservoir storage on kerala floods 2018: A copula approach. *Modeling Earth Systems and Environment, 5*, 1283–1296.

Bacopoulos, P. (2017). Tide-surge historical assessment of extreme water levels for the st. johns river: 1928–2017. *Journal of hydrology, 553*, 624–636.

Balistrocchi, M., Moretti, G., Orlandini, S., & Ranzi, R. (2019). Copula-based modeling of earthen levee breach due to overtopping. *Advances in Water Resources, 134*, 103433.

Bevacqua, E., Maraun, D., Hobæk Haff, I., Widmann, M., & Vrac, M. (2017). Multivariate statistical modelling of compound events via pair-copula constructions: Analysis of floods in ravenna (italy). *Hydrology and Earth System Sciences, 21*(6), 2701–2723.

Bevacqua, E., Maraun, D., Vousdoukas, M., Voukouvalas, E., Vrac, M., Mentaschi, L., & Widmann, M. (2019). Higher probability of compound flooding from precipitation and storm surge in europe under anthropogenic climate change. *Science advances, 5*(9), eaaw5531.

Bilskie, M. V., Zhao, H., Resio, D., Atkinson, J., Cobell, Z., & Hagen, S. C. (2021). Enhancing flood hazard assessments in coastal louisiana through coupled hydrologic and surge processes. *Frontiers in Water, 3*, 609231.

Cazenave, A., & Le Cozannet, G. (2014). Sea level rise and its coastal impacts, earth's future, 2, 15–34.

Chao, S. R., Ghansah, B., & Grant, R. J. (2021). An exploratory model to characterize the vulnerability of coastal buildings to storm surge flooding in miami-dade county, florida. *Applied geography, 128*, 102413.

Chen, X., Wu, L., & Zhang, J. (2011). Increasing duration of tropical cyclones over china. *Geophysical Research Letters, 38*(2), L02708.

Cipollini, P., Calafat, F. M., Jevrejeva, S., Melet, A., & Prandi, P. (2017). Monitoring sea level in the coastal zone with satellite altimetry and tide gauges. *Integrative Study of the Mean Sea Level and Its Components*, 35–59.

Cooper, M. J., Beevers, M. D., & Oppenheimer, M. (2008). The potential impacts of sea level rise on the coastal region of new jersey, usa. *Climatic Change, 90*(4), 475–492.

Deltares. (2018). D-flow flexible mesh.

Du, S., Scussolini, P., Ward, P. J., Zhang, M., Wen, J., Wang, L., Koks, E., Diaz-Loaiza, A., Gao, J., Ke, Q., et al. (2020). Hard or soft flood adaptation? advantages of a hybrid strategy for shanghai. *Global Environmental Change, 61*, 102037.

Edmonds, D. A., Caldwell, R. L., Brondizio, E. S., & Siani, S. M. (2020). Coastal flooding will disproportionately impact people on river deltas. *Nature communications*, *11*(1), 4741.

Fang, J., Wahl, T., Fang, J., Sun, X., Kong, F., & Liu, M. (2021). Compound flood potential from storm surge and heavy precipitation in coastal china: Dependence, drivers, and impacts. *Hydrology and Earth System Sciences*, *25*(8), 4403–4416.

Feng, D., & Beighley, E. (2020). Identifying uncertainties in hydrologic fluxes and seasonality from hydrologic model components for climate change impact assessments. *Hydrology and Earth System Sciences*, *24*(5), 2253–2267.

Hallegatte, S., Green, C., Nicholls, R. J., & Corfee-Morlot, J. (2013). Future flood losses in major coastal cities. *Nature Climate Change*, *3*(9), 802–806.

He, Q., & Silliman, B. R. (2019). Climate change, human impacts, and coastal ecosystems in the anthropocene. *Current Biology*, *29*(19), 1021–1035.

Higgins, S. A., Overeem, I., Steckler, M. S., Syvitski, J. P., Seeber, L., & Akhter, S. H. (2014). Insar measurements of compaction and subsidence in the ganges-brahmaputra delta, bangladesh. *Journal of Geophysical Research: Earth Surface*, *119*(8), 1768–1781.

Holgate, S. (2007). On the decadal rates of sea level change during the twentieth century. *Geophysical research letters*, *34*(1), L01602.

Holland, G. J., Belanger, J. I., & Fritz, A. (2010). A revised model for radial profiles of hurricane winds. *Monthly weather review*, *138*(12), 4393–4401.

Hoque, M. A.-A., Phinn, S., Roelfsema, C., & Childs, I. (2018). Assessing tropical cyclone risks using geospatial techniques. *Applied geography*, *98*, 22–33.

Idier, D., Rohmer, J., Pedreros, R., Le Roy, S., Lambert, J., Louisor, J., Le Cozannet, G., & Le Cornec, E. (2020). Coastal flood: A composite method for past events characterisation providing insights in past, present and future hazards—joining historical, statistical and modelling approaches. *Natural Hazards*, *101*(2), 465–501.

Jebbad, R., Sierra, J. P., Mösso, C., Mestres, M., & Sanchez-Arcilla, A. (2022). Assessment of harbour inoperability and adaptation cost due to sea level rise. application to the port of tangier-med (morocco). *Applied Geography*, *138*, 102623.

Karim, M. F., & Mimura, N. (2008). Impacts of climate change and sea-level rise on cyclonic storm surge floods in bangladesh. *Global environmental change*, *18*(3), 490–500.

Ke, Q. (2014). Flood risk analysis for metropolitan areas–a case study for shanghai.

Ke, Q., Jonkman, S. N., Van Gelder, P. H., & Bricker, J. D. (2018). Frequency analysis of storm-surge-induced flooding for the huangpu river in shanghai, china. *Journal of Marine Science and Engineering*, *6*(2), 70.

Ke, Q., Yin, J., Bricker, J. D., Savage, N., Buonomo, E., Ye, Q., Visser, P., Dong, G., Wang, S., Tian, Z., et al. (2021). An integrated framework of coastal flood modelling under the failures of sea dikes: A case study in shanghai. *Natural Hazards*, *109*(1), 671–703.

Khanal, S., Ridder, N., De Vries, H., Terink, W., & Van den Hurk, B. (2019). Storm surge and extreme river discharge: A compound event analysis using ensemble impact modeling. *Frontiers in Earth Science*, *7*, 224.

Knapp, K. R., Kruk, M. C., Levinson, D. H., Diamond, H. J., & Neumann, C. J. (2010). The international best track archive for climate stewardship (ibtracs) unifying tropical cyclone data. *Bulletin of the American Meteorological Society*, *91*(3), 363–376.

Kossin, J. P. (2018). A global slowdown of tropical-cyclone translation speed. *Nature*, *558*(7708), 104–107.

Kulp, S. A., & Strauss, B. H. (2019). New elevation data triple estimates of global vulnerability to sea-level rise and coastal flooding. *Nature communications*, *10*(1), 1–12.

Leonard, M., Westra, S., Phatak, A., Lambert, M., van den Hurk, B., McInnes, K., Risbey, J., Schuster, S., Jakob, D., & Stafford-Smith, M. (2014). A compound event framework for understanding extreme impacts. *Wiley Interdisciplinary Reviews: Climate Change*, *5*(1), 113–128.

Li, M., Kwan, M.-P., Yin, J., Yu, D., & Wang, J. (2018). The potential effect of a 100-year pluvial flood event on metro accessibility and ridership: A case study of central shanghai, china. *Applied geography*, *100*, 21–29.

Li, W., Wen, J., Xu, B., Li, X., & Du, S. (2018). Integrated assessment of economic losses in manufacturing industry in shanghai metropolitan area under an extreme storm flood scenario. *Sustainability*, *11*(1), 126.

Liu, Q., Xu, H., & Wang, J. (2022). Assessing tropical cyclone compound flood risk using hydrodynamic modelling: A case study in haikou city, china. *Natural Hazards and Earth System Sciences*, *22*(2), 665–675.

Moftakhari, H., Salvadori, G., AghaKouchak, A., Sanders, B. F., & Matthew, R. A. (2017). Compounding effects of sea level rise and fluvial flooding. *Proceedings of the National Academy of Sciences*, *114*(37), 9785–9790.

Moftakhari, H., Schubert, J. E., AghaKouchak, A., Matthew, R. A., & Sanders, B. F. (2019). Linking statistical and hydrodynamic modeling for compound flood hazard assessment in tidal channels and estuaries. *Advances in Water Resources*, *128*, 28–38.

Neumann, B., Vafeidis, A. T., Zimmermann, J., & Nicholls, R. J. (2015). Future coastal population growth and exposure to sea-level rise and coastal flooding-a global assessment. *PloS one*, *10*(3), e0118571.

Park, Y. H., & Suh, K.-D. (2012). Variations of storm surge caused by shallow water depths and extreme tidal ranges. *Ocean Engineering*, *55*, 44–51.

Salvadori, G., & De Michele, C. (2004). Frequency analysis via copulas: Theoretical aspects and applications to hydrological events. *Water resources research*, *40*(12), W12511.

Santos, V. M., Casas-Prat, M., Poschlod, B., Ragno, E., Van Den Hurk, B., Hao, Z., Kalmár, T., Zhu, L., & Najafi, H. (2021). Statistical modelling and climate variability of compound surge and precipitation events in a managed water system: A case study in the netherlands. *Hydrology and Earth System Sciences*, *25*(6), 3595–3615.

Shen, Y., Morsy, M. M., Huxley, C., Tahvildari, N., & Goodall, J. L. (2019). Flood risk assessment and increased resilience for coastal urban watersheds under the combined impact of storm tide and heavy rainfall. *Journal of Hydrology*, *579*, 124159.

Sklar, A. (1973). Random variables, joint distribution functions, and copulas. *Kybernetika*, *9*(6), 449–460.

Sklar, M. (1959). Fonctions de répartition à n dimensions et leurs marges. *Annales de l'ISUP*, *8*(3), 229–231.

Sohn, W., Bae, J., & Newman, G. (2021). Green infrastructure for coastal flood protection: The longitudinal impacts of green infrastructure patterns on flood damage. *Applied Geography*, *135*, 102565.

Sweet, W. W. V., Zervas, C. E., & Gill, S. K. (2009). Elevated east coast sea level anomaly: June-july 2009.

Takagi, H., & Wu, W. (2016). Maximum wind radius estimated by the 50 kt radius: Improvement of storm surge forecasting over the western north pacific. *Natural Hazards and Earth System Sciences*, *16*(3), 705–717.

Visser-Quinn, A., Beevers, L., Collet, L., Formetta, G., Smith, K., Wanders, N., Thober, S., Pan, M., & Kumar, R. (2019). Spatio-temporal analysis of compound hydrohazard extremes across the uk. *Advances in Water Resources*, *130*, 77–90.

Wahl, T., Haigh, I. D., Nicholls, R. J., Arns, A., Dangendorf, S., Hinkel, J., & Slangen, A. B. (2017). Understanding extreme sea levels for broad-scale coastal impact and adaptation analysis. *Nature communications*, *8*(1), 16075.

Wahl, T., Jain, S., Bender, J., Meyers, S. D., & Luther, M. E. (2015). Increasing risk of compound flooding from storm surge and rainfall for major us cities. *Nature Climate Change*, *5*(12), 1093–1097.

Wang, J., Gao, W., Xu, S., & Yu, L. (2012). Evaluation of the combined risk of sea level rise, land subsidence, and storm surges on the coastal areas of shanghai, china. *Climatic change*, *115*, 537–558.

Xu, H., Xu, K., Bin, L., Lian, J., & Ma, C. (2018). Joint risk of rainfall and storm surges during typhoons in a coastal city of haidian island, china. *International journal of environmental research and public health*, *15*(7), 1377.

Yan, B., Li, S., Wang, J., Ge, Z., & Zhang, L. (2016). Socio-economic vulnerability of the megacity of shanghai (china) to sea-level rise and associated storm surges. *Regional environmental change*, *16*, 1443–1456.

Yin, J., Lin, N., Yang, Y., Pringle, W. J., Tan, J., Westerink, J. J., & Yu, D. (2021). Hazard assessment for typhoon-induced coastal flooding and inundation in shanghai, china. *Journal of Geophysical Research: Oceans*, *126*(7), e2021JC017319.

Zellou, B., & Rahali, H. (2019). Assessment of the joint impact of extreme rainfall and storm surge on the risk of flooding in a coastal area. *Journal of Hydrology*, *569*, 647–665.

Zhang, W., Chang, W. J., Zhu, Z. C., & Hui, Z. (2020). Landscape ecological risk assessment of chinese coastal cities based on land use change. *Applied Geography*, *117*, 102174.

Zheng, F., Westra, S., & Sisson, S. A. (2013). Quantifying the dependence between extreme rainfall and storm surge in the coastal zone. *Journal of Hydrology*, *505*(21), 172–187.

Zscheischler, J., Westra, S., Van Den Hurk, B. J., Seneviratne, S. I., Ward, P. J., Pitman, A., AghaKouchak, A., Bresch, D. N., Leonard, M., Wahl, T., et al. (2018). Future climate risk from compound events. *Nature Climate Change*, *8*(6), 469–477.

4

ASSESSING COMPOUND FLOODING USING HYDRODYNAMIC MODELLING

To advance the modelling and quantification of compound flood characteristics, e.g., extent and depth, in coastal cities, in this chapter we introduce a hydrodynamic model. It combines a storm surge model and overland flooding model using Delft3D Flexible Mesh (D-Flow FM), to characterize the physical interaction between storm surges and rainfall during the typhoon period.

The results demonstrate that the coupled methodology, which integrates storm surge and overland flooding models, enabled the quantitative assessment of compound flood hazards with high model performance. It was observed that storm tide serves as the predominant driver of compound flood inundation, whereby tide levels directly influence the extent of inundation. A comparative analysis of compound flooding with rainstorm inundation and storm flooding showed that compound flooding exhibits greater destructive potential than single-driven flood hazards, surpassing the cumulative effects of rainstorm and storm tide flooding. This study focuses on Haikou City but its methodology offers a valuable framework for assessing compound flooding hazards in other coastal cities, particularly in the challenges of climate change-induced TCs and rising sea levels.

This chapter has been published as: Qing Liu[†], Hanqing Xu[†], Jun Wang. Assessing tropical cyclone compound flood risk using hydrodynamic modelling: a case study in Haikou City, China. ***Natural Hazards and Earth System Sciences***, 2022: 22(2), 665-675.

4.1. INTRODUCTION

Flood hazards, especially those happening during tropical cyclones (TCs), have become the most devastating and expensive natural hazards in coastal cities (Gutierrez et al., 2011; Hallegatte et al., 2013 Patricola and Wehner, 2018; van Oldenborgh et al., 2017). Storm tides brought on by TCs can lead to coastal flooding, and rainstorms occurring during TCs can lead to urban inundation. The simultaneous or consecutive occurrence of storm tides and rainstorms in time and space can lead to compound flooding (Gori et al., 2020; Leonard et al., 2014; Wahl et al., 2015).

In the past decade, many compound flood hazards occurred in coastal regions worldwide due to TCs, such as Typhoon Irma (2017) in Jacksonville and Typhoon Lekima on the southeast coast of China. An extremely destructive flood event in Houston–Galveston during Hurricane Harvey (2017) was confirmed to be a compound flood hazard (Huang et al., 2021). It was caused by land-derived runoff (mainly considered to be rainfall) and ocean-derived forcing (mainly considered to be storm tide) (Valle-Levinson et al., 2020). The coastal region suffered a major economic loss of more than USD 125 billion from Harvey. Thus, it is important to investigate the compound flood risk during TCs to comprehend flood hazards in coastal cities better.

The projection of future climate change indicates that TCs occur more frequently with greater intensity. Accordingly, the likelihood of the co-occurrence of storm tide and rainstorm would increase drastically (Emanuel, 2017; Keellings and Hernández Ayala, 2019; Lin et al., 2012; Marsooli et al., 2019), which may cause more extreme compound flood hazards (Bevacqua et al., 2019; Rasmussen et al., 2018). Due to global warming, sea level rise, land subsidence, and urban expansion, coastal cities are confronted with the critical threat of TC compound flooding (Wang et al., 2018; Yin et al., 2021). Recent studies evaluated compound flood risk at the regional scale (Bevacqua et al., 2019; Fang et al., 2021; Wahl et al., 2015). Wahl et al. (2015) assessed the risk of compound flooding from rainfall and storm surge in major US cities. Bevacqua et al. (2019) estimated the probability of compound flooding from precipitation and storm surges in Europe. Both studies showed that there would be an increase in compound flood risk in coastal cities in the future. A study conducted by Fang et al. (2021) investigated the compound flood potential from precipitation and storm surge in coastal China, indicating that low-latitude (<30 $^{\circ}N$) coastal areas in southeast China are more prone to compound flood hazards from storm tide and rainfall during TCs.

Only several urban-scale studies on compound flooding have been carried out in China (Wang et al., 2018; H. Xu et al., 2018). J. J. Lian et al. (2013) investigated the joint impact of rainfall and tidal level on flood risk in Fuzhou City. K. Xu et al. (2014) analyzed the joint probability of rainfall and storm tide under changing environments, concluding that the probability of compound flooding would increase by more than 300 % in Fuzhou. J. Lian et al. (2017) identified the major hazard-causing factors of compound flooding and classified the floodplains into tidal, hydrological, and transition zones in Haikou City. Although studies such as these have investigated the joint risk of hazard-causing factors in compound floods, they seldom pay attention to the compound flooding that occurs during TCs.

Most studies concerned with compound flooding rely on historical data, which contains information on hourly storm tide and daily rainfall (Zellou and Rahali, 2019). The

recorded data are often used to investigate the statistical correlation between flood drivers. For example, based on the recorded storm tide from 49 tide gauges and daily precipitation from 4890 rainfall stations in Australia, Zheng et al. (2013) quantified the dependence between rainfall and storm surge to investigate flood risk in coastal zones. However, for many coastal regions in the world, it is difficult to obtain sufficient recorded data that can be used to analyze the mechanism of TC compound flooding from storm tides and rainfall. An alternative approach is applying a hydrodynamic model to simulate storm tides (Gori et al., 2020). For example, Yin et al. (2021) constructed a storm surge model to simulate the storm tide derived from 5000 synthetic TCs to estimate TC-induced coastal flood inundation.

Hydrodynamic models can also be employed to simulate flood events (Kumbier et al., 2018; Zellou and Rahali, 2019). It is an effective method to model the flood extent and inundation depth, and this method has generally been applied in research on single-driven flood hazards (Yin et al., 2013). Recently, many studies have used hydrodynamic models to simulate compound flood events driven by historical TC events or synthetic TC scenarios (Bilskie et al., 2021; Santiago-Collazo et al., 2019). Gori et al. (2020) developed an integrated framework comprising three models for simulating storm surges and compound flood events. This approach offers the advantage of monitoring the spatiotemporal dynamics of rainfall and storm surges during TCs. However, assessing the compound flood risk by constructing a coupled model is not commonly used in current studies on compound flood hazards, mainly because the simulation of compound flooding involves multiple driving condition settings and requires combining multiple physics-based models.

D-Flow FM, developed by Deltares, the Netherlands, has been widely applied to build storm-surge numerical models for research on storm surge because of its capability of simulating 2D and 3D shallow water flow (Deltares, 2018). It integrates D-Flow FM and uses flexible unstructured grids, convenient for partial grid refinement. A recent study on compound flooding utilized this model to simulate storm surges for characterizing extreme sea levels, investigating the probability of compound floods from precipitation and storm surge in Europe (Bevacqua et al., 2019). Meijer and Hutten (2018) developed a 2D urban model with D-Flow FM for the downtown area of Shanghai. The results indicated that D-Flow FM was capable of modeling rainfall–runoff and could be used to construct urban flood models. Therefore, it is feasible to simulate storm surge and rainfall–runoff based on D-Flow FM to assess compound flooding.

This study investigates the compound effect of flooding from storm tides and rainstorms during TCs in Haikou. We set up a storm surge model and overland flooding model based on the D-Flow FM model to simulate the floodplain under TC events. We select 66 TC events that influenced Haikou to explore the probability distribution of storm tide, further selecting 5 TC events that correspond to the 5-, 10-, 25-, 50-, and 100-yr return periods, respectively. The risks of rainstorm inundation, storm tide flooding, and compound flooding are quantitatively assessed and compared based on the simulation results under different return periods. The conclusions drawn from this study can provide insight into mitigating compound flood risk in coastal areas.

To the best of our knowledge, this is the first study that applies a coupled model by D-Flow FM to assess TC compound flood risk in Haikou. The objectives of this study in-

clude (1) investigating the probability of storm tide by modelling TCs influenced Haikou; (2) quantifying the compound effects of rainfall and storm surge under TC events of different return periods; (3) assessing and comparing the flood severity of rainstorm inundation, storm tide flooding, and compound flooding.

This study is organized as follows: Section 4.2 presents the background information about the study area and data requirements. Section 4.3 describes the model configuration and explains how TCs that influenced Haikou were selected. The method of how to assess the compound flood risk is also in this section. Model verification and the analysis of the probability distribution of storm tides are reported and discussed in Section 4.4. The assessment and comparison of rainstorm inundation, storm tide flooding, and compound flooding are also discussed in this section. Finally, conclusions are given in Section 4.5.

4.2. MATERIALS

4.2.1. STUDY AREA

Haikou is located in the north of Hainan Island, China, where the geographical position is relatively independent (Figure 4.1). The coastal area of Haikou is low and flat. In particular, the elevation of the downstream plain and areas along Nandu River (Figure 4.1) is less than 3.0 m. Haikou is frequently affected by TCs and rainstorms from June to October. The annual rainfall is around 1660 mm. Storm tide flooding caused by TCs is one of the main natural hazards in Haikou, roughly three storm surges have occurred in Haikou every year in recent decades. The combination of storm tides and rainstorms will increase the probability of extreme compound flooding, posing a threat to social infrastructure and urban traffic in Haikou. For example, during Typhoon Kalmaegi (2014), a total of 219.8 mm (24 h) of precipitation was produced and the highest tide level reached 4.3 m in Haikou. The occurrence of heavy rainfall and strong storm tides caused serious compound flooding with an economic loss of USD 220 million. Under the changing environment, Haikou will face greater compound flooding risks and challenges from TCs, storm surges, and rainstorms in the future.

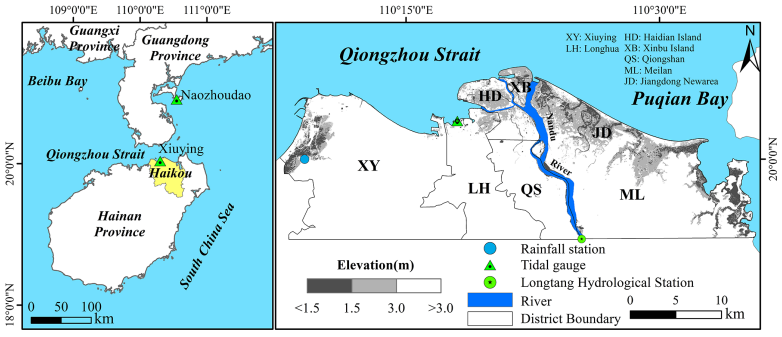

Figure 4.1: The geographic location of tide stations and Nandu River in Haikou and the basic geographic information of Haikou.

Table 4.1: Data profile of this study.

Name	Attributes	Source
DEM, Haikou	2018, 5 m	Department of Emergency Management of Hainan Province
DEM, bathymetry	2019, 500 m	https://www.gebco.net/
TC tracks	1949 – 2019, 3 hourly	Shanghai Typhoon Institute of China Meteorological Administration
Rainfall	1960 – 2017, daily	http://data.cma.cn/
Discharge	1960 – 2020, daily	Hainan Hydrology Resources Bureau

4.2.2. DATA

The geographic and meteorological data of the study area were systematically collected in this study (Table 4.1). The topographic map of the study area was provided by the Hainan Emergency Management Department, and the bathymetry data of the South China Sea and Beibu Bay were obtained from the General Bathymetric Chart of the Oceans (GEBCO). The spatial resolution of the topographic map is 5 m, and the bathymetry data are 500 m. The meteorological data include historical TC track data and daily rainfall data from 1960 to 2017. The historical TC track data, which includes the TCs' location (latitude and longitude), 2 min mean maximum sustained wind (MSW, m s^{-1}), and minimum pressure (hPa) near the TC center, were provided by the Shanghai Typhoon Institute of China Meteorological Administration. The daily rainfall data of Haikou were downloaded from the CMA (http://data.cma.cn/) and can be transferred to hourly rainfall by interpolation for inundation simulation. The annual river discharges at Longtang hydrological station from 1960 to 2020 were provided by the Hainan Hydrology and Water Resources Survey Bureau.

4.3. METHODS

4.3.1. MODEL CONFIGURATION AND VALIDATION METHODS

Delft3D Flexible Mesh (DFlow FM), developed by Deltares in 2011, is a practical unstructured shallow water flow calculation model (De Goede, 2020). It can be used for ocean hydrodynamic and surface runoff numerical simulations (Kumbier et al., 2018; Meijer and Hutten, 2018). In this study, the DFlow FM model was established to calculate the hydraulic boundary conditions needed to estimate the overland flow boundary and simulate the overland inundation during the TC period (Gori et al., 2020).

STORM SURGE MODEL

The calculation domain of the storm surge model covers Hainan Province, the South East Sea, and Beibu Bay and roughly ranges from 15-24.5°N and 105.5-118.5°E (Figure 4.1). The minimum mesh grid size is 100 m, and the maximum mesh grid size is 12000 m. The astronomical tide is simulated by importing the phase and amplitude of tidal constituents (Q1, P1, O1, K1, N2, M2, S2 and K2) extracted from the global tidal model (TPXO 8). These constituents represent the primary components of the tidal spectrum

and influence the tidal dynamics in coastal regions. A built-in module in the Delft3D WES (Wind Enhance Scheme) module is employed to calculate the TC wind field according to Holland's formula (Holland, 1980). We use the statistical measures RMSE (root mean square error) and R^2 to evaluate the model performance of the simulated tide (Kumbier et al., 2018). The storm surge model is validated against measured astronomical tides and storm tides (astronomical tide plus storm surge). Storm tide series (TC1415, "Kalmaegi") at Xiuying gauge station were collected from Haikou Municipal Water Authority to validate this model. For the validation of astronomical tide, we also collected astronomical tide for TC1415 from Xiuying and Naozhoudao tide gauge stations. All tide levels were recorded every hour (from 00:00 on 15 September 2014 to 00:00 on 17 September 2014).

OVERLAND FLOODING MODEL

The overland flooding model combines regular and irregular triangular mesh. This model is a surface runoff numerical model, and the mesh grid resolution is set as 50 m. The high-resolution topography of the study area is imported into the model, and it can roughly reflect the effect of the seawall. The average annual discharge (165.81 m^3s^{-1}) at Longtang hydrological station is calculated as the upstream boundary condition. In this model, the storm tide series extracted from the storm surge model serves as the coastal boundary conditions. This model is validated against the measured inundation area and depth. We collect the inundation data of TC1415 and conduct fieldwork in Haikou to validate this model. The overland inundation model can be approximately validated by comparing the inundation map of TC1415 with the measured inundation area and depth.

4.3.2. TCS INFLUENCING HAIKOU

The TCs that pass through the region (18–22 $^\circ N$, 109–113 $^\circ E$) and stay for over 24 hours have an apparent effect on Haikou. According to this, we analyze historical TC tracks and give priority to the TCs passing between latitudes 18 and 22 $^\circ N$ and longitudes 109 and 113 $^\circ E$. TC tracks lasting less than 24 hours in this region are removed in this study. Therefore, 66 TCs from 1960 to 2017 are selected in this study (Figure 4.2), and we construct typhoon wind fields and simulate the storm tide of these TCs. Each TC event has a code; for example, the ninth typhoon in 1963 is coded as TC6309.

4.3.3. COMPOUND FLOODING ASSESSMENT

In this study, we investigate the probability distribution of storm tides to assess compound flood hazards. Based on the storm surge model, the storm tide series of 66 TCs is simulated. The highest storm tides during TCs are used to calculate the probability distribution function at the Xiuying tide gauge station.

Exploring the storm tide distribution can offer comprehension of the probability of compound flood hazards from storm surges. Extreme value distribution (EVD) is widely applied to investigate storm tide probability distribution (Yum et al., 2021). We assume that the storm tide fits either Gumbel or Weibull extreme value functions, then calculate their function fitting parameters. We compare the goodness of fit of two distribution functions (Gumbel, Weibull) with the Kolmogorov–Smirnov (K-S) test. The k-S test is

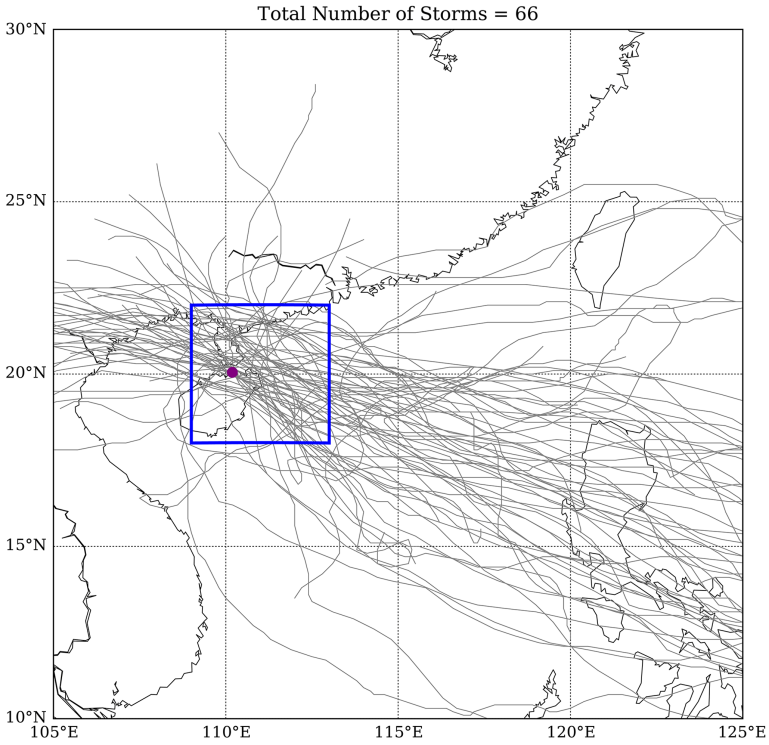

Figure 4.2: Location map for the study area. The purple dot indicates the location of Haikou. Grey-colored lines indicate major historical TC tracks within the region. Blue box indicates the selection region (18-22 °N, 109-113 °E).

an appropriate method to explore the distribution of continuous random variables and can be used to select the best-fitting distribution function. According to the storm tide distribution, we can determine tide levels at different probabilities (P). To investigate the possibility of an extreme storm tide, we replace P with storm tide return periods (T), which is equal to $1/P$. The corresponding TC events in 5-, 10-, 25-, 50-, and 100-yr return periods can be found to compare the compound flood hazards with different storm tides.

4.4. RESULTS AND DISCUSSION

4.4.1. MODEL VALIDATION

We use TC1415 to verify the astronomical tide and storm tide of the storm surge model. In the validation of the astronomical tide, we use the predicted astronomical tide at two gauge stations: Naozhoudao (Zhanjiang, Guangdong) and Xiuying (Haikou, Hainan). The calculation results show that the RMSE is 0.18 and 0.14 m for Naozhoudao and Xiuying gauge stations; the R^2 values of both the Naozhoudao and Xiuying gauge stations are 0.91.

Figure 4.3(a) and Figure 4.3(b) depict simulated and predicted water levels at Xiuying

and Naozhoudao gauge stations. The curves of the simulated astronomical tide at the two stations fit the observed tide level points well. Thus, this model has a good ability to simulate astronomical tides. In the validation of storm tide, we add the wind field of TC1415 in the model and only use the observed tide level at the Xiuying gauge station for validation (Figure 4.3(c)). The calculation of RMSE is 0.34 and R^2 is 0.83. It can be seen from Figure 4.3(c) that the curve of the simulated storm tide is consistent with the observation, and the highest storm tide is well simulated.

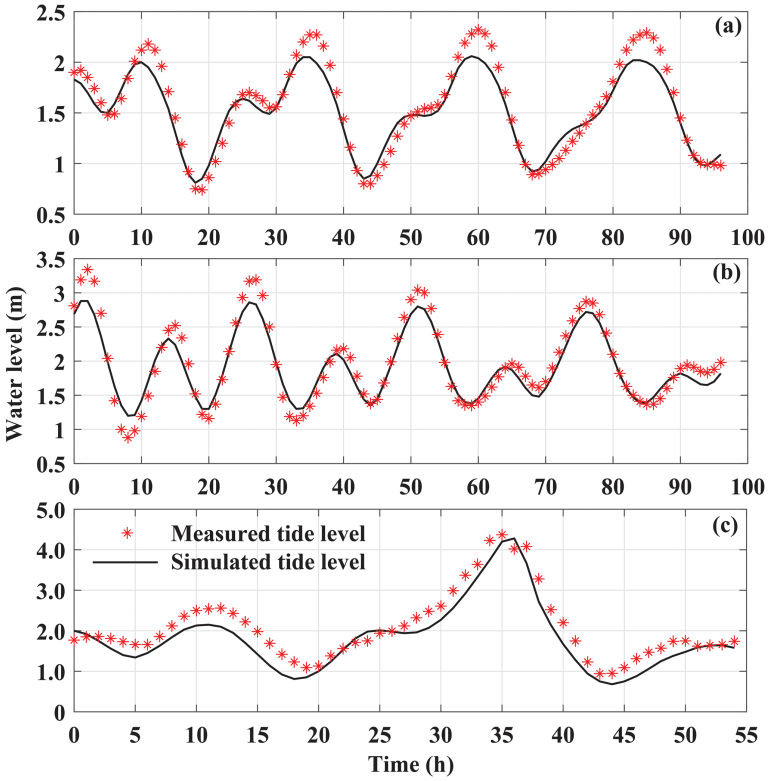

Figure 4.3: The simulation results of astronomical tide and storm tide compared to measured tide levels. (a) Astronomical tide at Xiuying gauge station. (b) Astronomical tide at Naozhoudao gauge station. (c) Storm tide at Xiuying gauge station. Black lines indicate the simulated tide level; red asterisk points indicate measured tide level.

Tide levels along the coastline extracted from the storm surge model serve as coastal boundary conditions for the overland flooding model. We utilize the TC1415 event also to validate the overland flooding model. Comparing the simulation of compound flooding with the measured inundation of roads during TC1415, the main inundation area in the simulation is coincident with the flooded roads (Figure 4.4). Furthermore, the distribution of the simulated inundation area is also consistent with the actual flood distribution. Hence this overland flooding model has a good capacity for modeling and demonstrating TC flood hazards.

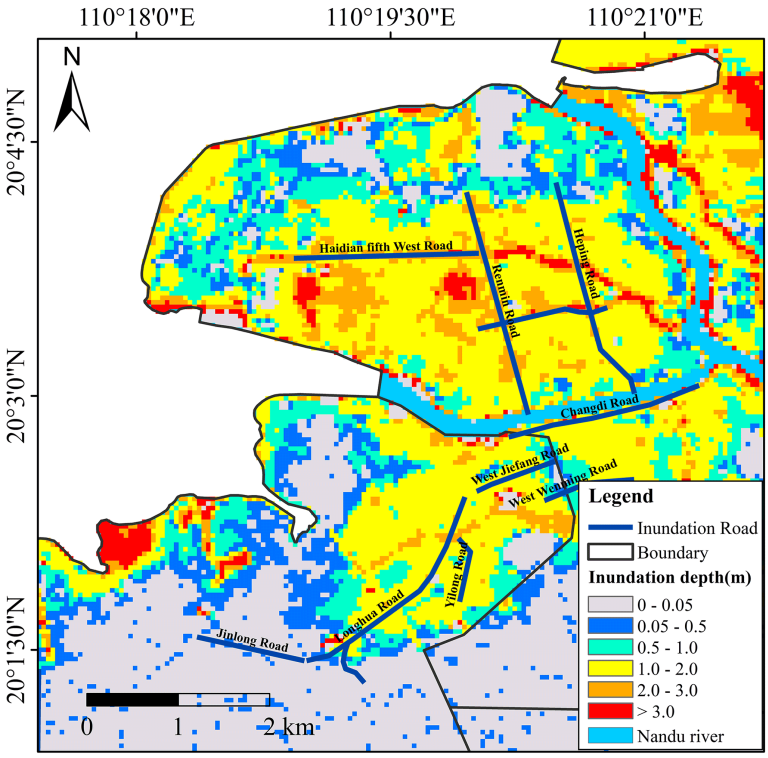

Figure 4.4: Spatial extent of simulated and measured inundation area and depth during TC1415.

4.4.2. STORM TIDE PROBABILITY DISTRIBUTION

The Xiuying gauge station is selected as a representative location to examine the probability exceedance of TC storm tide. The storm tide return period is calculated based on the maximum storm tide in the past 58 years simulated for 66 TCs. The results of the K-S test show that the D value and P value of GUM are 0.0615 and 0.9995, while the D value and P value of WEI are 0.0769 and 0.9876. Thus, the Gumbel extreme value (GEV) distribution function can fit TC storm tide better. Figure 4.5 shows that GEV fits storm tide well, presenting the corresponding TCs under different return periods. Red circles represent the maximum storm tide from the 66 TCs in the past. The solid line represents the estimation of the GEV fitting.

Table 4.2 shows the corresponding TC events and their highest storm tide and accumulated rainfall under different return periods. TC1415, with the highest storm tide, is considered a 100-year event. In order to investigate the compound effects of storm tide and rainstorm on the overland inundation, TCs with higher accumulated rainfall is selected. As a result, TC6311, TC8616, TC8007, and TC7109 are assigned to 50, 25, 10, and 5 years based on GEV fitting, respectively.

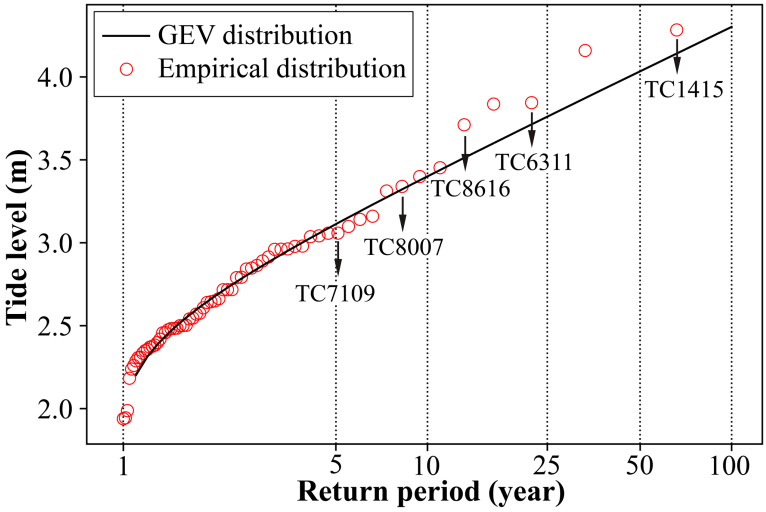

Figure 4.5: Storm tide at Xiuying gauge station as a function of return period based on GEV fitting (solid line).

Table 4.2: The different return periods of TC storm tide and the related TC events.

Return period	Event	Water level (m)	Rainfall (mm)
5Y	TC7109	3.04	137.7
10Y	TC8007	3.31	196.0
25Y	TC8616	3.71	128.0
50Y	TC6311	3.84	191.0
100Y	TC1415	4.28	219.8

4.4.3. COMPOUND FLOODING ASSESSMENT IN DIFFERENT STORM TIDE RETURN PERIODS

Figure 4.6 presents the compound flood inundation maps under 5-, 10-, 25-, 50-, and 100-year return period. For the 5-year inundation map, the major inundation area is distributed along the Jiangdong New Area and Xinbu Island on the northeast coast. The inundation area with sporadic distribution is caused by rainfall in the inland urban area. As return periods increase, Haidian Island, north Longhua district, and northwest Xiuying district begin to have serious flood extents, and the compound flooding severity of Jiangdong New Area and Xinbu Island increases. For 100-yr return period, the inundation depth regions are above 1.0 m, and the floodplain depth is above 3.0 m in most of Jiangdong New Area. Regions with inundation depth below 0.05 m are not evaluated in this study due to their low risk.

Table 4.3: Inundation depth (m) and area (ha) under different return periods.

Flooding depth (m)	5-year	10-year	25-year	50-year	100-year
0–0.5	2139	3757	2364	3957	3704
0.5–1.0	1349	1623	2037	1965	2065
1.0–2.0	1884	1980	3035	3513	3927
2.0–3.0	818	879	1389	1511	2055
> 3.0	29	112	384	516	862
Total	6219	8351	9209	11,462	12,613

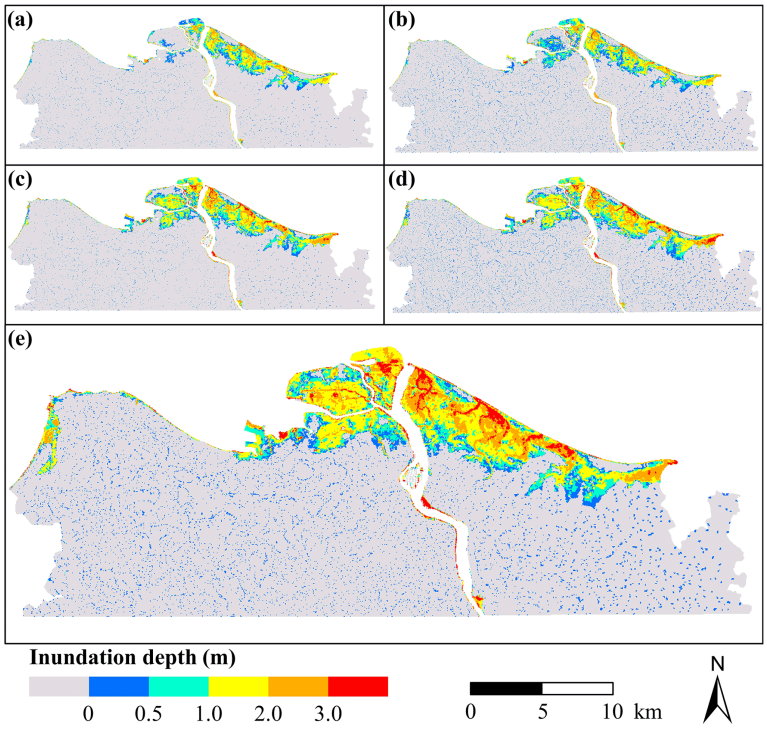

Figure 4.6: The compound flood inundation maps under different return periods: (a) 5-year event, (b) 10-year event, (c) 25-year event, (d) 50-year event, and (e) 100-year event.

Table 4.3 indicates the inundation depth and area under different return periods. In the 100-yr TC event, the total inundation area is 12,613 ha, with 29.4% and 31.1% accounted for by the inundation areas between 0-0.5 m and 1.0-2.0 m, respectively. The combined inundation area between 0.5-1.0 m and 2.0-3.0 m makes up 32.7%. For other TC events, the most extensive inundation areas occur at depths of 0-0.5 m and 1.0-2.0 m. In the case of a 100-yr TC event, areas with depths exceeding 1.0 m expand by approximately 2.5 times compared to a 5-yr TC event.

4.4.4. QUANTITATIVE COMPARISON SINGLE-DRIVEN FLOOD HAZARD AND COMPOUND FLOOD HAZARD

Figure 4.7 illustrates the maps of rainstorm inundation and storm tide flooding under different return periods. In each rainfall scenario, the overall inundation depth is below 1.0m, while in each storm tide scenario, the overall inundation depth is above 1.0m. When comparing the rainstorm inundation map and storm tide flooding map in the same TC event, it is obvious that storm tide flooding is significantly worse than rainstorm inundation.

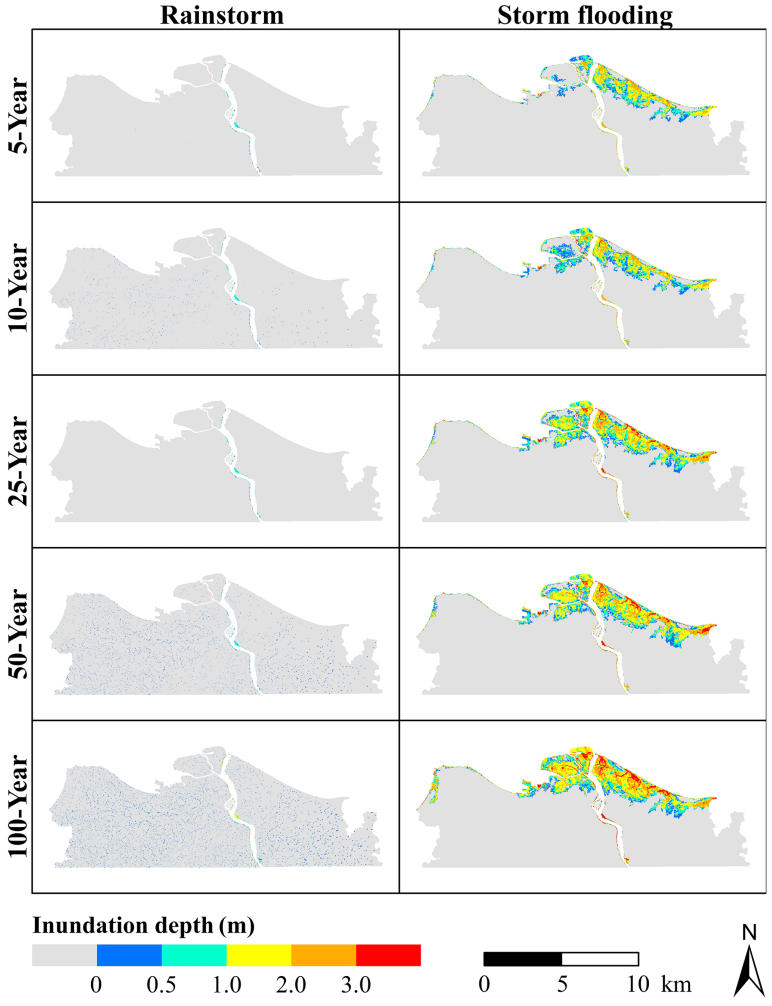

Figure 4.7: The inundation maps of rainstorm and storm flooding under different return periods.

Figure 4.8 compares the overall inundation area of rainstorms, storm tides, and compound flooding under different return periods. The inundation area of compound flood-

ing exceeds the inundation area of rainstorm inundation and storm tide flooding in each TC event. Thus, compound flood hazards can have more serious consequences than rainstorms and storm flooding (Bevacqua et al., 2019; Zscheischler et al., 2018). Moreover, it can be seen from Figure 4.8 that compound flooding has more inundation area than the accumulation of rainstorm and storm tide flooding under different return periods. For example, in the TC6311 scenario, the total inundation area of compound flooding is 11462 ha, exceeding the sum of rainstorm inundation and storm tide flooding, which is 10616 ha. Therefore, compound flood hazards are more destructive than the combination of single-driven flood hazards and have a certain amplification effect.

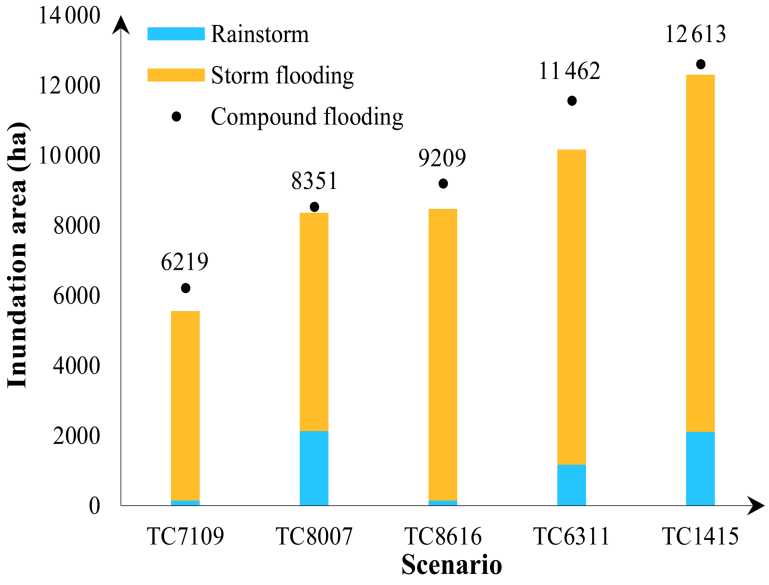

Figure 4.8: The comparison of the overall inundation area of rainstorm, storm flooding and compound flooding in each TC event.

However, storm tides and rainstorms are the driving factors in a compound flood hazard (Hsiao et al., 2021). This study investigates the compound effect of flood hazards by studying the probability distribution of the highest storm tides during TCs. Many studies have confirmed that rainfall and storm surge have statistically positive dependence (Wahl et al., 2015). Hence, it is of practical significance to reveal compound flood risk considering the statistical dependence of rainfall and storm surge. Copula is a kind of function connecting joint distributions and marginal distributions. Zhang et al. (2021) calculated the overtopping occurrence by determining the correlations between tidal levels and wave heights based on the copula function. In recent years, the copula function has been confirmed to model and describe the dependence between flood variables and express compound flood risk (Zellou and Rahali, 2019). H. Xu et al. (2019) employed the copula function to investigate the bivariate return period of compounding rainfall and storm tide events, finding that the joint probability analysis can reveal more adequate and comprehensive risk about compound events than univariate analy-

sis. Therefore, in future works, we will adopt the copula function to investigate the joint occurrence of rainfall and storm surge during TCs, further assessing extreme compound flooding severity.

4.5. CONCLUSIONS

This study applies a coupled methodology of combining the storm surge model and the overland flooding model to investigate the compound effect of flood hazards during TCs. We simulate and assess compound floods under different return periods of storm tides. The results show that storm tide is the key driving factor of compound flood inundation in Haikou, and the tide level decides the inundation extent. When quantitatively comparing compound flooding with rainstorm inundation and storm flooding, we find that it is more destructive than single-driven flood hazards, and the compound effect exceeds the accumulated effects of single-driven floods. The co-occurrence of heavy rainfall and strong storm surges in extreme TCs could intensify compound flood inundation. Simply accumulating every single-driven flood hazard to define compound flooding may cause underestimation.

In this study, we selected the typical TC scenarios based on storm tide probability distribution. The high storm tide has been confirmed to be the main driving factor of flooding. Considering that rainfall is also the driving factor of TC compound flooding, we will focus on the joint probability distribution of rainfall and storm tide in future research. Although this study is limited to Haikou City, we confirmed that other coastal cities can adopt the methodology of coupling two hydrodynamic models to quantitatively assess compound flooding risks. It can conveniently capture the dynamic of rainfall and storm surge and directly observe the change of inundation area to display the effect of rainfall and storm surge in compound events. For future research on extreme TC compound flooding, climate change factors should be taken into consideration, such as sea level rise and land subsidence, and the copula function can be applied to study the statistical dependence between heavy rainfall and strong storm surge under the changing environment to reveal extreme flood risk in coastal cities.

BIBLIOGRAPHY

Bevacqua, E., Maraun, D., Vousdoukas, M., Voukouvalas, E., Vrac, M., Mentaschi, L., & Widmann, M. (2019). Higher probability of compound flooding from precipitation and storm surge in europe under anthropogenic climate change. *Science advances*, *5*(9), eaaw5531.

Bilskie, M. V., Zhao, H., Resio, D., Atkinson, J., Cobell, Z., & Hagen, S. C. (2021). Enhancing flood hazard assessments in coastal louisiana through coupled hydrologic and surge processes. *Frontiers in Water*, *3*, 609231.

De Goede, E. D. (2020). Historical overview of 2d and 3d hydrodynamic modelling of shallow water flows in the netherlands. *Ocean Dynamics*, *70*(4), 521–539.

Deltares. (2018). D-flow flexible mesh.

Emanuel, K. (2017). Assessing the present and future probability of hurricane harvey's rainfall. *Proceedings of the National Academy of Sciences*, *114*(48), 12681–12684.

Fang, J., Wahl, T., Fang, J., Sun, X., Kong, F., & Liu, M. (2021). Compound flood potential from storm surge and heavy precipitation in coastal china: Dependence, drivers, and impacts. *Hydrology and Earth System Sciences*, *25*(8), 4403–4416.

Gori, A., Lin, N., & Xi, D. (2020). Tropical cyclone compound flood hazard assessment: From investigating drivers to quantifying extreme water levels. *Earth's Future*, *8*(12), e2020EF001660.

Gutierrez, B. T., Plant, N. G., & Robert, T. E. (2011). A bayesian network to predict coastal vulnerability to sea level rise. *Journal of Geophysical Research Atmospheres*, *116*(F2), 167–177.

Hallegatte, S., Green, C., Nicholls, R. J., & Corfee-Morlot, J. (2013). Future flood losses in major coastal cities. *Nature Climate Change*, *3*(9), 802–806.

Hsiao, S.-C., Chiang, W.-S., Jang, J.-H., Wu, H.-L., Lu, W.-S., Chen, W.-B., & Wu, Y.-T. (2021). Flood risk influenced by the compound effect of storm surge and rainfall under climate change for low-lying coastal areas. *Science of the total environment*, *764*, 144439.

Huang, W., Ye, F., Zhang, Y. J., Park, K., Du, J., Moghimi, S., Myers, E., Pe'eri, S., Calzada, J. R., Yu, H., et al. (2021). Compounding factors for extreme flooding around galveston bay during hurricane harvey. *Ocean Modelling*, *158*, 101735.

Keellings, D., & Hernández Ayala, J. J. (2019). Extreme rainfall associated with hurricane maria over puerto rico and its connections to climate variability and change. *Geophysical Research Letters*, *46*(5), 2964–2973.

Kumbier, K., Carvalho, R. C., Vafeidis, A. T., & Woodroffe, C. D. (2018). Investigating compound flooding in an estuary using hydrodynamic modelling: A case study from the shoalhaven river, australia. *Natural Hazards and Earth System Sciences*, *18*(2), 463–477.

Leonard, M., Westra, S., Phatak, A., Lambert, M., van den Hurk, B., McInnes, K., Risbey, J., Schuster, S., Jakob, D., & Stafford-Smith, M. (2014). A compound event frame-

work for understanding extreme impacts. *Wiley Interdisciplinary Reviews: Climate Change*, *5*(1), 113–128.

Lian, J. J., Xu, K., & Ma, C. (2013). Joint impact of rainfall and tidal level on flood risk in a coastal city with a complex river network: A case study of fuzhou city, china. *Hydrology Earth System Sciences*, *17*(1), 679–689.

Lian, J., Xu, H., Xu, K., & Ma, C. (2017). Optimal management of the flooding risk caused by the joint occurrence of extreme rainfall and high tide level in a coastal city. *Natural Hazards*, *89*, 183–200.

Lin, N., Emanuel, K., Oppenheimer, M., & Vanmarcke, E. (2012). Physically based assessment of hurricane surge threat under climate change. *Nature Climate Change*, *2*(6), 462–467.

Marsooli, R., Lin, N., Emanuel, K., & Feng, K. (2019). Climate change exacerbates hurricane flood hazards along us atlantic and gulf coasts in spatially varying patterns. *Nature communications*, *10*(1), 3785.

Meijer, D., & Hutten, R. (2018). 2d urban modelling using delft3d fm.

Rasmussen, D., Bittermann, K., Buchanan, M. K., Kulp, S., Strauss, B. H., Kopp, R. E., & Oppenheimer, M. (2018). Extreme sea level implications of 1.5 c, 2.0 c, and 2.5 c temperature stabilization targets in the 21st and 22nd centuries. *Environmental Research Letters*, *13*(3), 034040.

Santiago-Collazo, F. L., Bilskie, M. V., & Hagen, S. C. (2019). A comprehensive review of compound inundation models in low-gradient coastal watersheds. *Environmental Modelling & Software*, *119*, 166–181.

Valle-Levinson, A., Olabarrieta, M., & Heilman, L. (2020). Compound flooding in houston-galveston bay during hurricane harvey. *Science of the Total Environment*, *747*, 141272.

Wahl, T., Jain, S., Bender, J., Meyers, S. D., & Luther, M. E. (2015). Increasing risk of compound flooding from storm surge and rainfall for major us cities. *Nature Climate Change*, *5*(12), 1093–1097.

Wang, J., Yi, S., Li, M., Wang, L., & Song, C. (2018). Effects of sea level rise, land subsidence, bathymetric change and typhoon tracks on storm flooding in the coastal areas of shanghai. *Science of the total environment*, *621*, 228–234.

Xu, H., Xu, K., Bin, L., Lian, J., & Ma, C. (2018). Joint risk of rainfall and storm surges during typhoons in a coastal city of haidian island, china. *International journal of environmental research and public health*, *15*(7), 1377.

Xu, H., Xu, K., Lian, J., & Ma, C. (2019). Compound effects of rainfall and storm tides on coastal flooding risk. *Stochastic Environmental Research and Risk Assessment*, *33*, 1249–1261.

Xu, K., Ma, C., Lian, J., & Bin, L. (2014). Joint probability analysis of extreme precipitation and storm tide in a coastal city under changing environment. *PLoS One*, *9*(10), e109341.

Yin, J., Lin, N., Yang, Y., Pringle, W. J., Tan, J., Westerink, J. J., & Yu, D. (2021). Hazard assessment for typhoon-induced coastal flooding and inundation in shanghai, china. *Journal of Geophysical Research: Oceans*, *126*(7), e2021JC017319.

Yin, J., Yu, D., Yin, Z., Wang, J., & Xu, S. (2013). Modelling the combined impacts of sea-level rise and land subsidence on storm tides induced flooding of the huangpu river in shanghai, china. *Climatic change*, *119*, 919–932.

Yum, S.-G., Wei, H.-H., & Jang, S.-H. (2021). Estimation of the non-exceedance probability of extreme storm surges in south korea using tidal-gauge data. *Natural Hazards and Earth System Sciences*, *21*(8), 2611–2631.

Zellou, B., & Rahali, H. (2019). Assessment of the joint impact of extreme rainfall and storm surge on the risk of flooding in a coastal area. *Journal of Hydrology*, *569*, 647–665.

Zhang, M., Dai, Z., Bouma, T. J., Bricker, J., Townend, I., Wen, J., Zhao, T., & Cai, H. (2021). Tidal-flat reclamation aggravates potential risk from storm impacts. *Coastal Engineering*, *166*, 103868.

Zheng, F., Westra, S., & Sisson, S. A. (2013). Quantifying the dependence between extreme rainfall and storm surge in the coastal zone. *Journal of Hydrology*, *505*(21), 172–187.

Zscheischler, J., Westra, S., Van Den Hurk, B. J., Seneviratne, S. I., Ward, P. J., Pitman, A., AghaKouchak, A., Bresch, D. N., Leonard, M., Wahl, T., et al. (2018). Future climate risk from compound events. *Nature Climate Change*, *8*(6), 469–477.

5

COMBINING STATISTICAL AND HYDRODYNAMIC MODELS TO ASSESS COMPOUND FLOOD HAZARDS

While the statistical dependence between flood drivers, i.e., rainfall and storm surges, has been extensively studied, the sensitivity of the inundated areas to the relative timing of the driver's peaks is less understood and location-dependent. To fill this gap, in this chapter, we propose a framework combining a statistical dependence model for compound event definition and a hydrodynamic model to assess inundation maps of compound flooding from storm surges and rainfall during typhoon season in Shanghai. First, we determine the severity of the joint design event, i.e., peak surge and precipitation, based on the copula model. Second, we use the Same Frequency Amplification (SFA) method to transform the design event values in hourly time series to represent boundary conditions to force hydrodynamic models. Third, we assess the sensitivity of inundation maps to the "time lag" between storm surge peak and rainfall. Finally, we define flood zones based on the primary flood driver and we delineate flood zones under the worst compound flood scenario.

The research emphasizes the importance of the timing between storm surges and rainfall in causing flooding. Specifically, the most severe flooding occurs when rainfall happens before the peak of the storm surge. In Shanghai, flooding is primarily driven by storm surges, especially in the city's eastern part. These surges move upstream in the Huangpu River, causing flooding in the city center and nearby districts.

The study highlights the need for an improved system to control flooding from the river, particularly addressing the backwater effect during high surges in the upper and middle Huangpu River. This is crucial for enhancing flood resilience in both established and

newly urbanized areas.

This chapter is currently accepted after peer review: Hanqing Xu, Elisa Ragno, Sebastiaan N. Jonkman, Jun Wang, Jeremy D. Bricker, Zhan Tian, Laixiang Sun. Combining statistical and hydrodynamic models to assess compound flood hazards from rainfall and storm surge: a case study of Shanghai. ***Hydrology and Earth System Sciences***, 2023.

5.1. INTRODUCTION

Despite significant advancements in flood management systems (e.g., forecasting and early warning systems), recent compound flood events such as Hurricane Harvey (2017) and Super Typhoon Lekima (2019), have demonstrated the vulnerability of coastal cities (Hendry et al., 2019; Valle-Levinson et al., 2020; Zscheischler et al., 2018). Compound flood events are defined as events generated by the combined effect of multiple physical drivers, e.g., heavy rainfall and storm surge. Due to the interaction between flood drivers, the magnitude of compound events can be greater than the magnitude of events generated by a single driver, e.g., either heavy rainfall or storm surge. Hence, it is important to understand how such interaction is realized in coastal areas prone to compound floods.

According to the Intergovernmental Panel on Climate Change (IPCC), adapting coastal cities to the adverse impacts of climate change is crucial for their long-term resilience and sustainability (Adler et al., 2022). Consequently, a comprehensive assessment of the processes leading to compound floods is crucial to develop targeted and innovative adaptation strategies.

Chinese southeastern coastal cities are highly susceptible to flood hazards caused by typhoons due to their unique geographical location and complex ecological environment (Xu et al., 2023). During the occurrence of typhoons, the simultaneous presence of heavy rainfall and strong storm surge can result in severe and destructive flood events (Ridder et al., 2020; Santiago-Collazo et al., 2019). In this context, the effective management of flood risk relies on the integration of statistical and hydrodynamic modeling to assess the extent and potential impact of a flooding event.

In recent years, a growing body of research has focused on the probabilistic characterization of compound flooding (Gori et al., 2020; Moftakhari et al., 2019; Xu et al., 2023). Bevacqua et al. (2019) assessed the potential probability of compound flood hazards triggered by heavy precipitation coinciding with high tidal levels across Europe. Gori et al. (2020) simulated a large number of realistic TC events to examine TC flooding driven by rainfall and storm surges.

At the same time, hydrodynamic models have been widely used to simulate flood extent due to single or multiple flood drivers (Shi et al., 2020; Wang et al., 2018; Yin et al., 2016). Hydrodynamic models are effective in simulating the consequences of rainfall-runoff and storm surge during typhoon events (Kumbier et al., 2018; Zellou and Rahali, 2019) and can improve our understanding of region-specific hydrodynamics and the genesis mechanisms of compound flooding scenarios (Xu et al., 2022). Such numerical models necessitate boundary conditions, which include hourly time series of sea water level and rainfall data, to ensure precise and effective simulations of inundation extent and depth. Paprotny et al. (2017) combine a Bayesian-network-based model and a one-dimensional steady-state hydraulic model in place of conventional rainfall-run-off models to carry out flood mapping for Europe. Moftakhari et al. (2019) proposed a method linking bivariate statistical models and hydrodynamic models to estimate compound floods resulting from upstream discharge and downstream water levels in tidal estuaries. Gori et al. (2020) conducted an investigation into compound flood hazards under climate change by combining physical models and joint probability analysis, highlighting its effectiveness in reducing computational expenses.

Generally, copula models can provide information on the joint severity of multiple flood drivers, like rainfall, river discharge and storm surge, which needs to be further processed to become hydraulic boundary conditions. However, in the case of multiple flood drivers (e.g., surge and rainfall), it is essential to consider not only the statistical dependence of the drivers but also the physical interactions between them in terms of flooding processes. This comprehensive approach is crucial for a more accurate assessment of compound floods and the development of effective flood management strategies. For example, when high sea levels from storm surges coincide with increased river water flow due to heavy rainfall, it would lead to backwater effects for drainage and result in localized flooding. This implies the need to investigate methods to move from the definition of the severity of the event to the physical interaction of the flood drivers at a sub-daily time scale.

Moreover, when sub-daily observations are available to force a hydrodynamic model, to obtain a better understanding of the generation process of a compound flood, it is necessary to investigate the sensitivity of the flood extent to the relative timing between the drivers, i.e., between storm surge peak and rainfall. This enables a clear identification of inundation zones and their respective drivers, which are key information, especially in urban planning to improve the resilience of the system. Currently, there is limited research on how to clearly define flood zones in coastal cities based on their main flood sources (Jane et al., 2020; Muñoz et al., 2021) since a systematic numerical analysis is required to delineate flood zones, which are very sensitive to the relative occurrence of the tidal fluctuation and the rainfall event.

The objective of this study is to combine dependence models for the probabilistic characterization of compound events with hydrodynamic models to improve the identification of flood zones prone to compound floods. To assess flood hazards and the associated main physical drivers we propose the following framework (Figure 5.1): (1) determine events of surge and rainfall from their joint probability of occurrence; (2) select historical events to derive sub-daily signal of surge and rainfall; (3) merge (1) and (2) via the SFA method to generate boundary conditions; (4) simulate flood zones for various time lags between peak surge and rainfall to enable adaptation strategies specific to the type of flood driver(s). A comprehensive urban hydrodynamic inundation model is used to assess the sensitivity of the inundation maps to the relative timing between peak surge and rainfall. This quantitative assessment methodology of compound flooding can assist engineers and urban planners in designing resilient structures in flood-prone areas.

5.2. MATERIALS

5.2.1. STUDY AREA

Shanghai, a coastal megacity located in the Yangtze River delta, spans a total area of 6,340.5 km^2 and had a population of 24.87 million in 2020 (Figure 5.2). The city experiences an annual rainfall of approximately 1,200 mm, with the rainy months falling between June and September. During this period, Shanghai is prone to frequent typhoons and rainstorms, which often result in storm flooding, leading to severe damage. In 1997, Typhoon Winnie caused economic damage exceeding USD 100 million. Despite the

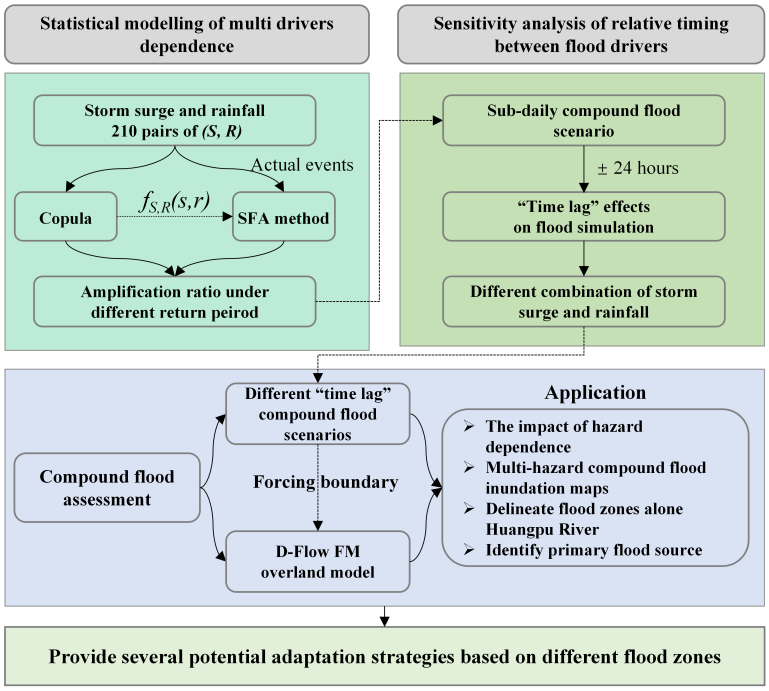

Figure 5.1: Flowchart of this study.

presence of Shanghai's extensive flood mitigation measures (e.g., 523 km seawall, comprehensive drainage systems and advanced water level monitoring systems), the city experienced significant impacts during Typhoon Winnie in 1997 (killed 342 people and caused a direct economic loss of USD 4.3 billion). These instances highlight Shanghai's persistent vulnerability to extreme weather events.

In 1997, Typhoon Winnie caused economic damage exceeding US $100 million, with water levels rising to 5.99 m, a level equivalent to an event expected on average once every 1000 years (Xu et al., 2022). In 2013, Typhoon Fitow broke records at Mishidu gauge along the Huangpu River with water levels reaching 4.61 m (Ke et al., 2018). Despite the presence of Shanghai's extensive flood mitigation measures (e.g., 523 km seawall, comprehensive drainage systems and advanced water level monitoring systems), the city experienced significant impacts during Typhoon Winnie in 1997 and Typhoon Fitow in 2013. These instances highlight Shanghai's persistent vulnerability to extreme weather events.

5.2.2. DATASET

Two flood drivers are considered in this study: storm surge peaks and associated daily rainfall. Daily rainfall is collected from the China Meteorological Administration (CMA, http://data.cma.cn/) Meteorological Data Center, covering the period from 1961 to 2018. More specifically, the reanalysis dataset of storm surge peaks from 1961 to 2018 located

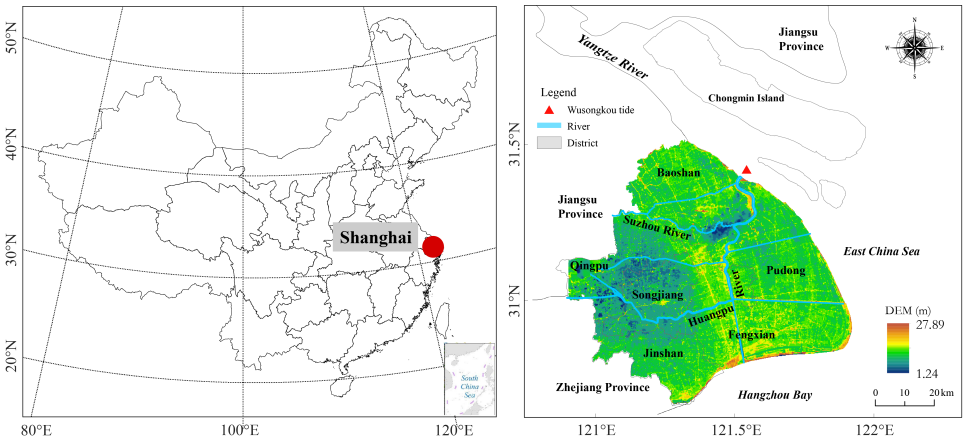

Figure 5.2: Location map of the study area and digital elevation map of Shanghai (red dot in the left graph is the location of Shanghai in China. The red triangle in the right graph shows Wusongkou tide gauge. The DEM data use the Wusong datum).

5

at the mouth of the Huangpu River (Figure 5.2) and associated rainfall used here is the same as the one described and used in Xu et al. (2022) and the reader is referred to that paper for further details on data processing. To obtain hourly boundary conditions, a representative hourly storm surge pattern and hourly rainfall hyetograph are selected from the Shanghai Municipal Water Authority and CMA.

In addition to flood drivers, we use land use data to analyze the potential impact of compound floods. Our approach involves directly coupling the inundation maps with land use data to identify the potential impacts, without employing a separate damage function. In this study, impacts are thus quantified in terms of the affected area for different land use types in different flood zones. The land use type data of Shanghai in 2010 comes from the Shanghai Institute of Surveying and Mapping. This represents the most detailed data available for Shanghai; however, it's important to recognize that land use patterns and urban development may have evolved since then. The land use type is further divided into 4 categories, which are residential land (including urban residential land and rural homestead), transportation and public service land (including commercial service land, public management and railway, highway, port and other transportation facilities), industrial land, green and agricultural land (including farmland, garden land, woodland and park green space).

5.3. METHODS

5.3.1. SAME FREQUENCY AMPLIFICATION FOR GENERATING BOUNDARY CONDITIONS

Drawing on the concept of an amplifier, we implement the Same Frequency Analysis (SFA) method to establish boundary conditions for hydrodynamic modelling (Xiao et al., 2009). The SFA method amplifies observed events ($V_0(t)$) to meet the design criteria ($V_i(t)$) via a constant amplification factor (A), then $V_i(t) = A \cdot V_0(t)$. In this specific case

study, hourly storm surge and hourly hyetograph over a window of 24 hours are amplified based on predetermined design events expressed in terms of storm surge peaks and total daily rainfall.

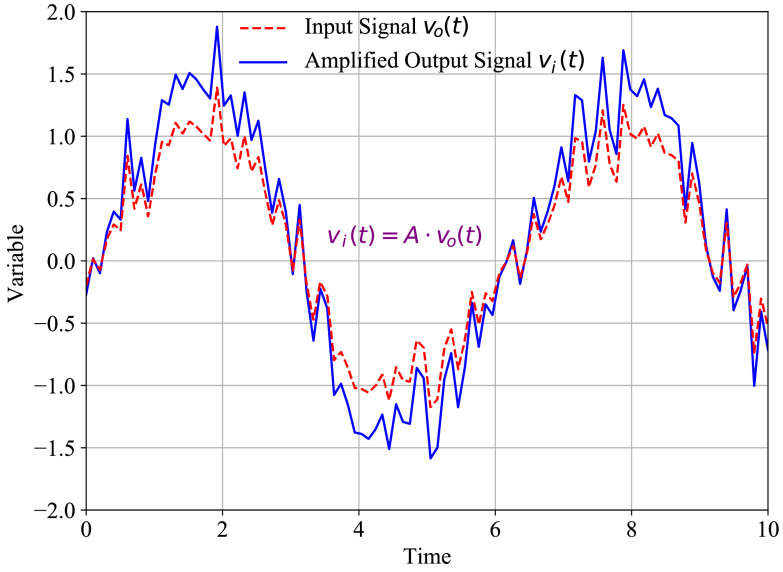

Figure 5.3: Principal of the Same Frequency Analysis (SFA) based on the principle of signal amplification.

These design values are derived from the probabilistic dependence model presented in Xu et al. (2022). Readers are referred to Xu et al., 2022 for details on the selection of the severity and magnitude of the event of interest.

Since design values are single values, to obtain hourly storm surge and rainfall time series the following steps are considered. First, a local typical storm surge pattern and rainfall hyetograph over a window of 24 hours are selected from historical observations. According to the peak surge and cumulative rainfall volume obtained from the joint probability model, we then calculate the amplification ratio by dividing the peak of the typical surge pattern and the cumulative value of rainfall by the corresponding design event, Figure 5.4. The amplification factor is estimated by dividing the design value of the peak surge or cumulative rainfall signal from the typical storm event. By applying this amplification factor, we ensure the amplification ratio essentially adjusts the typical storm event to match the desired design criteria based on the design value from the copula function.

5.3.2. HYDRODYNAMIC OVERLAND INUNDATION MODEL

D-Flow FM, developed by Deltares in the Netherlands, has been widely applied for water flow simulations, including storm surge and overland inundation, because of its capability of simulating 2D and 3D shallow water flow. It integrates structured and unstructured grids, which is convenient for partial grid refinement and predicts the behaviour of water flow for flood modelling in coastal regions (Deltares, 2018). Ke et al. (2021) developed

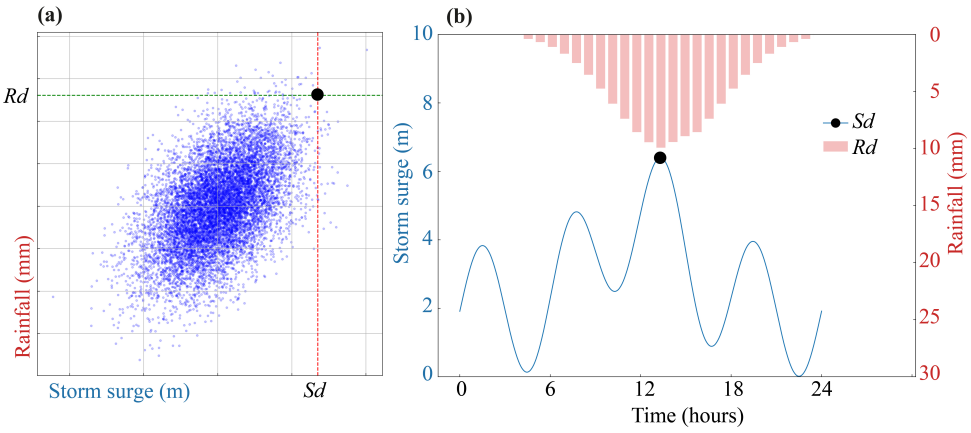

Figure 5.4: Sketch graph to illustrate the combination of the copula and SFA method. Panel (a) represents the dependence model of surge peaks and accumulated rainfall to derive their respective design values S_d and R_d. Panel (b) illustrates the amplified signals where the highest peak corresponds to the design value S_d and the volume of rainfall corresponds to the design value R_d.

5

a 2D urban model for Shanghai with D-Flow FM capable of reproducing coastal, fluvial, pluvial and interacting flood dynamics. Hence, we use the D-Flow FM hydrodynamic model, equipped with flexible meshing, efficient numerical schemes and comprehensive physical equations, to simulate overland flood inundation maps. The model used in this study incorporates rainfall and storm surge boundary conditions and takes into account floodwalls along the Huangpu River in Shanghai, as developed and validated by Ke et al. (2021). We use the digital elevation model data acquired from the Institute of Geographic Sciences and Natural Resources Research, Chinese Academy of Sciences. River, flood wall and discharge data obtained from the Shanghai Municipal Water Authority, to develop the urban inundation model. The overland flooding model combines regular rectangular and irregular triangular meshes. This model is a surface runoff numerical model, and the mesh grid resolution is set as 150 m. The storm surge at the Wusongkou gauge is used as the downstream boundary condition for the overland inundation model. The hourly rainfall hyetograph data from the CMA is input to the overland inundation model to determine the spatial and temporal distribution of rainfall across Shanghai.

5.3.3. DEFINITION OF DIFFERENT FLOOD ZONES

To discern the principal flood contributor, namely storm surge and/or precipitation, for a particular region, Bilskie and Hagen (2018) proposed a floodplain division into three zones based on the dominant contributor: fluvial (surge), transition (surge and precipitation) and pluvial (precipitation) zones. Here, we are interested in defining such zones in the city of Shanghai since they represent key information to develop targeted adaptation strategies. Hence, we run the hydrodynamic model for three different cases (Table 5.1). In Case 1, only the tidal level time series is taken as input, with no rainfall, to identify fluvial zones. In Case 2, rainfall and a fixed tidal level of 0 meters are taken as the

Table 5.1: Cases used in flood zone delineation.

Case	Inundation Types	Description of Modelling Approach
Case 1	Fluvial Zones	Tidal level without rainfall
Case 2	Pluvial Zones	Rainfall with a fixed tidal level of 0 meters
Case 3	Transition Zones	Tidal level and corresponding return period rainfall

boundary conditions to identify pluvial zones. In Case 3, both storm surge and rainfall-runoff processes are considered to identify transition zones. We expect that areas along the river floodplain are more prone to flooding due to high surges and backwater effects. On the other hand, we expect that inland areas are prone to pluvial flooding since rainfall becomes the predominant contributor to flooding.

5.4. RESULTS

5.4.1. HOURLY BOUNDARY CONDITIONS MERGING COPULAS AND SFA

In this study, we use the hourly storm surge curve at the Wusongkou tidal gauge and rainfall hyetograph in Shanghai recorded during Typhoon Winnie (9711), between 18th August to 19th August, as the basic curves to construct boundary conditions. This specific event stands out as it represents a noteworthy combination of extreme storm surge and heavy rainfall. Typhoon Winnie brought historical records of a storm tide of 5.99 m at Wusongkou tide gauge and 134.3 mm rainfall in 24 hours. Since this event is representative of a combination of extreme storm surge and heavy rainfall, it is suitable for studying the impacts of compound floods.

The amplification factor for storm surge and rainfall is estimated so that the amplified storm and rainfall match the design values derived from the probabilistic-dependent model presented by Xu et al. (2022) and shown in Figure 5.5. Since Shanghai is generally more vulnerable to fluvial flooding, we select the joint design values such that the surge design value corresponds to the event with a return period of 1000 years (the design standard of flood wall alone middle and lower reaches of Huangpu River) when yearly maximum water level from 1912 to 2013 are analyzed independently (Ke et al., 2018). The associated rainfall design value is obtained from the dependence model, Figure 5.5(a). By fixing the design value of the surge peak, the pairs of surge and rainfall with the highest density correspond to a joint event with a return period of 200 years considering the "AND" scenario, i.e., the probability that both surge and rainfall are higher than their respective thresholds is 0.005 (Figure 5.5(a)). The SFA is then applied to the surge and rainfall during Typhoon Winnie and amplified based on the designed value identified (Figure 5.5(b)).

5.4.2. SENSITIVITY OF INUNDATION MAPS TO THE TIME LAG BETWEEN HOURLY PEAK STORM SURGE AND RAINFALL

To understand the combined effect of storm surge and rainfall, it is important to investigate the relative timing between the peaks of these two drivers. Hence, we investigate how the relative timing of the peak surge and rainfall affect flood inundation depth

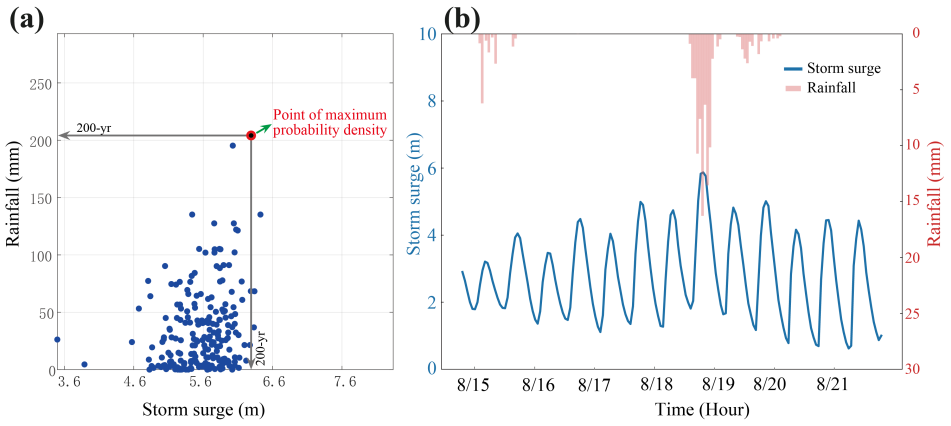

Figure 5.5: (a) Bivariate statistical analysis of joint distribution with "AND" scenario between peak storm surge and corresponding cumulative rainfall by MvCAT; (b) The boundary conditions for the hydrodynamic model based on a scenario of no time lag between the peak storm tide and the corresponding cumulative rainfall observed during typhoon Winnie.

5

by running the D-Flow FM hydrodynamic model multiple times, each time with a predefined distance between the peaks spanning over a temporal window of ±24 hours. For each run, the average inundation depth overall flooded locations (here labeled as the cumulative inundation depth) are recorded.

We observe that maximum cumulative inundation depth occurs when the rainfall event occurs 2 hours prior to the surge peak and is considered. In this scenario, floods mainly occur in the Upper Huangpu River, the maximum cumulative inundation depth exceeds 1.0 m in the southwestern Qingpu district and the southern Songjiang district, while some areas in the downtown area are covered by flood water with depths over 2 m (Figure 5.6(a-b)). The water level in rivers is high, potentially exceeding the capacity of drainage systems and pumping infrastructure to mitigate the inundation. This results in more extensive flooding in low-lying areas. In contrast, when rainfall takes place after the surge peak (e.g. +12 hours later), the water levels in the river have time to recede. This allows for improved drainage and pumping capacity in the city, reducing the cumulative inundation depth to 0.21 m (Figure 5.6(c-d)).

Generally, we observed a cumulative inundation depth greater than 0.25 m when the rainfall event precedes the peak of the surge, i.e., between -24 to 0 hours. Rainfall events occurring after the storm surge peak (> 0 hours) do not increase the cumulative inundation depth (Figure 5.6(e)). The cumulative inundation depth stabilizes at around 0.21 m when rainfall peaks about 12 hours after the surge peak. Therefore, the observed difference in flooding between these scenarios can be attributed to the combination of high water levels in rivers following the surge peak and the capacity of the drainage and pumping systems. This highlights the critical importance of considering the relative timing of events when determining the flood extent and severity in fluvial urban regions.

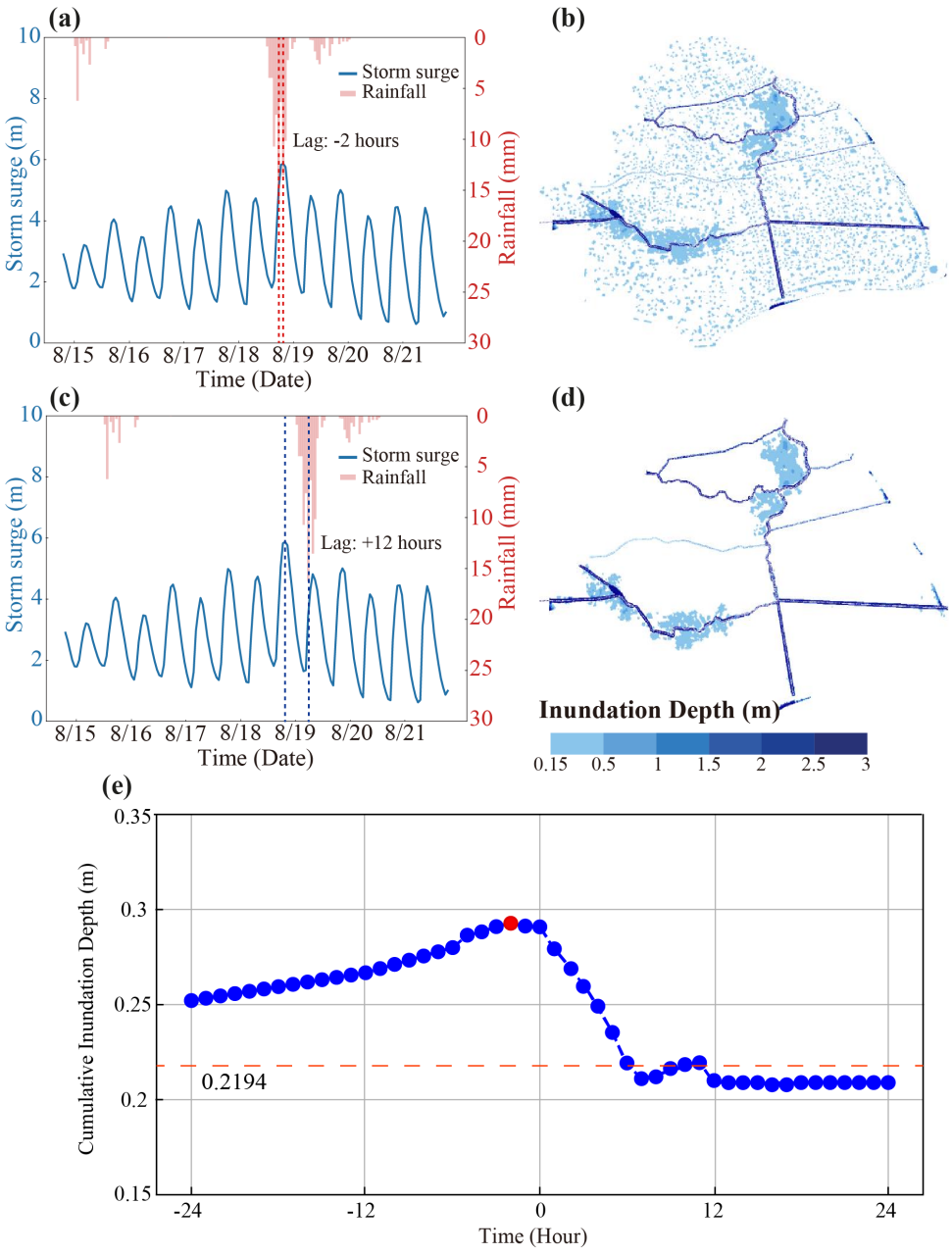

Figure 5.6: Cumulative inundation depth under the combined impact of storm surge and rainfall with -2 and +12 hour lags. (a) The boundary conditions of -2h time lag between the peak storm surge and the corresponding cumulative rainfall; (b) Flooding inundation under the -2h time lag scenario. (c) The boundary conditions of the scenario with +12h time lag between the peak storm surge and the corresponding cumulative rainfall; (d) Flooding inundation under the +12h time lag scenario. (e) Cumulative inundation depth with different time lags. (the horizontal dashed line is the maximum cumulative inundation depth for uniform rainfall. The red dot means the maximum cumulative inundation depth by -2 hours lag of compound event).

5.4.3. FLOOD ZONES

The distribution of flood zones would vary significantly given different storm events due to the different timing between rainfall and storm surge; here, we investigate the average response of the basin for the worst cumulative inundation depth event (rainfall peaks 2 hours prior to the surge peak). Flood zones are delineated in the entire study area based on the criteria established (Table 5.1).

In general, storm surges are the primary cause of inundation within and along the Huangpu River (represented by red), while the areas situated far from the river, mostly inland, experience inundation primarily due to rainfall (represented by blue). Distinct transitional zones, marked in yellow in Figure 5.7, can be seen surrounding the Huangpu River. We observe three main critical areas (Region A, B and C) due to the obvious cumulative inundation depth. Region A (inundated by 39.68 km^2), with its immediate fluvial adjacency, is dominated by fluvial flooding. Similarly, Region C (inundated by 23.88 km^2) is also dominated by fluvial flooding even though located about 100 km from the coast. This could be due to the river configuration and the backwater effect that prevents the normal discharge of the river into the sea when a high surge occurs. In contrast, Region B (inundated by 34.27 km^2) is the most prone to the combined effect of rainfall and storm surge with the largest transition zone recorded, 2.3 times greater than the transition zone in Region A and 4.4 times greater than the transition zone in Region C. The combination of low elevation and low flood wall makes Region B susceptible to fluvial flooding, which can result in overtopping and further exacerbate flooding.

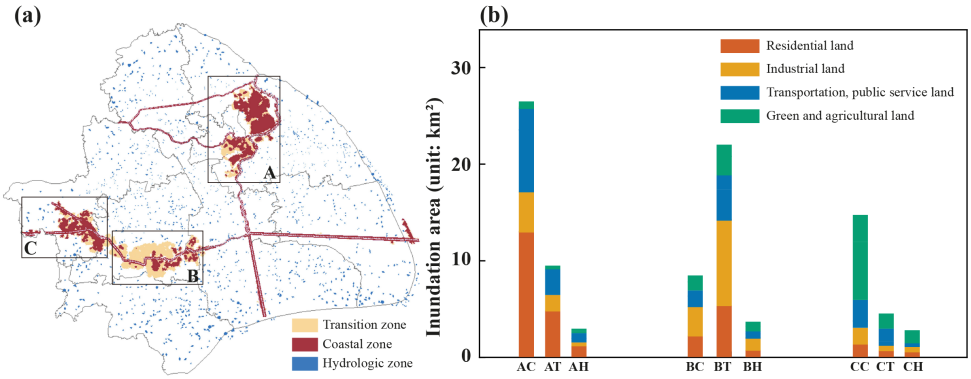

Figure 5.7: (a) Flood zones under 200-yr return period flooding events; (b) The inundation area of different land use combination under 200-yr return period flooding events (C: fluvial zone; T: transition zone; H: pluvial zone). The letters in front of the fluvial zones (A, B, and C) refer to the region investigated.

To gain additional insight into the population exposed in the regions identified as the most affected by a flood event, we investigate urban land use maps. Figure 5.7(b) clearly shows that Region A is mostly residential land, Region B is mostly industrial land and Region C is mostly green and agricultural land. This implies that a different approach is needed when developing strategies for flood control, especially in Region B where the industrial sector is prone to compound flooding (a larger transition zone). These results give insights on how to effectively realize the developmental goals for the year 2035 in Shanghai's new city expansion endeavours. These results suggest that the focal point

should be on reducing the risk in the system for fluvial flooding. This would protect also the upper and middle reaches of the Huangpu River, as well as the newly established urbanized region, with particular attention to low-lying areas in the upper reach of the Huangpu River.

5.5. DISCUSSION

The primary objective of this study was to develop a methodology to quantify flood inundation depth accounting from the relative timing of surge and rainfall and their respective magnitudes, when the dependence between the two events cannot be neglected, such as during typhoon season. In our simulations, the time lag between rainfall and surge peak is equal to -2 hours, i.e., the peak rainfall occurring 2 hours before the surge peak, causes the largest total inundation depth. However, this result depends on our initial choice of the hourly storm tide elevation and rainfall hyetograph amplified based on design requirements. The availability of higher quality data at finer temporal resolution could provide a different and more accurate insight into the sensitivity of the area to the combined effect between rainfall and storm surge. At the same time, we showed that this framework is a valuable option to generate boundary conditions when there is a lack of data.

From a design perspective, this study emphasizes the need for a comprehensive and case-specific understanding of the interaction between surge and rainfall and their relative timing to identify the most suitable adaptation strategy. For example, our results showed that storm surge protection systems can prevent flooding in the upstream reaches of the Huangpu River. Indeed, the river's susceptibility to backwater effects can result in river flooding even during moderate rainfall events. Alternatively, flood protection measures along riverbanks and within the city can also be considered but they should be developed considering storm surge and backwater effects as major drivers for high water in the river. Along with interventions to reduce inundation due to storm surges, implementing rainwater storage and hydrograph peak reduction facilities, such as detention basins, can enhance the capabilities of the urban flood protection system and improve the city's safety, particularly in cases when high rainfall precedes high surge.

However, it is crucial not to overlook hydrological factors, including topography, land use, soil type, and vegetation cover, as neglecting these elements may lead to an inaccurate representation of flood risk. For example, comprehensive land use maps offer an effective tool for delineating flood prevention and mitigation strategies because they rule out solutions not suitable for a specific category. In this study, we combined the land use types with inundation maps, thereby establishing a more holistic understanding of the areas at risk. Within the context of this investigation, we put forth a range of prospective adaptation strategies that can be employed by various vulnerable areas to reduce the impact of compound flooding. We underscore the paramount importance of adopting a comprehensive flood risk management approach that encompasses the entire system, while also emphasizing the necessity for integrated and coordinated measures to effectively tackle the intricate and dynamic nature of compound flooding events. Among these strategies is the proposal for constructing floodgates at the mouth of the Huangpu River, a measure designed to substantially diminish the impact of storm floods on the inner river basin and to prevent or reduce the necessity to raise floodwalls. Insights from

the completed and ongoing designs for international storm surge barriers could serve as valuable references for this investigation (Mooyaart and Jonkman, 2017).

Concurrently, it is imperative to reinforce the flood wall of vulnerable sections on the upstream reach of the Huangpu River and newly urbanized regions to ensure the preservation of their designated flood control capacity until the floodgates at the river mouth are completed. Additionally, in accordance with the latest analysis of Huangpu River tide levels, it is advisable to augment floodwalls to maintain their intended flood control capacity (Ke et al., 2018). By prioritizing these targeted efforts, Shanghai can make significant strides toward achieving its developmental aspirations while effectively managing the risk from compound flooding events.

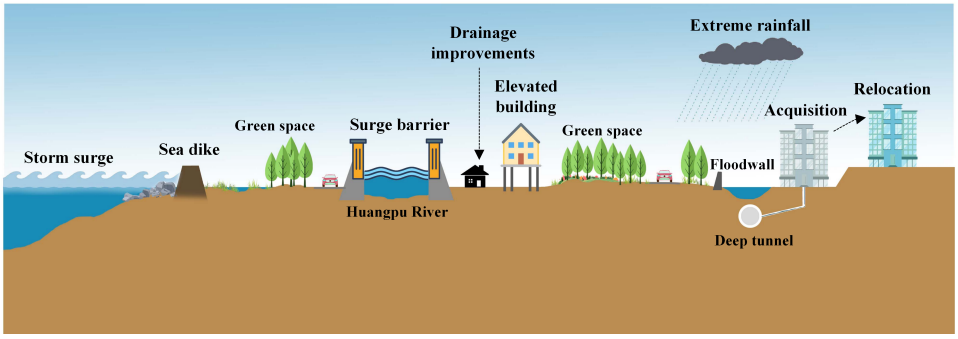

Figure 5.8: Visual of various measures applicable to Shanghai.

5.6. CONCLUSIONS

In this study, we highlight the importance of understanding how the interactions between multiple flood mechanisms change flood hazard maps, in contrast with the current Chinese flood policy which focuses on floods due to only a single driver. Although this study is specific to Shanghai City, the methodology of quantitatively assessing compound flood hazard via a coupled statistical-hydrodynamic model framework is available for other coastal cities.

1) The study allowed us to analyze the dynamics of storm surge and rainfall interactions and their effect on the inundation area under various return periods.

2) The investigation into the impact of temporal windows spanning ±24 hours revealed that the maximum cumulative inundation depth occurs at a temporal lag of -2 hours, highlighting the importance of assessing compound flood hazard "time lag" between different flood driving factors.

3) Storm surge is the primary driver of fluvial flood inundation in Shanghai, with inundated regions primarily situated on both sides of the Huangpu River, and concentrated in the city center and other specific districts.

4) Based on the worst-case inundation map caused by storm surge and rainfall, the flood zones are delineated into fluvial, pluvial and transition zones, enabling us to propose potential adaptation strategies to cope with inundation in Shanghai.

BIBLIOGRAPHY

Adler, C., Wester, P., Bhatt, I., Huggel, C., Insarov, G., Morecroft, M., Muccione, V., & Prakash, A. (2022). Cross-chapter paper 5: Mountains. In H. O. Pörtner, D. C. Roberts, M. Tignor, E. S. Poloczanska, K. Mintenbeck, A. Alegría, M. Craig, S. Langsdorf, S. Löschke, V. Möller, A. Okem, & B. Rama (Eds.), *Climate change 2022: Impacts, adaptation and vulnerability. contribution of working group ii to the sixth assessment report of the intergovernmental panel on climate change* (pp. 2273–2318). Cambridge University Press. https://doi.org/10.1017/9781009325844.022.2273

Bevacqua, E., Maraun, D., Vousdoukas, M., Voukouvalas, E., Vrac, M., Mentaschi, L., & Widmann, M. (2019). Higher probability of compound flooding from precipitation and storm surge in europe under anthropogenic climate change. *Science advances*, *5*(9), eaaw5531.

Bilskie, M., & Hagen, S. (2018). Defining flood zone transitions in low-gradient coastal regions. *Geophysical Research Letters*, *45*(6), 2761–2770.

Deltares. (2018). D-flow flexible mesh.

Gori, A., Lin, N., & Xi, D. (2020). Tropical cyclone compound flood hazard assessment: From investigating drivers to quantifying extreme water levels. *Earth's Future*, *8*(12), e2020EF001660.

Hendry, A., Haigh, I. D., Nicholls, R. J., Winter, H., Neal, R., Wahl, T., Joly-Laugel, A., & Darby, S. E. (2019). Assessing the characteristics and drivers of compound flooding events around the uk coast. *Hydrology and Earth System Sciences*, *23*(7), 3117–3139.

Jane, R., Cadavid, L., Obeysekera, J., & Wahl, T. (2020). Multivariate statistical modelling of the drivers of compound flood events in south florida. *Natural Hazards and Earth System Sciences*, *20*(10), 2681–2699.

Ke, Q., Jonkman, S. N., Van Gelder, P. H., & Bricker, J. D. (2018). Frequency analysis of storm-surge-induced flooding for the huangpu river in shanghai, china. *Journal of Marine Science and Engineering*, *6*(2), 70.

Ke, Q., Yin, J., Bricker, J. D., Savage, N., Buonomo, E., Ye, Q., Visser, P., Dong, G., Wang, S., Tian, Z., et al. (2021). An integrated framework of coastal flood modelling under the failures of sea dikes: A case study in shanghai. *Natural Hazards*, *109*(1), 671–703.

Kumbier, K., Carvalho, R. C., Vafeidis, A. T., & Woodroffe, C. D. (2018). Investigating compound flooding in an estuary using hydrodynamic modelling: A case study from the shoalhaven river, australia. *Natural Hazards and Earth System Sciences*, *18*(2), 463–477.

Moftakhari, H., Schubert, J. E., AghaKouchak, A., Matthew, R. A., & Sanders, B. F. (2019). Linking statistical and hydrodynamic modeling for compound flood hazard assessment in tidal channels and estuaries. *Advances in Water Resources*, *128*, 28–38.

Mooyaart, L., & Jonkman, S. N. (2017). Overview and design considerations of storm surge barriers. *Journal of Waterway, Port, Coastal, and Ocean Engineering*, *143*(4), 06017001.

Muñoz, D. F., Muñoz, P., Moftakhari, H., & Moradkhani, H. (2021). From local to regional compound flood mapping with deep learning and data fusion techniques. *Science of the Total Environment*, *782*, 146927.

Paprotny, D., Morales-Nápoles, O., & Jonkman, S. N. (2017). Efficient pan-european river flood hazard modelling through a combination of statistical and physical models. *Natural Hazards and Earth System Sciences*, *17*(7), 1267–1283.

Ridder, N. N., Pitman, A. J., Westra, S., Ukkola, A., Do, H. X., Bador, M., Hirsch, A. L., Evans, J. P., Di Luca, A., & Zscheischler, J. (2020). Global hotspots for the occurrence of compound events. *Nature communications*, *11*(1), 5956.

Santiago-Collazo, F. L., Bilskie, M. V., & Hagen, S. C. (2019). A comprehensive review of compound inundation models in low-gradient coastal watersheds. *Environmental Modelling & Software*, *119*, 166–181.

Shi, X., Han, Z., Fang, J., Tan, J., Guo, Z., & Sun, Z. (2020). Assessment and zonation of storm surge hazards in the coastal areas of china. *Natural Hazards*, *100*, 39–48.

Valle-Levinson, A., Olabarrieta, M., & Heilman, L. (2020). Compound flooding in houston-galveston bay during hurricane harvey. *Science of the Total Environment*, *747*, 141272.

Wang, J., Yi, S., Li, M., Wang, L., & Song, C. (2018). Effects of sea level rise, land subsidence, bathymetric change and typhoon tracks on storm flooding in the coastal areas of shanghai. *Science of the total environment*, *621*, 228–234.

Xiao, Y., Guo, S., Liu, P., Yan, B., & Chen, L. (2009). Design flood hydrograph based on multicharacteristic synthesis index method. *Journal of Hydrologic Engineering*, *14*(12), 1359–1364.

Xu, H., Tian, Z., Sun, L., Ye, Q., Ragno, E., Bricker, J., Mao, G., Tan, J., Wang, J., Ke, Q., Wang, S., & Toumi, R. (2022). Compound flood impact of water level and rainfall during tropical cyclone periods in a coastal city: The case of shanghai. *Natural Hazards and Earth System Sciences*, *22*(7), 2347–2358. https://doi.org/10.5194/nhess-22-2347-2022

Xu, H., Ragno, E., Tan, J., Antonini, A., Bricker, J. D., Jonkman, S. N., Liu, Q., & Wang, J. (2023). Perspectives on compound flooding in chinese estuary regions. *International Journal of Disaster Risk Science*, 1–11.

Yin, J., Yu, D., Yin, Z., Liu, M., & He, Q. (2016). Evaluating the impact and risk of pluvial flash flood on intra-urban road network: A case study in the city center of shanghai, china. *Journal of hydrology*, *537*, 138–145.

Zellou, B., & Rahali, H. (2019). Assessment of the joint impact of extreme rainfall and storm surge on the risk of flooding in a coastal area. *Journal of Hydrology*, *569*, 647–665.

Zscheischler, J., Westra, S., Van Den Hurk, B. J., Seneviratne, S. I., Ward, P. J., Pitman, A., AghaKouchak, A., Bresch, D. N., Leonard, M., Wahl, T., et al. (2018). Future climate risk from compound events. *Nature Climate Change*, *8*(6), 469–477.

6

CONCLUSIONS AND RECOMMENDATIONS

6.1. MAIN FINDINGS

This dissertation aims to advance the understanding, modelling, and quantification of compound flood hazards in Chinese coastal cities. Assessing the compound flood hazards involves a comprehensive understanding of the interaction between flood drivers. However, the limited historical data poses challenges in accurately estimating compound flood hazards. Additionally, traditional coastal flood models often overlook the interactions between rainfall and storm surges, leading to underestimation of the hazard. Uncertainty remains regarding how climate change would affect compound floods and joint probability distributions between storm surges and rainfall along the Chinese coast.

This dissertation addresses these challenges by proposing methodologies to quantify compound flood hazards at both regional and local scales. The findings from this thesis have the potential to guide the design and implementation of compound flood management systems in Chinese coastal regions, improving the reliability and safety of infrastructure while mitigating the adverse effects of compound flooding.

First, the four research questions formulated in Chapter 1 are answered (section 6.2). Then, recommendations for further research are provided (section 6.3).

6.2. ANSWERS TO THE RESEARCH QUESTIONS

I. *What are the geographical and physical factors determining the relationship between peak surge and rainfall along the Chinese coastline?*

Our analysis shows a positive and statistically significant correlation between surge peaks and rainfall in 10 out of 26 investigated catchments, meaning that high rainfall events are associated with high surges. However, we observe different patterns regarding extreme surge events in southern and northern China. Southern China experiences the highest frequency of such events during the typhoon season, while the majority of surge peaks in the northern part occur in the non-typhoon season. This geographic variation is consistent with expectations, as typhoons predominantly impact the southern region.

Subsequently, we employed a copula-based approach to calculate the joint probability and design value of peak water level and accumulated rainfall considering the impact of relative sea level rise (RSLR) in Shanghai. Seven potential compound flood events have been identified, wherein astronomic tide acts as the primary driver, with storm surge serving as a supplementary factor in one instance. The combined influences of astronomic tide, storm surge, and RSLR collectively contribute to peak water levels, emphasizing the importance of considering all relevant factors during the typhoon season. Hence, it is imperative to monitor and predict the interaction of these factors as integral components of future design standards aimed at enhancing flood preparedness.

II. *What is the added value of explicitly modelling the dependence between peak surge and rainfall when inferring design values for compound flooding in coastal regions?*

Explicitly modelling the dependence between peak surge and rainfall additional information in terms of design can be obtained. We showed that in southern China, specifically on Hainan Island, extreme rainfall events during the typhoon season exhibit greater intensity compared to the majority of annual maxima events, while this is not the case in the northern part of China. This implies that even in flood-prone areas, the actual impact depends on the geographical location and associated climate. These results are obtained by conditionalizing the dependence model between storm surge and rainfall on the level of storm surges of interest.

Moreover, copula functions are flexible to incorporate the effect of SLR on extreme water levels. At the Wusongkou tide gauge in Shanghai, the presented future scenario including relative sea-level rise shows an increase in the design value of extreme water level compared to the scenario without sea-level rise.

III. *Why do synthetic generated data provide valuable options for compound flooding hazards assessment when available observations are limited?*

In regions with limited historical data, synthetic data offers the possibility to generate potential real events. This allows for a more comprehensive exploration of various scenarios and combinations of extreme conditions, such as peak water levels and accumulated rainfall, which is essential for understanding compound flooding. Here, coupling storm surge and overland inundation model shows that storm tide is the primary driver of compound flood inundation in Haikou. In summary, synthetically generated data complement traditional data sources, enhancing our understanding of complex flooding dynamics and contributing to more effective resilient coastal planning efforts.

IV. *What are the potential benefits of combining probabilistic modelling and hydrodynamic modelling for flood hazard quantification in urban environments?*

Statistical dependence models offer a general understanding of the potential of flood hazards with a certain severity and frequency. At the local scale, hydrodynamic models complement statistical models by providing detailed insights into how flood drivers interact with urban topography and infrastructure, leading to a more holistic assessment of flood hazards. The framework proposed combines a statistical dependence model for defining compound events with a hydrodynamic model to assess inundation maps. This combined model enables investigating the sensitivity of inundated areas to the relative timing of storm surge peaks and rainfall peaks during the typhoon season in Shanghai. The results reveal that the maximum cumulative inundation depth occurs when the peak rainfall happens two hours before the peak storm surge, highlighting the importance of assessing the time lag between different flood-driving factors in evaluating compound flood hazards.

Moreover, the combined model enables categorizing flood zones based on their main drivers, i.e., fluvial, pluvial, and transition zones. In Shanghai, storm surge emerges as the primary driver of fluvial flood inundation, concentrating flood risk in specific districts and the city center along both sides of the Huangpu River. This

knowledge is invaluable for engineers and urban planners, guiding the planning and design of both structural and non-structural measures in flood-prone areas to ensure resilience against potential combinations of hazards.

6.3. RECOMMENDATIONS

6.3.1. RECOMMENDATIONS FOR FUTURE RESEARCH

1. **Broadening the model scope and resolution.** Future studies should explore the integration of advanced modelling techniques, including machine learning algorithms and high-resolution numerical simulations, to improve the accuracy and predictive capabilities of compound flood models. There is a need to expand the scope of compound flood modelling to incorporate additional contributing variables such as local precipitation, wave impacts, and coastal flooding nuances. To improve the accuracy of predictive models for short-duration heavy precipitation events in urban environments, future research should also explore the interconnections within tightly coupled hydrodynamic models.

2. **Overcome the data limitations in coastal flood assessment.** One of the primary limitations of this study is the relatively small number of tide gauge sites and the limited length of the available time series, particularly from observations. Presently, the publicly accessible datasets considered in this study constitute the most comprehensive collection of hourly sea level data along Chinese coasts. There exists an urgent necessity for longer datasets to be employed to better evaluate compound flood risk, particularly for the southeastern coasts of China, which are susceptible to TCs. In this study, we solely address two flooding drivers: precipitation and storm surge. However, it is imperative to further investigate the role of other flooding drivers, as well as compound effects under nonstationary conditions. This includes conducting bivariate frequency analysis, evaluating the relationship to climate indices, and considering the implications for flood risk management. The latter aspect is of particular significance, given the limited capacity of drainage systems in many urban areas across China.

3. **Enhancing dimensionality of copula models.** This study explores historical compound flooding resulting from the combination of rain and tide, laying the fundamentals for examining future scenarios influenced by climate-altered typhoon dynamics and sea-level fluctuations. The change of typhoons is expected to greatly impact the frequency and intensity of compound flooding events in coastal regions under climate change. To effectively address the complexities of these future scenarios, enhancements to the current copula joint distribution model are necessary. This expansion includes incorporating higher-dimensional and higher spatiotemporal resolution details related to environmental factors, e.g. rainfall, storm surge, river discharge and sea level rise. Integration of these additional drivers into the copula model framework enables researchers to understand the interactive relationships between drivers in compound flooding, which would provide reliable predictions of compound flooding hazards in response to climate change.

6.3.2. RECOMMENDATIONS FOR PRACTICAL FLOOD MANAGEMENT

1. **Integration of additional values in design provided by joint probability analysis.** This supplementary data on likelihood offers insights for designers, planners, and decision-makers involved in flood management strategies. By incorporating this information into their planning processes, stakeholders can make more informed decisions regarding infrastructure design, land-use planning, and emergency response strategies. This approach enhances the resilience of urban areas against flood hazards by providing a more comprehensive understanding of the probabilistic nature of flooding events and their potential impacts. For example, flood management could be informed by conditional probabilities of rainfall given the 100-year return period storm surge.

2. **Simulating compound flooding using hydrodynamic models.** These models offer a robust framework for integrating multiple flood-driving factors, such as rainfall and storm surges, to simulate complex flood scenarios accurately. By employing hydrodynamic models, practitioners in flood management can gain valuable insights into the interactions and amplification effects of different flood drivers, thereby enhancing their ability to anticipate and respond to compound flooding events. Furthermore, leveraging hydrodynamic models enables the exploration of various mitigation strategies and adaptation measures tailored to address the specific challenges posed by compound flooding. Incorporating these simulation capabilities into practical flood management approaches can significantly improve resilience and preparedness in flood-prone regions, ultimately safeguarding lives, infrastructure, and livelihoods.

3. **Investment in resilience infrastructure.** To deal with compound flooding in Shanghai, investing in strong infrastructure is important. This means building more green spaces, surfaces that can absorb rainstorms, and strong coastal defences. These measures do two things: they help absorb and drain away excess water during compound floods, and they make the city better able to handle different compound flooding drivers. By including these improvements in city planning and development, Shanghai can become much less vulnerable to compound flooding and better prepared for future climate change.

ACKNOWLEDGEMENTS

I would like to thank my daily supervisor, Elisa Ragno, for her invaluable guidance, encouragement, and insightful feedback throughout my research journey. Her dedication and expertise have been instrumental in shaping this dissertation.

I am also grateful to my promoters, Sebastiaan N. Jonkman and Jun Wang, for their unwavering support and mentorship. their profound knowledge and constructive criticism have significantly contributed to the depth and quality of this work.

Special thanks to Matthijs Kok, Jie Yin, Oswaldo Morales Napoles, Davide Pasquali and Zhengbing Wang for being my committee members and providing me with valuable suggestions on the topic. Your thoughtful feedback and keen insights have greatly enhanced this research.

I would also like to express my sincere appreciation to Laixiang Sun, Zhan Tian, Jeremy D. Bricker, Qinghua Ye, Qian Ke and Alessandro Antonini, for their support and assistance during my PhD studies. Your contributions have been crucial to my academic development.

I am deeply thankful to my friends who have accompanied me over the difficult but wonderful years. Your companionship and encouragement have been a constant source of strength and joy.

Finally, I would like to express my profound gratitude to my wife, Minlan Wang, and my daughter, Zhiyu Xu. Completing my PhD would not have been possible without their love, patience, and continuous support. I am also grateful to my parents for their care and encouragement throughout my life. Their generosity, commitment, and resilience have consistently motivated me, propelling me forward.

Hanqing Xu
August, 2024, in Shanghai

CURRICULUM VITÆ

Hanqing XU

12-01-1993 Born in Lianyungang, Jiangsu, China.

EDUCATION

2011–2015 BSc in Geographic Information Science
Shanxi Normal University, Shanxi, China

2015–2018 MSc in Applied Chemistry
Shanghai Institute of Technology, Shanghai, China

2020–2024 PhD in Hydraulic Engineering
Delft University of Technology, Delft, the Netherlands

Thesis:	Compound flood hazards in Chinese coastal cities
Promotor:	Prof. dr. ir. Sebastiaan N. Jonkman
Promotor:	Prof. dr. Jun Wang
Co-Promotor:	Dr. Elisa Ragno

LIST OF PUBLICATIONS

11. **H.Q. Xu**, E. Ragno, B. Jonkman, J. Wang, J. Bricker, Z. Tian, L.X. Sun, *Combining statistical and hydrodynamic models to assess compound flood hazards from rainfall and storm surge: a case study of Shanghai*, Hydrology and Earth System Sciences (2023).

10. **H.Q. Xu**, E. Ragno, J.K. Tan, A. Antonini, J. Bricker, B. Jonkman, Q. Liu, J. Wang, *Perspectives on Compound Flooding in Chinese Estuary Regions*, International Journal of Disaster Risk Science **14**, 269–279, (2023).

9. **H.Q. Xu**, Z. Tian, L.X. Sun, Q. Ye, E. Ragno, J. Bricker, G.Q. Mao, J.K. Tan, J. Wang, Q. Ke, S. Wang, R. Toumi, *Compound flood impact of water level and rainfall during tropical cyclone period in a coastal city: The case of Shanghai*, Natural Hazards and Earth System Sciences **22**, 2347–2358, (2022).

8. Q. Liu^{+}, **H.Q. Xu**$^{+}$, J. Wang, *Assessing tropical cyclone compound flood risk using hydrodynamic modelling: a case study in Haikou City, China*, Natural Hazards and Earth System Sciences **22**, 665-675, (2022).

7. G.F. Wu, Q. Liu, **H.Q. Xu**, J. Wang, *Modelling the combined impact of sea level rise, land subsidence, and tropical cyclones in compound flooding of coastal cities*, Ocean & Coastal Management **252**, 107107, (2024).

6. X.J. Sun, R.N. Li, X.M. Shan, **H.Q. Xu**, J. Wang, *Assessment of climate change impacts and urban flood management schemes in central Shanghai*, International Journal of Disaster Risk Reduction **65**, 102563, (2021).

5. Y. Niu, J. Fang, R. Chen, Z. Xia, **H.Q. Xu**, *Network Modeling and Dynamic Mechanisms of Multi-Hazards—A Case Study of Typhoon Mangkhut*, Water **12**, 2198, (2020).

4. Z. Tian, Y.H. Ji, **H.Q. Xu**, H.G. Q, L.X. Sun, H.L. Zhong, J.G. Liu, *The potential contribution of growing rapeseed in winter fallow fields across Yangtze River Basin to energy and food security in China*, Resources, Conservation and Recycling **164**, 105159, (2021).

3. X.C. Liu, Z. Tian, L.X. Sun, J.G. Liu, W. Wu, **H.Q. Xu**, L.D. Sun, C.F. Wang, *Mitigating heat-related mortality risk in Shanghai, China: system dynamics modeling simulations*,Environ Geochem Health **42**, 3171–3184, (2020).

2. Z. Tian, **H.Q. Xu**, L.X. Sun, D.L. Fan, G. Fischer, H.L. Zhong, P.Q. Zhang, E. Pope, C. Kent, W. Wu, *Using a cross-scale simulation tool to assess future maize production under multiple climate change scenarios: An application to the Northeast Farming Region of China*, Climate Services **18**, 100150, (2020).

1. **H.Q. Xu**, Z. Tian, X.G. He, J. Wang, L.X. Sun, G. Fischer, D.L. Fan, H.L. Zhong, W. Wu, E. Pope, C. Kent, J.G. Liu, *Future increases in irrigation water requirement challenge the water-food nexus in the northeast farming region of China*, Agricultural Water Management **213**, 594-604, (2019).